Fabricating Multifunctional Composites via Transfer of Printed Electronics Using Additively Manufactured Sacrificial Tooling

Jacob Zachary Viar

Thesis submitted to the faculty of Virginia Polytechnic Institute and State University in partial fulfillment of the requirements for the degree of

Master of Science In

Materials Science and Engineering

Chair: Christopher B. Williams

Co-Chair: Bradley A. Davis

Scott W. Case

March 21,2022

Blacksburg, VA

Keywords: Multifunctional Composites, Printed Electronics, Additive Manufacturing

Fabricating Multifunctional Composites via Transfer of Printed Electronics Using Additively Manufactured Sacrificial Tooling

Jacob Zachary Viar

Abstract

Multifunctional composites have gained significant interest as they enable the integration of sensing and communication capabilities into structural, lightweight composites. Researchers have explored additive manufacturing processes for creating these structures through selective patterning of electrically conductive materials onto composites. Thus far, multifunctional composite performance has been limited by the conductivity of functional materials used, and the methods of integration have resulted in compromises to both structural and functional performance. Integration methods have also imposed limitations on part geometry due to an inability to adequately deposit conductive material over concave surfaces. Proposed methods of integrating functional devices within composites have been shown to negatively affect their mechanical performance.

This work presents a novel method for integrating printed electronics onto the interior surfaces of closed, complex continuous fiber composite structures via the transfer of selectively printed conductive inks from additively manufactured sacrificial tooling to the composite surface. The process is demonstrated by creating multifunctional composites via transferring printed electronics from sacrificial tooling onto structural composites without negatively affecting the mechanical performance of the structure. Additionally, this process expands the ability to pattern devices onto complex surfaces and demonstrates that the transferred functionality is well integrated (adhered) with the composite surface. The process is further validated through the successful completion of two separate case studies. The first is the integration of a functioning strain gauge onto an S-glass/epoxy composite, while a second process demonstration shows a composite surface featuring a band stop filter at the X-band, otherwise known as a frequency selective surface (FSS), to show the process' suitability for high performance, aerospace grade multifunctional composites.

Fabricating Multifunctional Composites via Transfer of Printed Electronics Using Additively Manufactured Sacrificial Tooling

Jacob Zachary Viar

General Audience Abstract

Significant interest has been given in the past few decades to strong, lightweight materials for structural purposes. Among these materials, specific interest has been paid to fiber-reinforced composites, which are made of strong fibers and advanced resins. Recently, researchers have tried to use electrically conductive inks and 3D printing techniques to put antennas and other devices onto composites. These composites could possess additional functions beyond their structural purpose and are therefore called multifunctional composites. So far, the performance of multifunctional composites has been limited by the methods used to add additional functions. These methods often result in a weaker composite material and poor performance of the added devices.

In this work, a new method for integrating devices onto complex-shaped composite structures is demonstrated. This is done by printing a mold for a composite, then putting a conductive ink onto the mold and transferring the ink to the composite surface. This process is demonstrated without weakening the composite. Additionally, this process allows researchers to put devices onto complex surfaces and demonstrates that the devices are secured to the composite surface. The process is used to make two separate devices and combine them with a composites surface. The first demonstration is the integration of a functioning strain gauge (used to measure a change in material dimension) onto a structural composite, while a second process demonstration shows a composite surface featuring an electromagnetic filter, otherwise known as a frequency selective surface (FSS), to show the process' suitability for high performance, aerospace grade multifunctional composites.

This work relates to Department of Navy award N00014-19-1-2736 issued by the Office of Naval Research.

Acknowledgements

I would like to here thank both of my advisors, Dr. Christopher Williams and Dr. Bradley Davis, for their willingness to accept me as a student and for providing the direction for this work, which has garnered so much interest in the last year. Indeed, I would not have been able to attend graduate school at all were it not for Dr. Davis taking a chance on me and bringing me into the MEEP program at the Hume Center. The tireless dedication to this project of both Dr. Davis and Dr. Williams as well as their generous patience with me during this program is the direct reason that I have achieved any success in pursuing this degree. Their work ethic has been an inspiration to me; one that I hope to emulate as I move on from Virginia Tech.

I owe a great deal of gratitude to my graduate and undergraduate colleagues who have contributed to my personal and professional development in ways I have yet to fully realize. John and Dallas, I could not have asked for finer friends through my time here; you both have been like brothers to me, and I can hardly state how grateful I am to have learned from and relied on you two. Ginny and Theresa, you both provided the support and kindness and baked goods that sustained me in my most stressful moments, thank you. My mentee, Julia: it was an absolute privilege to mentor you and to work on this project with you; you brought determination and an open mind to lab each day, and I firmly believe that this project would not have succeeded without that. Joseph, Lindsey, Ian, Nathan, Amanda, Sam, Keyton, Jack, Danny, Kazi, Yifeng, and Bemnet: each one of you were excellent towards me, and you inspired me to bring my best to lab, to contribute to the reputation of the lab. I am humbled to have spent my time here with researchers of such high quality, and each of you is a credit to your field.

I would like to also thank my family for their support through my time at Virginia Tech, and in particular I thank my dad for encouraging me to pursue engineering from a young age. The sacrifices made by them in support of my ambitions will continue to motivate me as I move forward.

Table of Contents

Table of Figures viii

Chapter 1: AM of Multifunctional Composites 1

1.1 Multifunctional composites: overview and value proposition 1

1.2 Printing Electronic Devices 3

1.2.1 Direct Ink Write (DIW) 5

1.2.2 Inkjet Printing 6

1.2.3 Aerosol Jet 6

1.2.2 Transfer printing 7

1.3 Multifunctional composite fabrication via printed electronics 9

1.3.1 Capabilities gap and limitations of current multifunctional composite methods 12

1.4 TEST Process: Transfer deposition onto composite surface 12

1.4.1 Process objectives 12

1.4.2 TEST Process Overview 13

1.4.3 Anticipated Process Advantages 13

1.4.4 Significant Contributions 13

1.4.5 Research Questions 14

Chapter 2: TEST Process for Multifunctional Composite Fabrication 15

2.1 Introduction 15

2.2 RQ1: What materials are compatible with this process? 15

2.2.1 Fiber reinforced polymer matrix composite 15

2.2.2 FFF Soluble Tooling 15

2.2.3 Solvent Selection 16

2.2.4 Conductive Ink 16

2.2.5 Analysis of material compatibility with TEST process 17

2.3 Empirical demonstration of TEST process 18

2.4 RQ2: How does solvent selection affect multifunctional composite mechanical performance using the TEST process? 23

2.4.1 Introduction 23
2.4.2 Sample preparation and experimental setup 23
2.4.3 Results 24
2.4.4 Conclusion 25
2.5 RQ3: How does the TEST process affect printed trace resistance? 25
2.5.1 Methods for fabricating TEST process specimen 26
2.5.2 Methods for determining TEST process effect on trace resistance 27
2.5.3 Results 27
2.6 RQ4: How does the TEST process affect dimensions of transferred electronics? 28
2.6.1 Introduction 28
2.6.2 Test setup and data collection 28
2.6.3 Results 29
2.6.4 Conclusion 32
2.7 RQ5: What is the quality of ink adhesion to the composite surface after TEST process? 32
2.7.1 Introduction 32
2.7.2 Methods 32
2.7.3 Results 33
2.7.4 Conclusion 34
2.8 TEST Process Conclusions 35
Chapter 3: Use of Test Method to Integrate Strain Gauge on Conformal Composite Structure 39
3.1 Introduction 39
3.2 Methods 40
3.2.1 Strain gauge design 40
3.2.2 Strain Gauge Printing via Direct Ink Write (DIW) 41
3.2.1 Print sacrificial tool: tool selection and preparation 41
3.2.2 Print conductive trace: DIW of strain gauges 41
3.2.3 Composite layup onto PES tooling 43
3.3 Measurement and Results 46
3.3.4 Results and discussion for CB028 strain gauge on fiberglass-epoxy 47
3.5 Conclusions 48
Chapter 4: Transfer Process Validation: Production and Characterization of a Composite Frequency Selective Surface at X-band 50
4.1 Introduction 50

4.2 Methods 51
4.2.1 FSS Design 51
4.2.2 Fabrication 53
Geometric modeling and DIW toolpath planning 53
Step 1: Print sacrificial tool: selection and preparation 54
Step 2:Print conductive trace - DIW of FSS onto ULTEM 1000 54
Step 3: Layup composite 55
Step 4: Wash away tool 55
4.3 Measurement 56
Measurement Setup 56
4.4 Results 58
4.5 Conclusions 61
Chapter 5: Summary, Conclusions, and Future Work 62
5.1 Summary of motivation 62
5.2 Summary of work and key results 63
5.3 List of key contributions 65
5.4 Future work 65
References 67
Appendices 71
A.1 TEST process using ExOne Printed Sand sacrificial tooling 71
A.2 Composite pressure vessel experiment 72

Table of Figures

Chapter 1

Figure 1.1 Fiber reinforced polymer composite lamina (a) with additional functionality embedded within a fiber reinforced polymer laminate (b)……...1

Figure 1.2 A comparison of subtractive IC processing and additive printing approach for thin film device development……4

Figure 1.3 A comparison of subtractive IC processing and additive printing approach for thin film device development……..5

Figure 1.4 Schematic of direct ink writing of silver ink at representative pressure condition of 25 psi.....6

Figure 1.5 Comparison of different digital manufacturing technologies. (a) Ink jetting low viscosity nanoparticle loaded inks; thousands of droplets per second (b) Aerosol spray low viscosity nanoparticle loaded inks; a steady stream of aerosol(c) microdispensing low, medium, and high viscosity particle loaded paste; continuous dispense (d) extruding thermoplastic that is heated to melt temperature; continuous extrusion……..8

Figure 1.6 Transfer process depicted via a printed layer on a donor substrate (a) being transferred via a stamp (b) onto a device substrate (c-d)……9

Figure 1.7 Direct Ink Write of Dupont CB-028 onto a woven glass reinforcement……..11

Figure 1.8 Conformal direct ink writing of Dupont CB-028 onto a cured S-glass/cyanate ester composite laminate (a) to form a conformal printed patch antenna array (b)……..12

Figure 1.9 Conformal metasurface antenna fabricated via laser-profiling (a) and after integration with a conformal composite laminate surface (b)……..13

Figure 1.10 Graphical representation of the TEST process…… 14

Chapter 2

Figure 2.1 Polysulfone sacrificial tool, block……20

Figure 2.2 Polysulfone sacrificial tool, airfoil……..20

Figure 2.3 Conformal DIW of Dupont CB-028 onto airfoil tool via 6-axis robotic arm……..21

Figure 2.4 Sintered CB-028 50mm 4-point probe lines on block PSU sacrificial tooling (a.) and conformal patch antenna geometry on airfoil PSU sacrificial tooling (b)……..21

Figure 2.5 Composite layup process onto block polysulfone sacrificial tool during layup (a), after layup (b), and after vacuum bagging (c) before curing. Composite laminate cured onto airfoil (d) and block polysulfone sacrificial tooling (e) with a cross-shaped access hole (f) after curing……22

Figure 2.6 Cured composite laminate structure after sacrificial tooling washout. Block tooling geometry (a), washed out with DCM, successfully transferred conductive traces onto the interior surface of the

composite shell (b). Airfoil tooling geometry (c), washed out with DMSO, also successfully transferred the simulated patch antenna onto the interior surface of the composite skin (d)……..…..23

Figure 2.7 Fibreglast E-glass/epoxy prepreg laminate layup (a). Laminate cured and cut into 3-point bend test coupons (b)……24

Figure 2.8 Visual comparison of 3-point bend test coupons after exposure to DMF (a-left) and DMSO (a-right) and during 3-point bend testing (b)……..25

Figure 2.9 Flexural response of composite coupons exposed to solvent for 27 hours……26

Figure 2.10 4-point probe resistance measurement CAD drawing with dimensions labelled in millimeters……...27

Figure 2.11 Printed CB-028 resistance measurement samples sintered on sacrificial PES composite tooling (a), during composite prepreg layup (b), and during tooling washout in DMSO bath (c)……28

Figure 2.12 Resistance values for CB-028 silver ink sample 50mm lines after sintering onto printed PES sacrificial tooling (left) and after transferring samples to the surface of S-glass/epoxy composite surface using the TEST process (right)……..29

Figure 2.13 Composite panel with printed resistance measurements embedded in the surface (a) being scanned via laser profilometer (b)……..…..30

Figure 2.14 Profilometry scans compiled into surface plot for printed conductive traces on sacrificial PES tooling (a) and cross-section showing four distinct traces (b). Similarly, profilometry scans compiled into surface plot for composite specimen after TEST process completion (c) and cross-section showing the four printed traces are no longer distinct from the surrounding surface (d)……31

Figure 2.15 Cut edge of composite test article with transferred trace cross-section exposed and outlined in red……..32

Figure 2.16 Composite sample holders with decreasing radius of curvatures, measuring from bottom to top: 635mm, 317.5mm, 158.75mm, 80.65mm, and 69.85mm……34

Figure 2.17 Resistance measurements for the unflexed and flexed composite specimen at decreasing radius of curvatures……..35

Figure 2.18 Fishbone diagram illustrating the factors at each step in the TEST process which was observed to directly affect the final part transfer quality……..……37

Chapter 3

Figure 3.1 Illustration of a uniaxial strain gauge……40

Figure 3.2 CAD image produced via SolidWorks of uniaxial strain gauge to be printed using conductive DIW……40

Figure 3.3 Strain gauges printed onto PES sacrificial tooling via conductive DIW……42

Figure 3.4 Copper solder tabs placed onto printed strain gauges……..……43

Figure 3.5 PES tooling after curing FRP composite laminate (a) and after tool dissolution in DMSO (b), showing the successful transfer of the printed strain gauges from the surface of the PES tooling to the FRP composite surface……44

Figure 3.6 Schematic of unbalanced Wheatstone bridge, thus necessitating the use of an additional resistor to increase the resistance of R4 to match the three 120Ω legs……..45

Figure 3.7 Strain gauges embedded onto FRP fiberglass-epoxy composite specimens……..45

Figure 3.8 Test configuration for tension testing including an extensometer to measure strain……..46

Figure 3.9 Extensometer results from Instron testing shows the linear relationship between stress and strain……47

Figure 3.10 Printed strain gauge output voltage versus strain of glass-fiber reinforced polymer (GFRP) composite……48

Chapter 4

Figure 4.1 Frequency selective surface unit cell with critical dimensions listed in the table on the left….51

Figure 4.2 Illustration of the test method orientation showing the coordinate system relative to the test specimen and the transmitted waves. Both alpha and beta angles are highlighted……52

Figure 4.3 Modeled S12 transmission characteristics for the FSS in the V-orientation (a) and H-orientation (b). Each orientation was modeled for beta angles of 0, 10, and 45, in order to visualize how the transmission response changes with changes in the beta angle……53

Figure 4.4 Printing of the FSS onto an Ultem 1000 substrate via conductive DIW……..54

Figure 4.5 From left to right: Sintered FSS pattern undergoing optical microscopy inspection (a). Hand layup of composite prepreg onto the surface of the Ultem 1000 tool(b). Vacuum bagging of the composite prepreg and the FSS on the Ultem 1000 sacrificial tooling(c)……..55

Figure 4.6 Successful transfer of the printed tripole FSS onto Fibreglast 7781 E-glass/Epoxy composite (a). Discoloration and defects occurred due to manual removal of the ULTEM sacrificial tooling from the composite surface (b). Four FSS panels aligned and sandwiched between two panels of polystyrene foam, forming the final test specimen (c)……56

Figure 4.7 Measurement setup for conducting transmission measurements on FSS……...57

Figure 4.8 Measured transmission response for FSS from 2-18GHz for H-orientation (a) and V-orientation (b). Modeled results at beta angles of 0, 10, and 45 are superimposed over the measured results for comparison……..60

Appendices

Figure A.1.1 TEST Process transfer demonstration using ExOne printed sand sacrificial composite tooling surface (a) and cured composite box (b)……..71

Figure A.2.1 Pressure vessel dimensions for FDM printed sacrificial tooling ……72

Figure A.2.2 DIW printing silver ink strain gauge onto Ultem pressure vessel sacrificial tooling……...73

Figure A.2.3 Cured composite pressure vessel on sacrificial tooling (left), interior of original size pressure vessel with undissolved Ultem and damaged strain gauge not fully adhered to composite (middle), and large-scale pressure vessel (2X original size) with undissolved Ultem covering the damaged printed strain gauge (right). ……74

Chapter 1: AM of Multifunctional Composites

1.1 Multifunctional composites: overview and value proposition

Increasingly lightweight, strong materials are necessary for structural applications across many industries ranging from aerospace, defense, automotive, and civil structures. Fiber reinforced polymer (FRP) composites have been used extensively in these industries for several decades due to their high strength to weight ratio and their tunable material properties. FRP composites derive their excellent mechanical properties primarily from the tensile strength of the reinforcement fiber which is held in place via the polymer matrix. The polymer matrix can be either a thermoplastic or a thermoset, although for most high performance applications (e.g., aerospace), thermosets are most commonly preferred. FRP composites consist of several layers of matrix coated reinforcing fibers stacked together against a composite tool to form a laminate.

Multifunctional composites are FRP composites that have been modified to possess some additional functionality beyond their structural function. Additional functionality can include sensing, EMI shielding, actuation, energy storage, RF communications, and more [1]–[5]. This additional functionality can be added through the use of fillers in the matrix [5], conductive fibers or patterns woven into the reinforcement fabric [6], or through the integration of electronics into the FRP structure during FRP fabrication [7]–[9]. Figure 1.1a illustrates an individual FRP lamina juxtaposed with a multifunctional composite laminate (Figure 1.1b), where the added functionality is represented as being embedded between the FRP layers. In this illustration, the method of integrating functionality involves patterning the functional element directly onto the uncured FRP composite material as the laminate is being formed. Approaches which embed functionality within the layers of a composite have the unique advantage that the device (antenna, circuit, high impedance surface, etc.) is completely protected from the environment after curing the structural laminate. Embedded approaches to fabricating multifunctional composites have been shown to negatively affect the structure of the laminate, particularly in bending. [10]–[12]

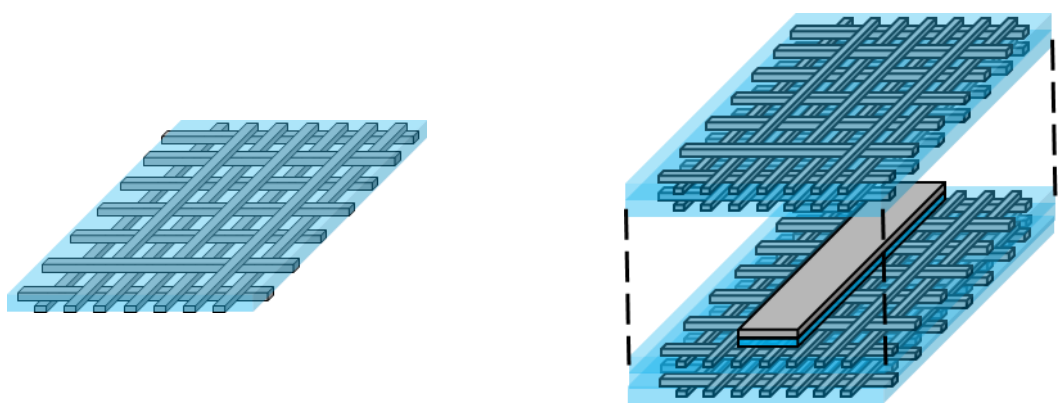

a. b.

Figure 1.1 Fiber reinforced polymer composite lamina (a) with additional functionality embedded within a fiber reinforced polymer laminate (b).

The ability to integrate additional functionality into the structure of FRP composites presents several benefits. Consolidation of structure and functionality leads to weight reduction of the part by removing the need for, and parasitic mass of, wiring harnesses and fasteners. Additionally, space and fabrication time are conserved by integrating conductive pathways into the structure of the laminate composite, as the need for cables and other non-structural/functional elements after installing the part are eliminated [1].

As previously mentioned, additional functionalities have been incorporated into the structure of FRP composites through fiber modification, matrix modification, or through the integration of printed electronics. Addition of functionality through the use of fiber or matrix modification takes place before the formation of the composite laminate, whereas the integration of printed electronics with the composite has been demonstrated both before and after the laminate cure process.

Mirotznik et al. provide examples of fiber modification by the selective weaving of carbon fibers with glass fiber reinforcement to form conductive pathways within individual FRP lamina. This technique is presented as hybridizing the reinforcement architecture using a CCI Tech SL8900 Sampling Loom to form electromagnetically heterogeneous laminae to be laid up within a composite laminate. Another method demonstrated by Mirotznik et al. involves selectively laying up carbon fiber reinforcing fabric within a glass fiber reinforced laminate in order to introduce heterogeneity. These methods are effective at producing large scale, rapidly produced multifunctional composites. The low conductivity of carbon fiber, approximately and order of magnitude less than silver, does present significant limitations on the types of functionalities that can be added using fiber modification techniques [4].

Yao et al. utilize a different approach in which a 3D orthogonal weaving machine is used to stitch bulk copper wires into a glass fiber reinforced vinyl ester composite in a patch antenna geometry. The top and bottom warp yarns of the laminate were replaced with copper wires and stitched in the through thickness direction to the laminate before curing. The patch antenna formed using this method was designed to transmit in the L-band (1-2GHz). The authors record satisfactory performance of the antenna but note a significant reduction in the tensile and bending strengths of the multifunctional laminate when compared to an unmodified laminate composite [13].

Baum et al. demonstrate a new approach of selectively embroidering silver coated polyamide and Kevlar reinforcement yarns onto HexPly 914E S-glass/epoxy prepreg to form microstrip transmission lines. The technique utilized a Brother PE-1000 embroidery machine to use different stitch patterns to integrate the conductive fibers into the prepreg lamina which was then laid up on the surface of a laminate structural composite of the same prepreg. The laminate was cured, and the microstrip transmission lines' RF performance was evaluated. Overall, the conductive fibers showed excellent performance when compared to the reference copper line; however, the authors do not assess the mechanical effects of such a process. Acknowledgment is given to the importance of a structural analysis, but it is labeled as future work, with the caveat that it is possible that the embroidering process may form delamination or failure points within the laminate. Once again, it is mentioned that the conductive fibers used possess significantly lower conductivity when compared with bulk copper, despite their similar RF performance. It is explicitly stated that in recent works, the isotropic conductivity of printed circuits has provided better performance [6].

With the introduction of additive and other advanced manufacturing methods, functionality can be conformally integrated into FRP structures, which is especially beneficial in cases where sensing or communication devices need to be applied to complex structures. There has been a quiet push in recent years for discreet electronics that are able to conform to highly irregular surfaces, as demonstrated by Baum et al. [6] and Perez et al. [14].

For example, Lee et al. have utilized a cold spray technique to deposit continuous silver strain gauges directly onto carbon and glass fiber reinforced prepreg lamina for structural health monitoring of laminate composites. The lamina with printed gauges were then laid up to form laminate composites and tested in axial strain. The resulting data showed the printed gauge factors varied from 5 to 30 and could measure strains up to 0.01mm/mm. [15] The motivation of the work is presented as leveraging advanced techniques to embed structural health monitoring sensors within a structural composite to measure strain at nonplanar and difficult to access areas.

Techniques which involve modification of the fiber reinforcement to add functionality appear in all cases to be limited in application by the conductivity of the functional material. In nearly all cases, a significant reduction in the mechanical strength of the resulting laminate is recorded. Furthermore, reduction in strength is attributed directly to the functionality integration method. By contrast, the most promising work in recent literature utilizes additive/advanced manufacturing methods to print electronic devices that are then incorporated with the FRP composite to form multifunctional composites. Before further analysis of these methods, a brief overview of printed electronics is necessary.

1.2 Printing Electronic Devices

Printed electronic techniques have enabled selective patterning of complex electrically conductive traces directly onto substrates, which is of particular importance in the fabrication of multifunctional composites. Direct patterning or printing of conductive traces has the potential to remove the need for solder and connectors, which can cause impedance mismatching in traditionally fabricated electronic devices [16].

Printed electronics have gained significant attention in recent years for both commercial and industrial applications. Figure 1.2 illustrates the differences between additive and subtractive processes used in the fabrication of integrated circuits. The ability to rapidly prototype electronic devices by only depositing conductive material where necessary eliminates waste and reduces fabrication time associated with conventional electronics manufacturing. Printed electronics have shown particular promise via their ability to be patterned on a wide variety of rigid and flexible substrates such as PET, organics (paper), polyimide, PTFE, and even cured laminate composites directly. [17]–[19]

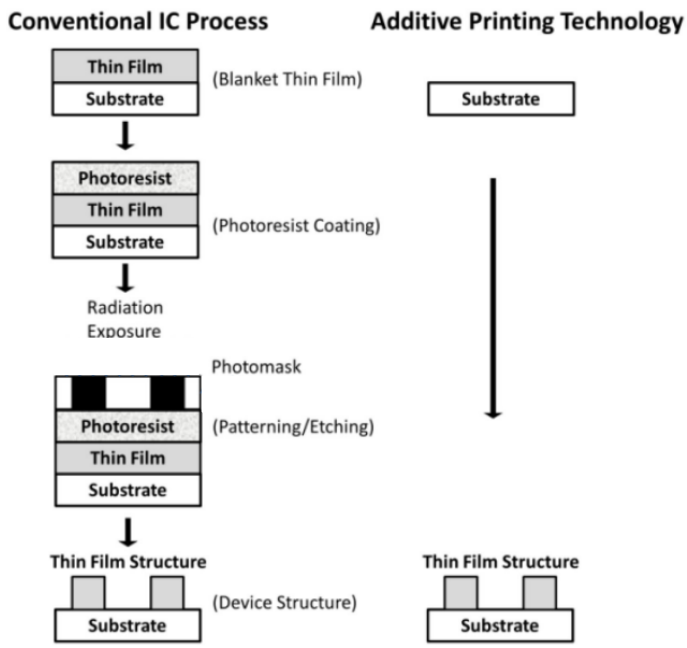

Figure 1.2 A comparison of subtractive IC processing and additive printing approach for thin film device development adapted from [20].

Additive methods for printing electronics are typically focused on selective deposition of conductive inks. These methods involve the patterning of a conductive ink or paste onto a desired substrate. Conductive inks consist in two categories: particle-based and particle-free. In particle-based inks, metal particles are suspended in a solution of surfactants, binders, and solvents to enable consistent deposition. These metal particles are typically silver, copper, or gold with silver particles being by far the most common due to their stability, superior conductivity, and reasonable affordability [21]. Particle-based inks typically require a sintering step after printing which takes place between 140°C-200°C. Particle-free inks are sometimes referred to as metal-organic decomposition (MOD) inks and are composed of metal organic salts dispersed in solvents and ligands. Particle-free inks are formed by the dissolution of a metal salt precursor in a solvent. Particle-free inks are able to be patterned by a variety of methods such as direct ink write and inkjet printing and require lower temperatures (120°-150°C) to reduce and sinter the metal salts into conductive films, making them appealing for deposition on a wide variety of substrates (PET, paper, low melt-temperature plastics, etc.). [22] Nearly all conductive inks require a post process to remove the polymer binder and establish conductivity. At present, both silver particle-based and particle-free inks possess, at best, approximately 3 times the bulk resistivity of silver after post processing. [23]–[26] As a general trend, the greater the temperature used to post process conductive inks, the lower the resistivity of that ink [24].

The method of depositing these conductive inks is primarily determined by the ink's viscosity, which is affected by the particle size, solids loading, and solvent selection. Methods of printing electronics are depicted in Figure 1.3 to illustrate the difference in subtractive and additive methods as they relate to resolution and throughput. From the figure, additive processes of patterning conductive inks offer as much as two orders of magnitude greater throughput than traditional subtractive methods. Inkjet and screen printing of conductive ink, in particular, are used extensively in multifunctional composite

fabrication techniques. Not listed in Figure 1.3 are direct ink write, aerosol jet, and transfer printing, which are also relevant to multifunctional composite fabrication.

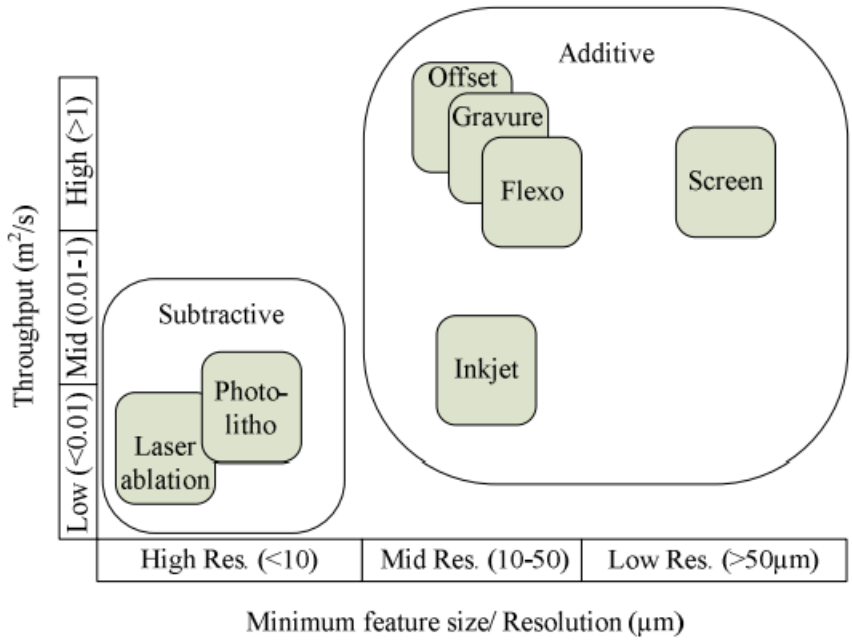

Figure 1.3 Comparison of various printing/patterning technologies [17]

1.2.1 Direct Ink Write (DIW)

DIW is referred to as a material extrusion-based process in which conductive ink is loaded into a syringe and extruded through a nozzle via pneumatically or mechanically pressurizing the ink onto a substrate. This syringe is mounted onto a 3-axis linear motion gantry system to enable controlled patterning of the ink in three dimensions. Figure 1.4 and Figure 1.5c depict the relevant elements in this process. Factors which affect the accuracy and precision of the print include pressure applied to the syringe, distance between the tip of the nozzle and the substrate, rate of travel of the syringe across the substrate, nozzle diameter, and wetting of the ink onto the substrate. For a more detailed analysis of DIW and its recent impacts on the field of printed electronics, the review written by Perez and coauthors [14] is referred to along with Chapter 8 of *Additive Manufacturing* by Parekh et al. [27].

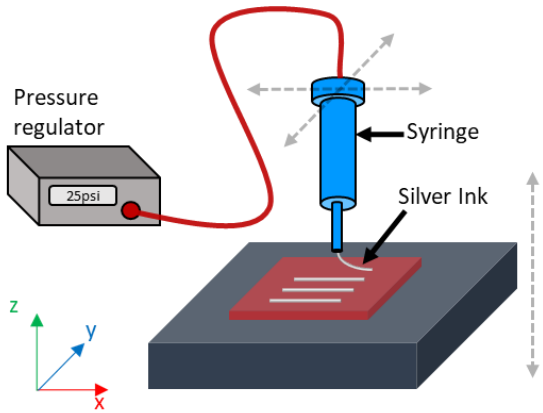

Figure 1.4. Schematic of direct ink writing of silver ink at representative pressure condition of 25 psi.

Inks processed in this method typically have higher viscosities when compared to aerosol jet and inkjet methods and conductivity values on the order of 30% the bulk conductivity of silver [18]. A benefit of DIW is the breadth of materials that it can process, including a broad range of dielectric resins and conductive inks that enable the fabrication of electronic devices. This process has been used extensively in recent years to fabricate antennas and metamaterials operating at a wide range of frequencies ranging from UHF to K bands [7], [28]–[33]. DIW is well suited to rapidly prototyping several design iterations or for small volume production due to its balance of resolution (0.1mm) with print speed. Additionally, DIW is not dependent upon gravity for proper deposition which means that the process can be used to realize conformal deposition. DIW is not particularly well suited to large prints where fine feature resolution is not necessary.

1.2.2 Inkjet Printing

Inkjet printing (IJ) is perhaps the most recognizable printing technology given its widespread use in household office printers. The most common form of IJ printing, drop-on-demand (DOD), utilizes thermal or piezoelectric actuators to jet ink in picolitre droplets onto a substrate (Figure 1.5a). Conductive inks for IJ are typically low viscosity inks with low solids loadings in order to form such small droplets. Alternatively, IJ often uses MOD inks in order to maintain consistent deposition quality [14]. IJ is capable of printing very precise thin films with high speed and precision, covering large areas in conductive films in very short spans of time. This method is particularly suited for thin film applications, such as printed solar cells of flexible printed electronics [34], [35]. Typically, IJ systems have the printhead move in the X-Y plane while the substrate travels linearly in the Z-direction. Because the droplets are carried via gravity to the substrate, the orientation of the inkjet head and the substrate must be precisely controlled. It is for this reason that IJ is not well suited to deposit conductive inks over conformal substrates.

1.2.3 Aerosol Jet

The aerosol jetting (AJ) process (Figure 1.5b) has the greatest resolution of current printed electronic techniques. AJ is capable of depositing conductive inks to form electronic devices with feature sizes as small as 20µm. AJ is a contactless printing process which atomizes conductive ink through ultrasonic or pneumatic means. An inert carrier gas (nitrogen or argon) transports the aerosolized ink particles through a deposition nozzle onto the substrate. Channels in the deposition nozzle are carefully designed to allow for a second gas, the sheath gas, to focus the aerosolized particles into a steady stream as they travel towards the substrate. Adjusting the flow rate of the sheath gas determines the printed

trace width, while adjusting the carrier gas and atomizing power determines the ink flow rate through the deposition nozzle. AJ is capable of printing conformally onto substrates that possess surface deviations up to 3mm. The deposition nozzle is typically mounted on an X-Y-Z gantry system to enable three dimensional depositions although, with few very impressive exceptions, most AJ printing of conductive traces is two dimensional[14], [36]–[38]. AJ is costly and labor intensive compared to other methods of printing electronics. This has prevented its more widespread use despite its superior resolution. Ink stability and deposition consistency are also reported as being hurdles for more universal adoption of the technology in industrial applications [36]. The reader is referred to a comprehensive review of printed electronic technologies by Hon et al. for further details on the applications of printed electronics [39].

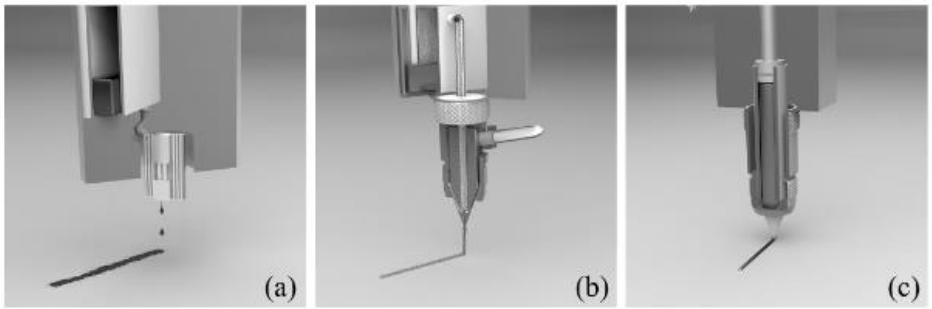

Figure 1.5 Comparison of different digital manufacturing technologies. (a) Ink jetting low viscosity nanoparticle loaded inks; thousands of droplets per second (b) Aerosol spray low viscosity nanoparticle loaded inks; a steady stream of aerosol(c) microdispensing low, medium, and high viscosity particle loaded paste; continuous dispense (d) extruding thermoplastic that is heated to melt temperature; continuous extrusion [16].

1.2.2 Transfer printing

Transfer printing is relatively new to the field of printed electronics. The process consists of four key components: a donor substrate, a transfer substrate, a printed layer, and a device substrate. In transfer printing, the electronic device (printed layer) is patterned onto a donor substrate. A transfer substrate is then “stamped” onto the donor substrate to transfer the printed layer from the donor substrate to the device substrate. In order for this to happen, the cohesive forces between the printed layer and the transfer substrate must be less than the adhesive forces between the printed layer and the device substrate [27]. Alternatively, the printed layer may in some cases be directly patterned onto a transfer substrate to be stamped onto the device substrate, eliminating the need for a donor substrate.

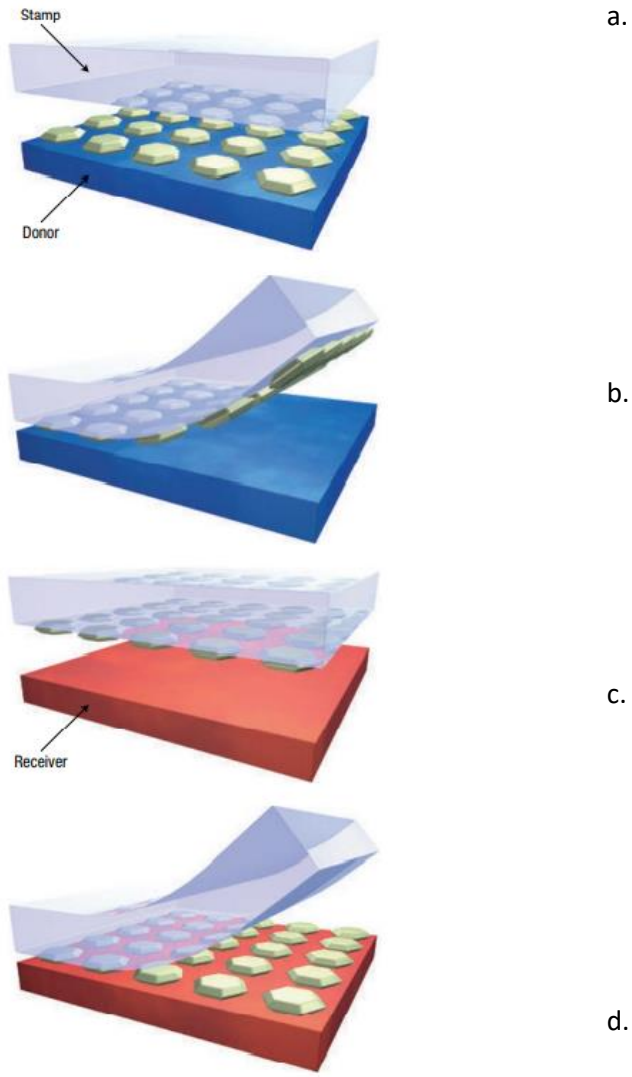

Figure 1.6 Transfer process depicted via a printed layer on a donor substrate (a) being transferred via a stamp (b) onto a device substrate (c-d) [40].

This method has been used to selectively pattern p-n junctions onto highly curved surfaces through the use of a switchable adhesion elastomeric stamp by Meitl et al. [40]. The process is used by Pfeiffer et al. to fabricate several electrically small helical antennas onto doubly curved device substrates through multi-stage plating-transfer-etching technique. The antennas were designed to operate at 1.12, 1.52, and 2.70GHz. The process is depicted in Figure 1.7

In this work, particular attention is paid to direct ink write (DIW) and transfer methods of patterning conductive inks. These methods are selected due to their ease of use and their ability to deposit inks over a large area and onto a variety of conformal substrates. Additionally, DIW and transfer printing

have shown promise in recent years as methods for multifunctional composite fabrication. DIW encompasses a broad category of deposition techniques illustrated in Figure 1.5, and in this work specific attention is paid to the continuous extrusion of conductive paste. (Figure 1.5c)

1.3 Multifunctional composite fabrication via printed electronics

As previously stated, the more promising approaches to multifunctional composite fabrication involve integrating printed electronics with FRP composites. This section presents a deeper dive into current multifunctional composite fabrication approaches which utilize printed electronics to add functionality. These approaches can be broadly categorized into two groups based on whether the integration of the added functionality occurs during or after the processing of the FRP laminate.

Integration of electronic functionality within the FRP laminate before layup as demonstrated by Pa et al. has been shown to embed transmission lines, frequency selective surfaces, and patch antennas. The process starts with the design of an electronic device from its simulated performance characteristics. Once a part file is made, the device is patterned via selective deposition of Dupont CB-028 conductive ink using a direct ink write method with an nScrypt 3Dn-300. The work also patterns Dupont CB-028 using a screen printing technique for comparison of the printing technologies' ability to form functional devices. In both cases, the ink is deposited onto a dry woven glass fiber reinforcing mat substrate (Figure1.7). The ink is then sintered onto the reinforcing mat at 160°C for one hour. The sintered components and dry fabric are laid up within a 4-layer balanced BTCy-1 6781 glass fiber/cyanate ester prepreg layup at different positions depending on the printed device. The laminate was vacuum bagged and cured at 176.6°C for 90min in accordance with manufacturers specifications. Connectors were then added to the laminate to interface with the printed device. Mechanical analysis of multifunctional composites formed using this embedded approach show adhesive bond failure between the sintered ink and composite resin as the failure mode for short beam shear tests. A reduction on flexural strength as high as 30% is recorded. Additionally, small surface voids were observed on the non-printed composite areas indicating insufficient resin content as a result of the addition of dry reinforcement fabric. In the RF characterization of the printed antenna multifunctional composite, impedance mismatching is significant due to the spreading/wicking of the printed ink along the fiber reinforcement before sintering. Ink spreading/wicking was attributed as the cause of the 500MHz discrepancy between the measured and modeled antenna reflection characteristics. [3], [9], [10] This embedded approach is likely to find its application in discreet electronics/sensing where structural requirements may not be as stringent. This process possesses significant promise over other methods that modify or use the reinforcement fiber as the functional element, as this embedding process allows for isotropic electrical conductivity of the functional elements. This method does have significant negative effects on mechanical performance, which limits its application.

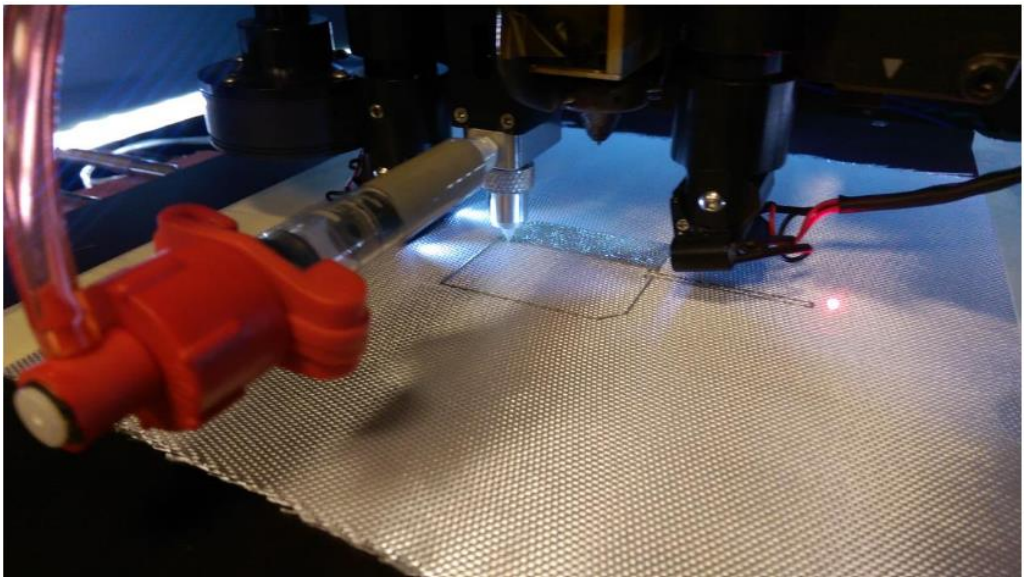

Figure 1.7 Direct Ink Write of Dupont CB-028 onto a woven glass reinforcement [3].

Functionality added after the formation of the FRP laminate involves patterning the desired device onto the surface of the cured laminate (Figure1.8). This has been demonstrated by Biswas et al through the conformal DIW deposition of a patch antenna array, designed to perform at 6GHz, onto the surface of a curved FRP laminate [7]. This process starts with the design and modeling of an array of patch antennas in a finite element simulator. The patch antenna part file is then uploaded to an nScrypt 3Dn-300 printer in order to pattern Dupont CB-028 conductive ink via a direct ink write onto a cured composite laminate substrate. The balanced composite laminate was composed of four layers of BTCy-1 6781 S-glass/cyanate ester prepreg that had been laid up and autoclave cured at 177°C under 344.74kPa for 90min. The cured laminate and conductive ink were then heated to 177°C for one hour in order to sinter the ink. An edge connector was then fixed to the final part to facilitate the RF characterization of the reflection properties of the antennas. Initial measured results showed excellent return losses when compared to the simulated return losses. Since the mechanical performance of the composite is not impacted by the deposition of conductive ink onto its surface, a mechanical study is not performed [7], [41], [42]. An adhesion study of the printed antennas to the composite surface is missing from the work, so the durability of electronics made in this process is unknown. This is a critical study to include because multifunctional composites formed using this method have their functionality exposed to the environment and lack the protection of embedded techniques. An adhesion study between the sintered ink and the composite surface is necessary to determine whether the flexural strains experienced by the composite structure will result in chipping, cracking, or delamination of the antennas. The authors cite geometry limitations with this method, as toolhead collisions will prevent the printing onto substrates angled at >45°. The benefits of this method are presented as allowing the radiating element to transmit normal to the surface of the composite, providing new RF design opportunities that have been largely unexplored. Additionally, this method does not reduce the mechanical strength of the composite laminate, as is noted in embedded approaches.

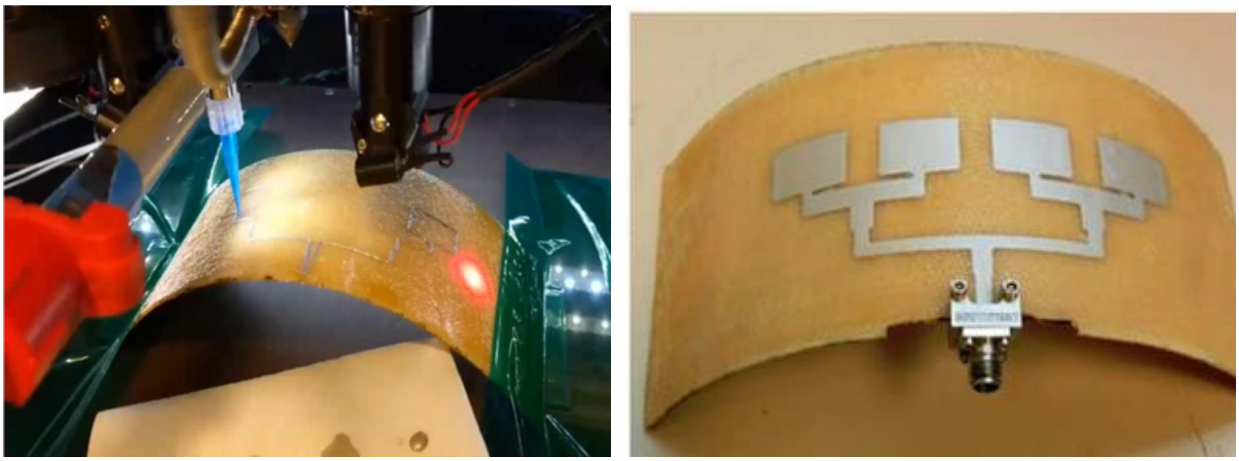

a. b.

Figure 1.8 Conformal direct ink writing of Dupont CB-028 onto a cured S-glass/cyanate ester composite laminate (a) to form a conformal printed patch antenna array (b)[7].

Nicholson et al. have demonstrated a form of transfer printing as a method of integrating planar and conformal metasurface antennas with an S-glass/epoxy laminate. The work is presented as being compatible with current laminate fabrication methods used in the aerospace industry, and it represents the most promising work on the deployment of truly conformal multifunctional composites. The process begins with the design of the metasurface antennas, which in this case are designed to operate at 10GHz. In the planar case, annealed copper foil (25µm thick) is held against an Airtech A4000 PTFE release film by a thin layer of spray adhesive. The copper foil is subtractively patterned into the designed metasurface antenna via laser-profiling with a Trotec Speedy Mark 700. Fifteen plies of HexPly914E twill weave prepreg are laid up onto the patterned metasurface antenna and cured at 175°C for one hour, per manufacturer specifications. After curing the laminate, the PTFE release liner is peeled away, leaving the patterned copper metasurface antenna adhered to the laminate surface. A nearly identical method is used to produce a conformal metasurface antenna. The major difference in the conformal case is that the copper foil and PTFE release liner are applied to a machined aluminum tool which acted as the inverse geometry to the final desired laminate (Figure 1.9). The prepreg laminate and inverse tool were cured in an autoclave as before. In both cases, the metasurface antennas possess nearly identical measured performance at 10GHz when compared to the simulated performance [8], [43]. In this process, three metasurface antennas are successfully integrated with a structural composite laminate through the use of transfer printing. The functional surface is adhered to the composite surface during laminate cure, and therefore does not embed a defect or delamination point within the composite laminate. Additionally, the use of annealed copper foil and traditional composite tooling materials means that this process requires minimal changes to existing composite processing methods. The use of a subtractive “printing” process (laser-profiling) can be wasteful and time consuming depending on the design and application of the conductive surface. It is proposed by Gupta et al. that this same integration process be repeated using a 6-axis robotic arm hybrid additive manufacturing technique to print the functional device. This work is ongoing, however, and results have not yet been presented [43].

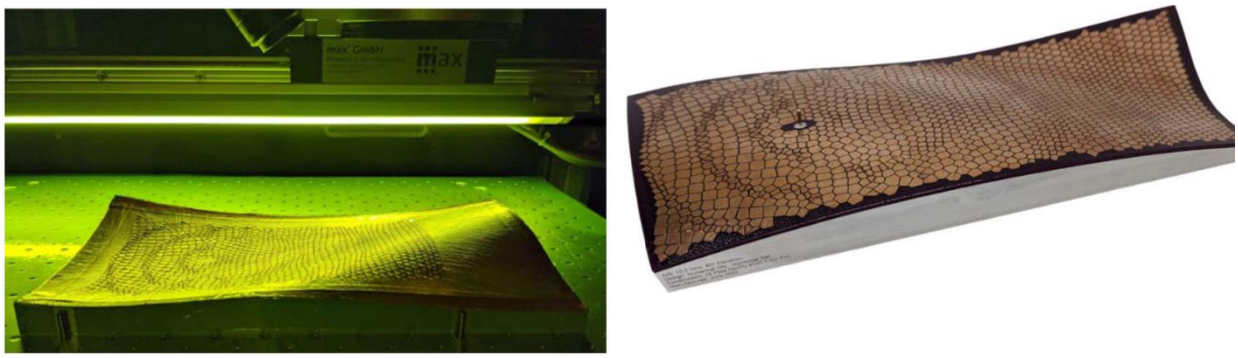

a. b.

1.9 Conformal metasurface antenna fabricated via laser-profiling (a) and after integration with a conformal composite laminate surface (b).

1.3.1 Capabilities gap and limitations of current multifunctional composite methods

Current approaches to multifunctional composite fabrication through the integration of printed electronics is still largely unexplored. At present, embedding of functional devices within a structural FRP laminate has been shown in nearly all cases to negatively affect mechanical performance [3]. Printing onto reinforcement fabric is also shown to cause spreading of the ink as it is wicked along the reinforcing fibers, resulting in final part infidelity.

Patterning of conductive inks onto the surface of cured FRP laminates inherently limits the viable sintering approaches in order to achieve the desired conductivity of the device [6]. Additionally, conformal DIW deposition is limited by the cured laminate geometry due to the potential for toolhead collisions.

Transfer printing techniques impose mechanical stresses onto the electronic device, and as sintered inks possess very brittle behavior, little if any work has been done to demonstrate transfer printing of printed electronics [43].

1.4 TEST Process: Transfer deposition onto composite surface

This work proposes a method that combines the ability of transfer processes to pattern onto conformal surfaces with the speed and resolution of conductive DIW. This novel process enables the fabrication of conformal, multifunctional composites without negatively affecting mechanical performance to achieve electromagnetic functionality. Furthermore, protection of the functional elements from the environment and secure integration of said functional elements is shown.

1.4.1 Process objectives

In order to achieve this objective, a novel transfer process is outlined in this work whereby additively manufactured sacrificial composite tooling is used as a transfer substrate for printed conductive devices to be transferred onto a structural FRP laminate. Additively manufactured sacrificial composite tooling is selected for its significant time and cost savings over traditional sacrificial composite tooling methods. The goal of this process is to enable the integration of electronic devices onto the interior surface of complex highly curved composite structures, where it would otherwise be inaccessible. The intent is to combine the environmental protection of embedded functionality with the performance of printed electronics without being limited by part geometry or sacrificing composite mechanical performance.

1.4.2 TEST Process Overview

The four primary steps in the TEST process (Figure 2.1) are:

1. printing a sacrificial tool in the desired shape of the composite structure via an additive manufacturing process (e.g., fused filament fabrication, binder jetting),
2. selectively patterning (e.g., via direct ink write) and sintering a conductive ink onto the surface of the printed sacrificial tool,
3. laying up and curing a composite prepreg onto the surface of the printed sacrificial composite tool (covering the deposited conductive trace),
4. and washing away the printed sacrificial composite tool via a solvent.

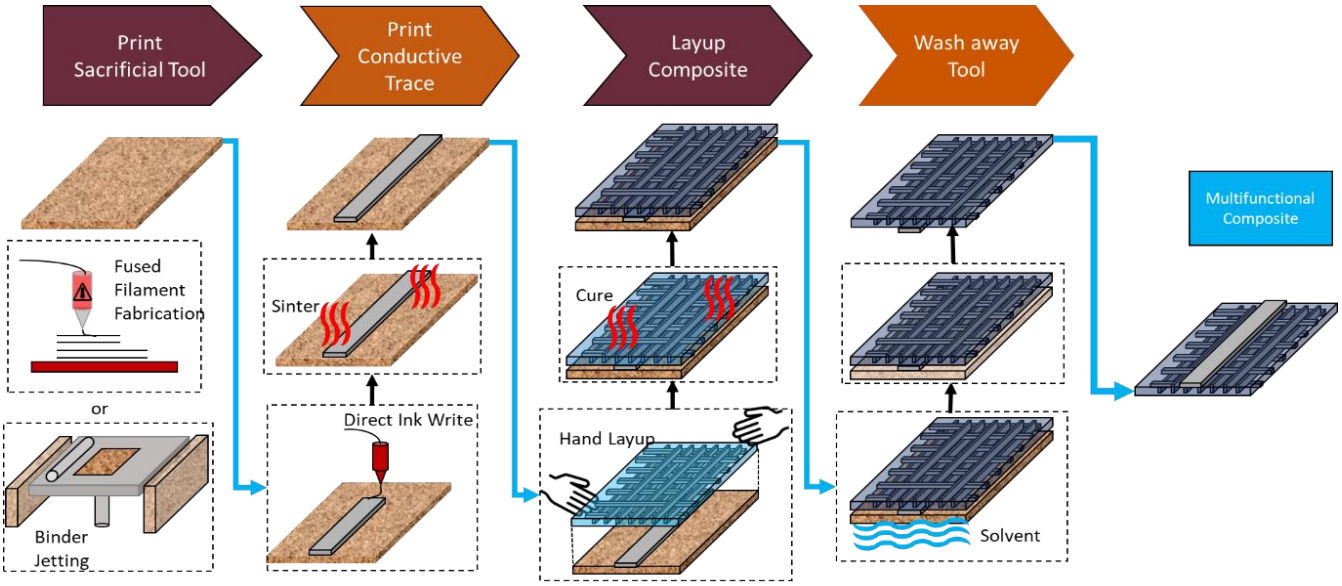

Figure 1.10 Graphical representation of the TEST process.

1.4.3 Anticipated Process Advantages

The advantages of such a process are in the tooling complexity enabled via additive manufacturing. Taking the ability to form complex, conformal composites with high temperature (>120C) FRP composite materials further expands the material limitations imposed on current multifunctional composite fabrication methods. without the need to manually remove the tooling through physical or mechanical means. By using chemical means for the removal of the composite tooling, there is no mechanical force applied to the printed electronics, which is known to be present in other transfer methods and can damage the conductive traces [25]. This process could enable the patterning of electromagnetic structures and sensing devices on the interior surfaces of conformal, complex aerospace composite structures. Such a capability presents a significant step forward for the integration of discreet electronics with composite structures.

1.4.4 Significant Contributions

This work demonstrates the following:

- The first instance of soluble composite tooling produced via FFF to form complex, high temperature curing composite structures using aerospace grade thermosetting composites.
- The first instance of multifunctional composite fabrication through the transfer of electrically conductive ink from a soluble composite tool surface to a FRP composite surface.

- The catalog of materials suitable for FFF of soluble composite tooling has been expanded to accommodate high temperature (>180°C) curing composites.

1.4.5 Research Questions

Identifying what factors are relevant to successfully transfer printed electronic devices from a composite tool to the surface of a FRP composite surface is critical to understanding whether this process is viable to fabricate multifunctional composite structures. In order to understand the viability of the TEST process to form multifunctional composite structures, the following research questions are addressed in this work:

RQ1: What materials are compatible with this process?

RQ2: How does solvent selection affect multifunctional composite mechanical performance using the TEST process?

RQ3: How does the TEST process affect printed trace resistance?

RQ4: How does the TEST process affect dimensions of transferred electronics?

RQ5: What is the quality of ink adhesion to the composite surface after TEST process?

Chapter 2: TEST Process for Multifunctional Composite Fabrication

2.1 Introduction

As shown in Chapter 1, multifunctional composite fabrication techniques have seen significant progress in recent years through the integration of printed electronics with aerospace grade FRP composites. However, embedding of printed electronics within composite laminates has been shown to negatively affect composite mechanical strength (Section 1.3). The most promising methods to date utilize a transfer printing method to pattern functional devices onto the surface of composite laminates. These methods are limited to traditional composite tooling geometries however, which require that the composite is able to be physically removed from the tool surface. Additively manufactured sacrificial composite tooling enables the formation of topographically complex composite structures by dissolving away the composite tool after part curing. In this chapter, multifunctional composite fabrication is demonstrated through the transfer of electronics via sacrificial tooling (TEST). At the time of writing this work, integration of printed electronics with structural FRP composites has not been demonstrated by transfer printing from additively manufactured sacrificial tooling due to a lack of suitable materials for such a process.

2.2 RQ1: What materials are compatible with this process?

The first step in bounding the TEST process is to identify what materials are compatible for each stage in this process and to gain understanding of the process interactions that could constrain material selection for this process. Generally, there are four classes of materials used in the TEST process that must be compatible:

- FRP composite
- additively manufactured sacrificial tooling
- conductive ink
- solvent

2.2.1 Fiber reinforced polymer matrix composite

The composite material selection for this project has been focused on high temperature curing thermosetting matrix composites to simulate the intended application space for this study due to their prevalence in aerospace applications. In theory, the TEST process is compatible with composite materials possessing lower cure temperatures. Additionally, the TEST process could be generally applied to thermoplastic composites and alternative composite layup techniques such as resin transfer molding (RTM). In practice, the specific fiber reinforcement and matrix material will be selected based on application requirements such as structural or electromagnetic properties.

2.2.2 FFF Soluble Tooling

The ability to leverage AM to produce soluble tools for forming high temperature, aerospace multifunctional composites is currently limited by the fact that solubility and thermal stability are generally considered opposing material properties. This process will thus require an exploration into high temperature, soluble materials that can be processed via AM. Current FFF soluble composite tooling is compatible with composites that have a maximum cure temperature equal to or less than 120°C [44]. Insoluble, or “breakout,” printed composite tooling can be used to form composites that have a maximum cure temperature up to 200°C [45]. Using these high temperature printable composite tooling materials as a starting point, it is necessary to identify solvents that can dissolve these materials without negatively

affecting the structure of the composite in order to make these high temperature printable composite tooling materials compatible with the TEST process.

In order to validate the feasibility of the TEST process to fabricate multifunctional composites, selected materials that are thermally compatible with each of the process constraints imposed in the four major steps shown above. The constraints imposed on the sacrificial tool are such that the material used for in the tool production

- must be printable through an AM process,
- must remain dimensionally stable during ink sintering (Sacrificial Tool Tg > Ink sinter temperature),
- must remain dimensionally accurate during the composite cure cycle (Sacrificial Tool Tg > Composite cure temperature), and
- must be soluble, preferably in a solvent that is used in industrial applications and readily available.

Current soluble tooling materials available for additive manufacturing are limited to low melt temperature polyvinyl alcohols and acrylic copolymers [46] and little work has been done investigating the use of solvent to remove high-temperature FFF materials [47].

2.2.3 Solvent Selection

The solvent selected must be able to fully dissolve the printed FFF tooling without affecting the mechanical performance of the composite structure. Because there are often several solvents that can successfully dissolve the printed tooling, the solvent's effect on the composite mechanical properties is often the driving factor in the decision.

Because it is infeasible to determine the effect of every solvent on every matrix material, it is suggested that as part of the TEST process, the solvent's effect on the composite's structure should be determined for each application of the TEST process. In this work we evaluate dichloromethane (DCM), dimethylformamide (DMF), and dimethyl sulfoxide (DMSO) to dissolve PSU, ULTEM 9085, and polyethersulfone tooling. Mechanical effects on the composite flexural strength are studied in our experimental analysis of this process (RQ2; Section 2.4).

2.2.4 Conductive Ink

The TEST process is generally compatible with. Instead, the selection for ink/deposition method should be made based on the specific application. As stated in Chapter 1, conductive inks are composed of metal particles, typically silver, copper, or gold, loaded in a polymer binder that acts to keep the metal particles in suspension until the ink undergoes a sintering process. This sinter stage is required for virtually all electrically conductive inks so that the polymer binder can be pyrolyzed and the metal particles can coalesce to form continuous, conductive traces [25].

Sintering of conductive inks is most often performed using a thermal, convection-based approach in which the deposited traces are heated until the metallic particles fuse together and coalesce to reduce the free surface area and mean free path of the conductive trace [48], [49]. The thermal approach to sintering conductive inks often begins at or above 150°C, which, due to their relatively low heat deflection temperatures, can make this process incompatible with many polymer sacrificial tooling material options.

In recent years, new approaches to sintering conductive inks at lower temperatures and reducing overall resistivity of printed inks have been explored, including the use of reactive inks, photonic sintering, microwave sintering, and electroless plating at or near room temperature [25], [48], [50]. These sintering techniques could enable the TEST process to work with low temperature (<120°C) additively manufactured sacrificial tooling by removing the high-temperature (>180°) thermal stability requirement necessary for thermal sintering of conductive inks.

2.2.5 Analysis of material compatibility with TEST process

In this section, the thermal and chemical properties of the materials listed in the previous sections are presented to illustrate the potential material combinations that would be plausibly compatible with the TEST process. In Table 2.1, commercially available FFF-printable sacrificial tooling materials are listed with their glass transition temperatures. The maximum tooling temperature in Table 2.1 is based on the previous studies which use the preliminary maximum processing temperature is set at or below the glass transition temperature (Tg) for each material [51]. The actual processing temperature at which each of the listed materials can survive will be dependent on many more factors than the Tg.

As previously stated, nearly all conductive ink deposition takes place at room temperature and therefore the deposition method is not relevant to the TEST process. Nearly all conductive inks do require sintering. The sintering methods compatible with the maximum tooling temperatures are reflected in the third column of Table 2.1. For printed sacrificial tooling materials with glass transition temperatures less than 150°C, it is recommended to print a reactive ink or to use an alternative method of increasing the conductivity of the printed traces. Alternatively, the patterned conductive ink can act as a seed layer, which can be electroplated to increase the conductivity to acceptable levels [33]. If a composite with a maximum cure temperature >177°C and a conductive ink with a sinter temperature >150°C are selected, the printed sacrificial tooling must be selected from those with a Tg >180°C to remain stable during both the thermal sintering of the conductive ink and the curing of the composite laminate. Such materials can be found in the bottom three rows of Table 2.1.

For the final column, the solvents listed are taken from literature as being able to fully dissolve the sacrificial tooling material listed in the first column. For the bottom three rows, the listed entries are not comprehensive, but rather, these solvents were those used in this work specifically. It has been reported in literature that polysulfones (PSU and PES) are not resistant to chlorinated organic solvents and ketones. Therefore, it could be proposed that methyl ethyl ketone (MEK) might also be considered a suitable solvent for these sacrificial tooling materials. [52] It should be noted that the entries listed are not comprehensive of all potential solvents, furthermore, the effect of the selected solvent on the desired composite prepreg must be understood before true compatibility of materials can be established.

In summary, Table 2.1 shows the temperature compatibility of available printable sacrificial tooling materials with a variety of conductive ink sintering techniques and composite prepreg cure temperatures.

Table 2.1 Material compatibility matrix for the TEST process.

Sacrificial Tooling material	Max tool temperature (°C)	Conductive ink compatibility	Composite maximum cure temperature (°C)					Washout solvents
			Ambient	50	120	180	200	
Stratasys ABS-M30/ASA	82	Reactive, plating, photonic	X					Acetone, MEK
Stratasys SR-30	91	Reactive, plating, photonic	X	X				Aqueous (NaOH)
Stratasys SR-100	98	Reactive, plating, photonic	X	X				Aqueous (NaOH)
Stratasys ST-130	120	Reactive, plating, photonic	X	X	X			Aqueous (NaOH)
Polycarbonate (PC)	132	Reactive, plating, photonic	X	X	X			DCM, MEK
Ultem 9085	180	Reactive, plating, photonic, thermal	X	X	X	X		DCM, DMF, DMSO
Polysulfone (PSU)	180	Reactive, plating, photonic, thermal	X	X	X	X		DCM, DMF, DMSO
Polyethersulfone (PES)	225	Reactive, plating, photonic, thermal	X	X	X	X	X	DCM, DMF, DMSO

2.3 Empirical demonstration of TEST process

Having determined those materials that satisfy the necessary conditions of the TEST process, the next step was to validate that TEST could be used to transfer electronically conductive traces onto aerospace, structural composites. This test was performed empirically as a first pass attempt to prove the conceptual validity of the TEST process. Two test geometries were used in this first attempt of the TEST process. The first was a simple 76.2mm X 76.2mm X 12.7mm block and the second was a representative airfoil geometry with a build volume of approximately 65mm X 65mm X 12.7mm, seen in Figure 2.1 and 2.2 respectively. These test geometries, hereafter referred to as “block” and “airfoil” respectively, were selected to validate the TEST process in both planar and complex geometries, particularly by utilizing AM processes to print a nonplanar sacrificial tool and conformally deposit conductive traces onto its surface.

Both tools were printed using an FDM Stratasys Fortus 400mc loaded with Ultem 9085 and Ultem 9085 Support filaments. When generating the toolpaths for these geometries, the part and support materials were inverted such that the final parts were printed using the Ultem 9085 Support material, which is polysulfone (PSU). The block was printed in XY orientation, and the airfoil was printed in the ZX. Once the sacrificial tooling had been printed, the area where conductive ink deposition was to be patterned was sanded using abrasive pads to produce a smooth surface. Surface abrasion was deemed necessary after it was observed that the as-printed surface exceeded the necessary surface roughness for the DIW process that was selected to pattern the conductive ink.

Figure 2.1 Polysulfone sacrificial tool, block

Figure 2.2 Polysulfone sacrificial tool, airfoil

For the block, Dupont CB-028 silver ink was patterned via pneumatically controlled extrusion with a custom 3-axis DIW machine. Due to its complex surface curvature, Dupont CB-028 silver ink was patterned conformally onto the sacrificial airfoil tool via pneumatically controlled extrusion with a 6-axis ABB robotic arm (Figure 2.3).

For the purposes of demonstration, the geometries of the conductive regions were kept relatively simple. Three 50mm long 4-point probe resistance measurement lines were patterned onto the sanded surface of the block sacrificial tool geometry. For the airfoil tool geometry, a small, simulated patch antenna geometry was selected as the conductive pattern to showcase a potential application of the TEST process.

For the block sacrificial tool, a 10cc syringe containing CB-028 was pressurized to 70psi to extrude the ink through a 0.15mm ID nozzle positioned 0.1mm away from the substrate's surface. A similar process was used for the airfoil sacrificial tool geometry, with the exception that the 10cc syringe barrel was pressurized to 15psi extruding ink through a 0.25mm ID nozzle that was positioned approximately 0.3mm away from the surface of the substrate. A larger print nozzle was selected for the airfoil sacrificial tool in order to make allow for greater ease in registering the 6-axis robotic arm with the tool surface.

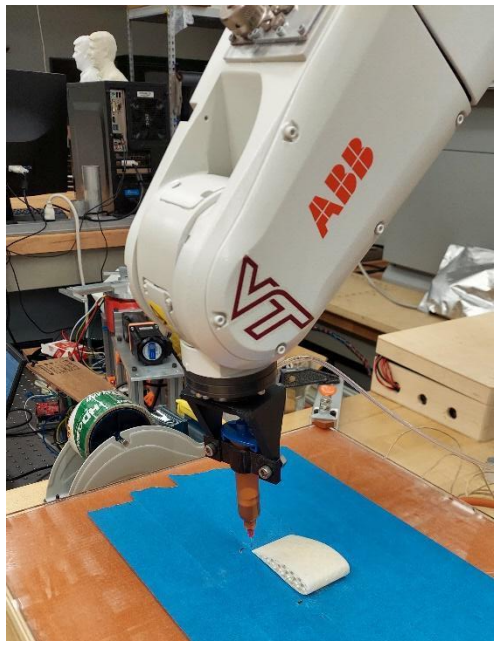

Figure 2.3 Conformal DIW of Dupont CB-028 onto airfoil tool via 6-axis robotic arm.

The printed conductive patterns were then thermally sintered on the printed sacrificial tools in air with a convection oven set to 180°C for 1hr per manufacturer recommendations. After the sintering was complete, the samples were removed from the oven, allowed to cool to room temperature, and then taken to be laid up in composite prepreg. Figures 2.4 show the sintered traces on the tools' surface.

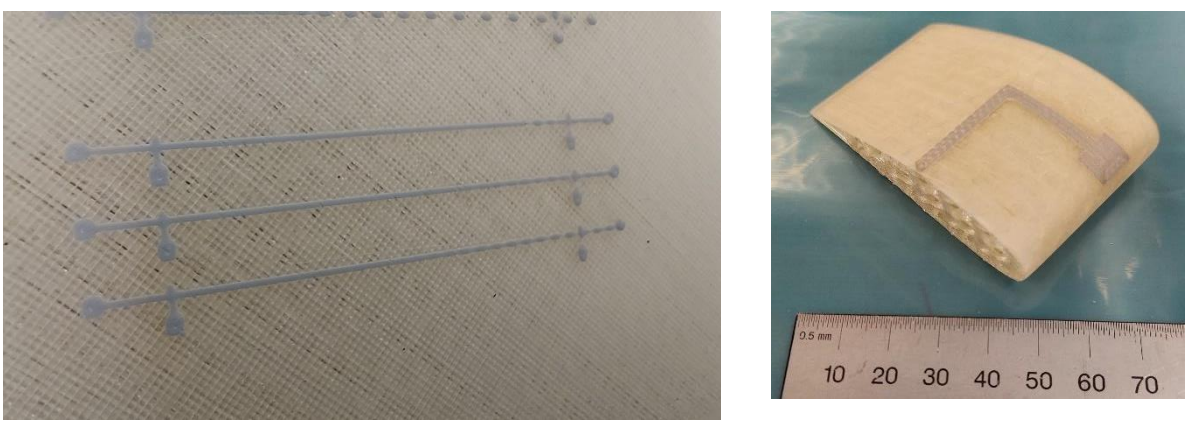

a. b.

Figure 2.4 Sintered CB-028 50mm 4-point probe lines on block PSU sacrificial tooling (a.) and conformal patch antenna geometry on airfoil PSU sacrificial tooling (b).

Hexcel HexPly S2GL/8552 unidirectional S-glass reinforced epoxy matrix composite prepreg was used in the hand layup for both sacrificial tooling geometries. An 8-layer, quasi-isotropic $[0,90]_{2S}$ stacking sequence was selected to simulate a representative structural composite. Prepreg was cut to the dimensions of each tool and laid up directly onto the sacrificial tools and conductive traces by hand. Vacuum was pulled after each layer of prepreg was applied to the tool to remove air pockets in the laminate and to apply even pressure from the prepreg onto the tool. The entire surface of the block tool

geometry was wrapped in prepreg, and a small cross-shaped hole was cut into the uncured laminate to provide a point for the solvent to access the tooling surface in the subsequent solvent removal of the sacrificial tooling (Figure 2.5a-c). The uncured laminate and tool were then vacuum bagged and cured in a Wabash Genesis series heated press. For both items in this study the cure parameters of the composite prepreg were kept identical. The laminate was placed under vacuum and 15 psig pressure, heated up to 107°C with a controlled rate of 2°C per minute, held at 107°C for 60 minutes, then held at 177°C for 120 minutes. The cure temperature and pressure (177°C@15psig) are lower than the heat deflection temperature of PSU (185°C@66psig) [44]

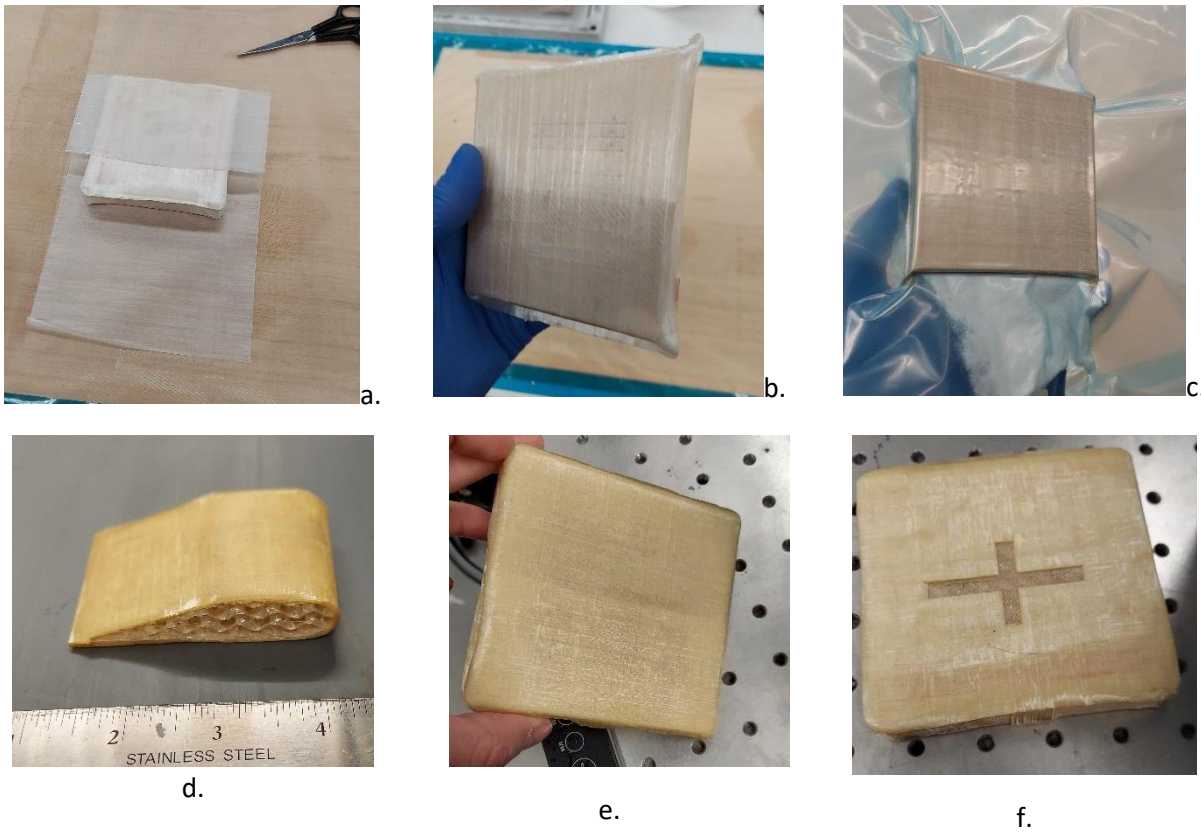

Figure 2.5 Composite layup process onto block polysulfone sacrificial tool during layup (a), after layup (b), and after vacuum bagging (c) before curing. Composite laminate cured onto airfoil (d) and block polysulfone sacrificial tooling (e) with a cross-shaped access hole (f) after curing.

The cured composite and sacrificial tool survived the composite cure schedule with no visible changes to the overall shape or dimensions (Figure 2.6d-f). The final stage of the TEST process was to washout the printed polysulfone sacrificial tooling through the use of a solvent. Without knowing the dissolution compatibility of the available solvents with the composite, two different solvents were selected for the washout process in this experiment. The block tool and composite were placed into a bath of methylene chloride (DCM) and left to sit at room temperature. The airfoil tool and composite were placed into a bath of dimethyl sulfoxide (DMSO) and sat at room temperature. After approximately 4 hours, both tools appeared to have fully dissolved and the composite structures appeared to remain intact. The composite shells were then removed from the solvent bath and let dry at room temperature for an additional hour.

The specimens were then visually inspected to determine if a successful transfer of the conductive traces from the sacrificial tool surface to the composite surface had occurred. Figure 2.6 shows that the printed conductive traces did transfer onto the composite surface, for both the planar and the conformal sacrificial tooling geometries. The composite box was cut open and multimeter probes were applied to the transferred conductive traces to verify continuity. These images can be taken as initial validation of the TEST process as a method for the integration of printed conductive traces within aerospace grade composite structures.

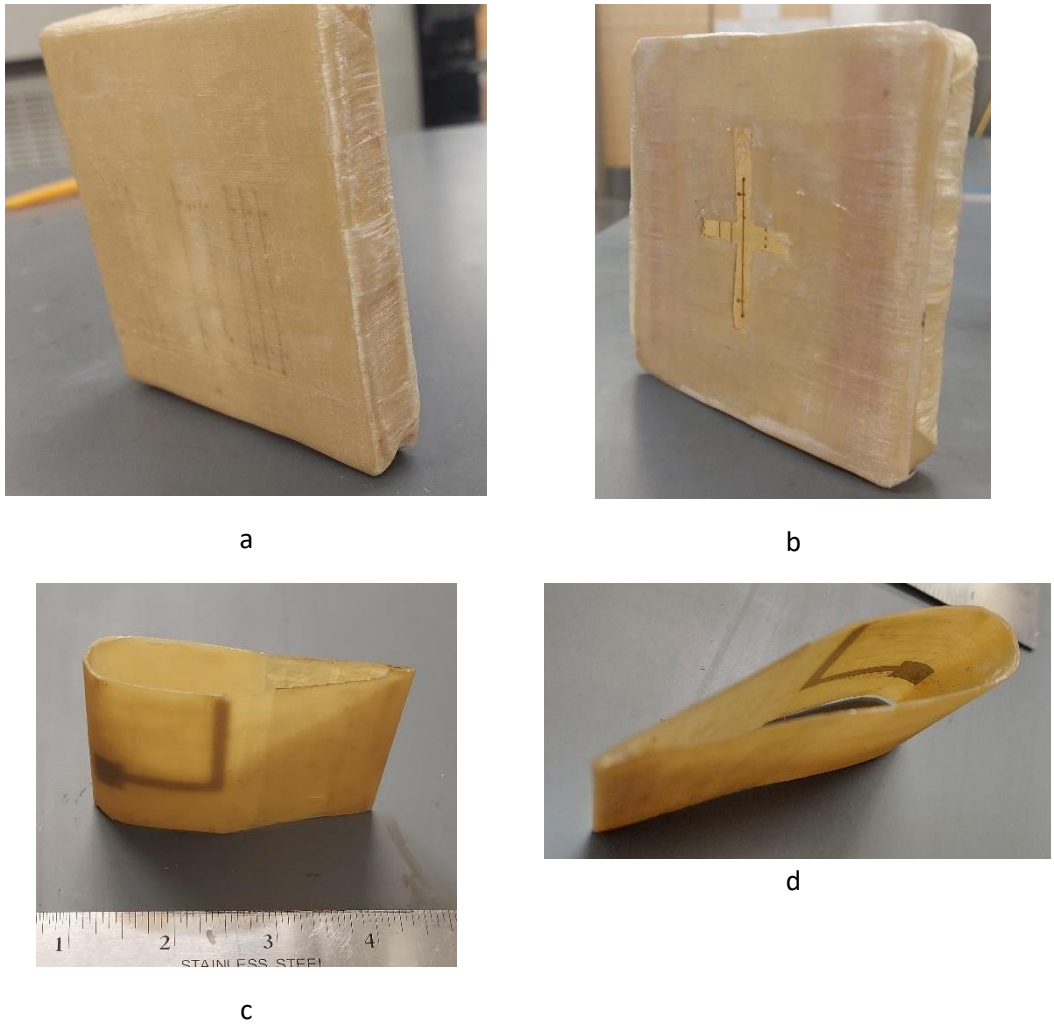

Figure 2.6 Cured composite laminate structure after sacrificial tooling washout. Block tooling geometry (a), washed out with DCM, successfully transferred conductive traces onto the interior surface of the composite shell (b). Airfoil tooling geometry (c), washed out with DMSO, also successfully transferred the simulated patch antenna onto the interior surface of the composite skin (d).

.

2.4 RQ2: How does solvent selection affect multifunctional composite mechanical performance using the TEST process?

2.4.1 Introduction

The purpose of this experiment is to explore if the solvent selection for the soluble tooling affects the mechanical strength of the composite structure during the washout step of the TEST process. This selection can have potentially significant impacts on the final composite and thus, this experiment should be performed for every solvent and composite material combination for this process. If the solvent selected is to affect the composite, it is assumed that it will be observed in the matrix material and not the fiber reinforcement. Based on this assumption, a test method is selected in that will measure a change in the matrix properties. In general, test methods for composites have the fiber direction primarily aligned with the direction that an applied stress is expected, since the reinforcement fiber strength dominates the composite material strength. From this, a three-point bend test to measure the flexural strength of our composite with and without exposure to solvents based on ASTM C581 and ASTM D790 standards [39], [40].

2.4.2 Sample preparation and experimental setup

Fibreglast E-glass 7781 epoxy prepreg was used as the composite material for this study as a representative aerospace composite suitable for use with the TEST process. In accordance with ASTM C581, 14 plies of the 8HS weave prepreg were laid up to form a 101.6mm x 127mm x 3.43mm planar laminate specimen. The specimen was vacuum bagged to remove air pockets between the layers. The prepreg laminate was cured in a Wabash Genesis series heated press. The specimen was heated from room temperature to 154°C at a ramp rate of 1°C/min and held for 1hr then cooled to 143°C at a ramp rate of 1°C and held for 2hr then cooled to 132°C at a ramp rate of 1°C/min and held for 4hr before being brought to room temperature and removed from the heated press. This process was identically repeated to form three cured laminates. Each cured laminate was then cut into four 3-point bend coupons measuring 76.2mm x 25.4mm x 3.43mm for a total of 12 coupons shown in Figure 2.7.

a. b.

Figure 2.7 Fibreglast E-glass/epoxy prepreg laminate layup (a). Laminate cured and cut into 3-point bend test coupons (b).

Four coupons were not to be exposed to any solvent and set aside as control specimens. For this study, dimethyl sulfoxide (DMSO) and dimethyl formamide (DMF) were selected as the solvents. Both DMSO and DMF are capable of fully dissolving the high temperature printed sacrificial tooling used in this work (Table 2.1) to demonstrate the TEST process.

Four 3-point bend coupons were placed in a bath of DMSO, and the remaining four coupons were placed in a bath of DMF. Both sets of coupons remained in their solvent baths for 27 hours, which is much

longer than a typical sacrificial tooling washout should take. Coupons were afterwards removed and blotted dry with a Kimwipe. Both sets of coupons were then dried in a convection oven set to 50°C for 30min to simulate a “worst-case” scenario and to maximize any observed changes to the flexural strength of the coupons. Comparison of test coupons after solvent exposure and drying can be seen in Figure 2.8.

The three sets of 3-point bend coupons were measured and marked for consistent placement in the Instron test apparatus. Flexural strain and modulus were measured in an Instron universal test system. Individual coupon dimensions were measured and recorded to calculate the flexural stress after testing. Coupons were strained at 1mm/min in accordance with the test procedure outlined in ASTM D790 and the recorded data was compiled and is presented in Figure 2.10. The statistical significance of the changes in flexural stress and modulus was determined using the F-test method.

a. b.

Figure 2.8 Visual comparison of 3-point bend test coupons after exposure to DMF (a-left) and DMSO (a-right) and during 3-point bend testing (b).

2.4.3 Results

No changes in the color of the solvent baths were observed after removing the coupons. After drying, the coupons exposed to DMF possessed visible changes in the color of the matrix material, possibly due to be the formation of micro-cracks. Test coupons subjected to DMSO did not show any visible differences after exposure.

From the p-values in Table 2.2, it can be seen that, at the 95% confidence interval, there is not a statistically significant decrease in flexural strength for composite specimens exposed to DMSO when compared to the coupons with no solvent exposure. There is, however, a statistically significant decrease in the flexural strength of composite coupons that were exposed to DMF when compared to both sets of coupons that had no solvent exposure and those which were exposed to DMSO (Figure 2.9). The negative effect due to solvent exposure could potentially be reduced by a longer, more thorough, drying process; however, solvent selection clearly plays an important role on the final composite properties.

Table 2.2 P-values for F-test analysis between data sets

Comparison	Stress P-value	Modulus P-value
Control vs DMSO	0.06819	0.06985
Control vs DMF	0.00067	0.00442
DMSO vs DMF	0.02657	0.00108

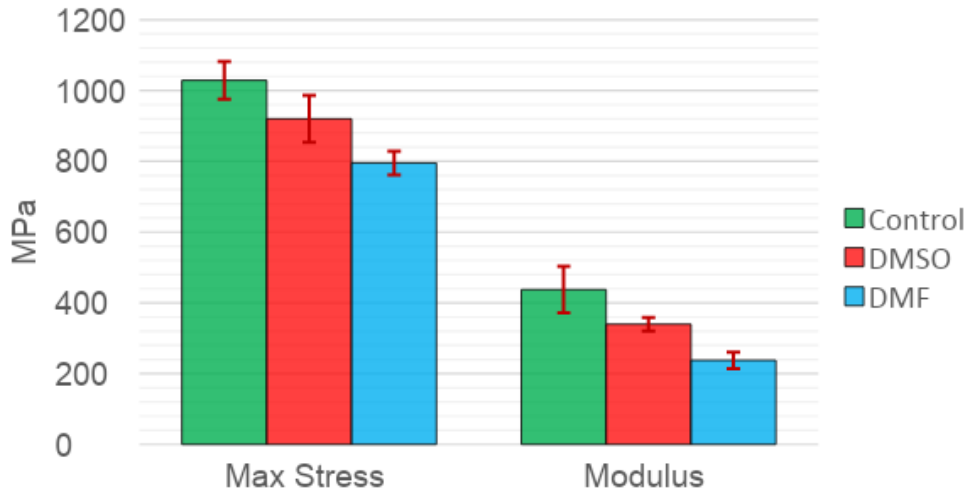

Figure 2.9 Flexural response of composite coupons exposed to solvent for 27 hours.

2.4.4 Conclusion

In this study, the effect of sacrificial tooling solvent selection on the flexural strength of cured composite is measured. The importance of solvent selection is highlighted by demonstrating the potential reduction in flexural strength of the composite matrix material. This study is necessary for the TEST process for every solvent-composite combination, especially when multiple solvents are capable of dissolving the selected sacrificial tooling material. In this study, DMF and DMSO were selected as the potential solvents because both are capable of dissolving PES, Ultem, and PSU which are high temperature sacrificial tooling materials used in this work. For the selected E-glass/epoxy composite material, DMSO was shown not to have a significant effect on the flexural strength, whereas DMF was shown to significantly decrease the flexural strength. From this experiment, it is determined that for this E-glass/epoxy composite, DMSO is the preferred solvent for the TEST process.

2.5 RQ3: How does the TEST process affect printed trace resistance?

It is important that methods of multifunctional composite fabrication do not significantly alter the performance of the device to be integrated. To that end, the TEST process is used to integrate conductive traces on a structural composite laminate. It is hypothesized that the electrical resistance of the sintered conductive traces remains unchanged after the transfer to the composite surface. To examine this, the resistance of the printed traces must be measured at after sintering onto the printed sacrificial tool and then compared to the measured resistance after the conductive elements are transferred onto the composite surface.

In order to determine the effect of the TEST process on the resistance of transferred elements, the TEST process was conducted, as in the initial process demonstration (Section 2.3), using PES as the sacrificial tooling material, Dupont CB-028 as the conductive ink, HexPly 8552 S-glass epoxy prepreg for the composite, and DMSO as the solvent.

2.5.1 Methods for fabricating TEST process specimen

- *Step 1: Sacrificial Tool Fabrication:* A 76.2mm x 50mm x 25.4mm rectangular prism was first modeled in Fusion 360. The resulting .stl was then processed using Stratasys Insight toolpath software and then printed out of PES on a Stratasys 400mc FFF system. The resultant PES tool was then abraded progressively down to 600grit to prepare the surface for DIW.
- *Step 2: Conductive DIW*: 4-probe resistance measurement samples were drawn in Fusion 360 with the dimensions listed in Figure 2.10. The CAD model was then exported as an .stl to Autodesk Netfabb in order to generate .gcode toolpaths. The resulting .gcode was manually edited to produce a single layer print file which would be the test sample once printed. Dupont CB-028 silver ink was printed onto the surface of the PES tool by extruding the silver ink through a 0.25mm nozzle at 15psi 0.2mm away from the tool surface. The 4-probe resistance geometry was patterned five times in total onto the surface of the PES tool to allow for several measurements to be taken in this study. The silver ink was then sintered onto the PES tool thermally, via a convection oven set to 180°C for 1hr (Figure 2.11a).

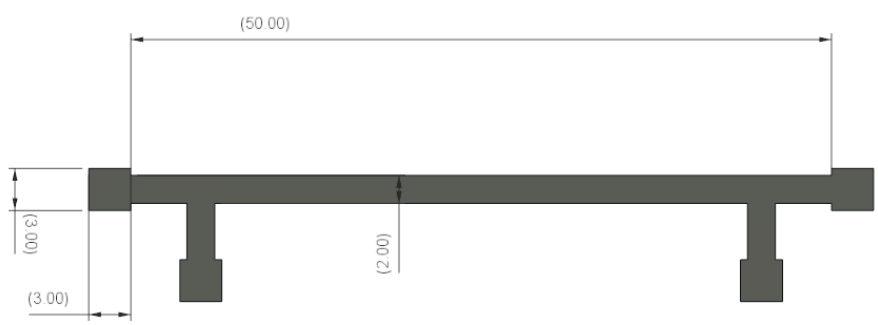

Figure 2.10 4-point probe resistance measurement CAD drawing with dimensions labelled in millimeters.

- *Step 3: Layup Composite:* After resistance values were recorded, HexPly 8552 S-glass epoxy prepreg was laid up in a $[0,90]_{2S}$ stacking sequence onto the surface of the PES sacrificial tooling with the sintered conductive traces. Layup was performed manually; only a planar laminate composite was necessary for this experiment (Figure 2.11b). The PES sacrificial tool specimen and prepreg laminate were then vacuum bagged and placed in a Wabash Genesis series heated press. The composite was then cured in the heated press pressurized under 15psig, while vacuum was pulled continuously. The laminate was taken from room temperature to 107°C at a ramp rate of 1°C/min, held for 45min, taken to 177°C at a ramp rate of 1°C/min, held for 120min, and finally allowed to cool to room temperature.
- *Step 4: Washout Tool:* The specimen was then placed in a bath of DMSO to dissolve away the PES sacrificial tool. A stir bar was placed in the bath and excess material was manually removed in order to expedite the tool removal process. The PES tooling was allowed to sit in the DMSO bath

for approximately 3hr until all PES had been visibly removed from the composite. All 5 printed traces were observed to have been transferred successfully onto the composite surface (Figure 2.11c).

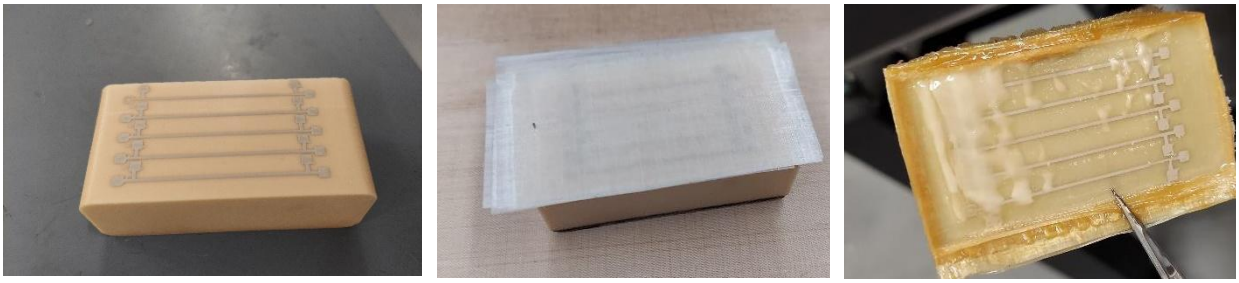

a. b. c.

Figure 2.11 Printed CB-028 resistance measurement samples sintered on (a) sacrificial PES composite tooling, (b) during composite prepreg layup, and (c) during tooling washout in DMSO bath.

2.5.2 Methods for determining TEST process effect on trace resistance

Resistance measurements were recorded at the conclusion of sintering with a Hewlett Packard 34401A Digital Multimeter for comparison at the end of the TEST process. Measurements were taken using two probes placed 50mm apart on the tabs of the print. Four measurements were taken per printed sample for 20 resistance measurements total. Measurements taken after between Steps 2 and 3 are labelled “before transfer,” while measurements taken after Step 4 are labelled “after transfer.”

2.5.3 Results

The measured resistance values across the 50mm lines before and after transferring to the composite surface are presented in Figure 2.12. The average resistance value after sintering the conductive ink onto the PES tooling was 0.364Ω +/- 0.004. After transferring the sintered conductive ink to the composite surface, the average resistance value recorded was 0.369Ω +/- 0.006. The average increase of 0.005Ω across a 50mm line was determined not to be statistically significant at the 95% confidence interval after conducting an F-test on both data sets. Thus, it is confirmed that the transfer process has no effect on the printed trace’s resistance.

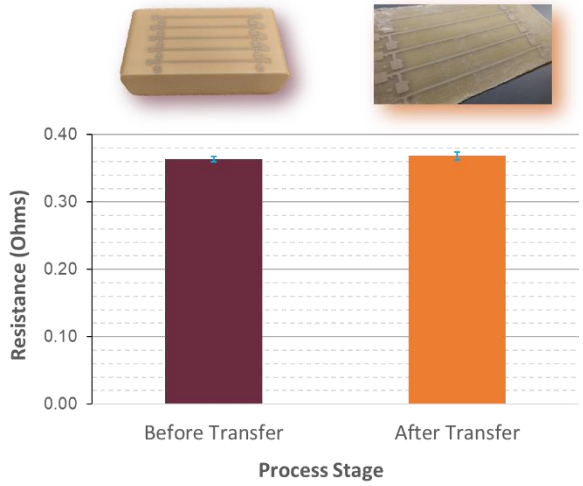

Figure 2.12 Resistance values for CB-028 silver ink sample 50mm lines after sintering onto printed PES sacrificial tooling (left) and after transferring samples to the surface of S-glass/epoxy composite surface using the TEST process (right)

2.6 RQ4: How does the TEST process affect dimensions of transferred electronics?

2.6.1 Introduction

Since the TEST process involves the transfer of the conductive trace from the tool surface to the surface of the composite, it is important to understand how the transferred trace cross section is affected. It is hypothesized that the surface features of the tooling will be imparted onto the surface of the conductive trace after it has been transferred. Since the conductive traces have been sintered before integration with the FRP composite, it is hypothesized that no change in trace cross section will occur. To understand this relationship, and to verify the above assumption, profilometry scans are taken after sintering on the printed sacrificial tool and again after transferring onto the composite surface.

2.6.2 Test setup and data collection

In order to measure what happens to the surface of the conductive trace as it transfers from the sacrificial tooling surface onto the composite surface, a Keyence Lj-v7000 laser profilometer was used to record the surface profile for the printed conductive traces after they had been sintered onto the sacrificial PES tooling and after the tooling had been dissolved at the conclusion of the TEST process. The test article in this study is the same article mentioned in Section 2.5.1 of this work. Profilometry scans were taken of the sample after Step 2 was complete and compared to scans taken after completing Step 4. The profilometer and test article are depicted in Figure 2.13. The laser profilometer traveled across the substrate surface at a velocity of 1mm/s, taking measurements at 10Hz. Approximately 600 data points were collected at 0.05mm between points along the raster width and 0.10mm along direction of travel for the profilometer.

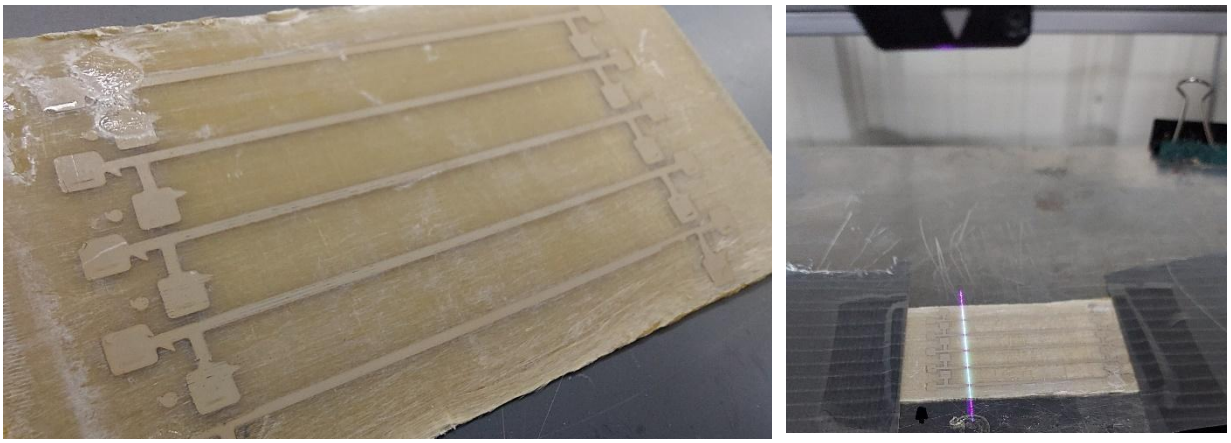

a. b.

Figure 2.13 Composite panel with printed resistance measurements embedded in the surface (a) being scanned via laser profilometer (b).

2.6.3 Results

Scans were compiled into surface plots of the printed conductive traces are seen in Figure 2.14. The scans were compiled into surface plots with individual scan widths presented to highlight the single cross-section for each substrate. The surface height values were not normalized to the composite substrate in the profilometry software, thus the numerical values on the vertical axes in the following plots are taken as relative values, not absolute.

a.

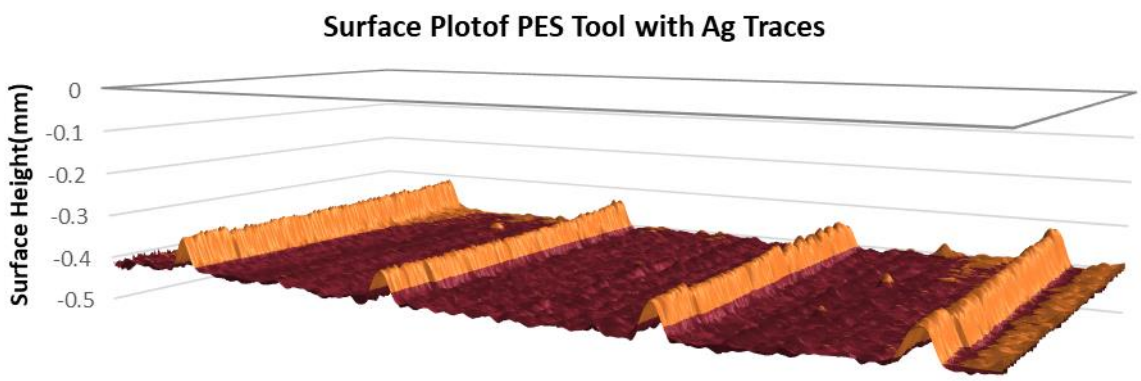

b.

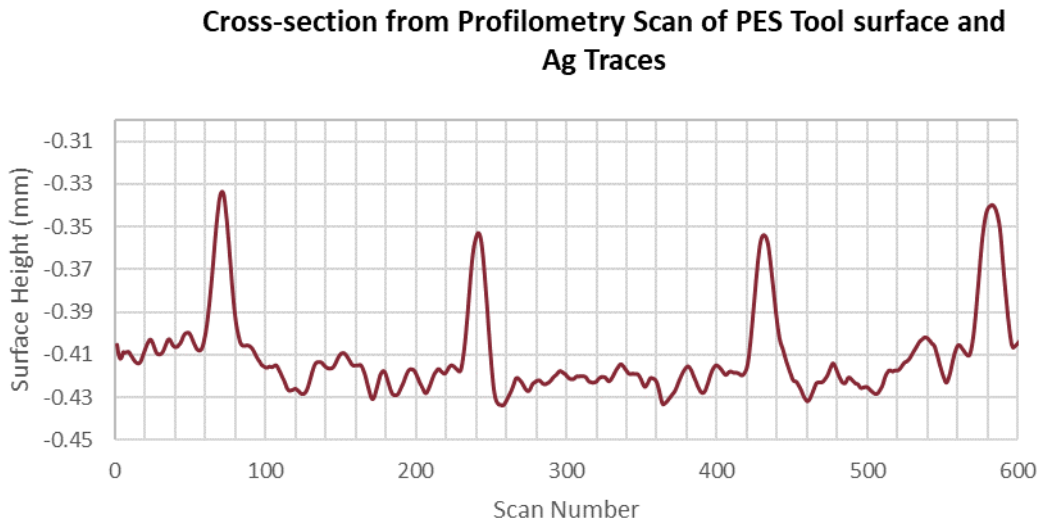

c.

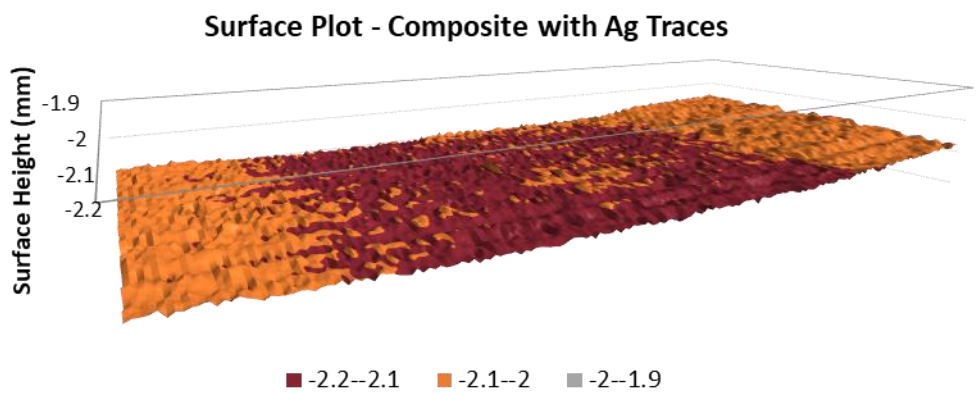

d.

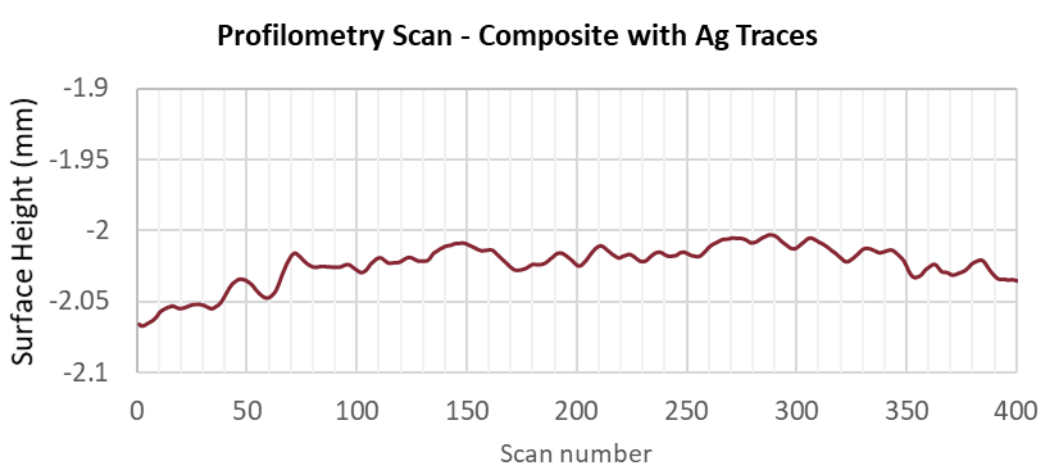

Figure 2.14 Profilometry scans compiled into surface plot for printed conductive traces on sacrificial PES tooling (a) and cross-section showing four distinct traces (b). Similarly, profilometry scans compiled into surface plot for composite specimen after

TEST process completion (c) and cross-section showing the four printed traces are no longer distinct from the surrounding surface (d).

In Figure 2.14b, the height of the printed traces can be calculated by comparing each trace peak with the point on plot where the trace begins. This shows that the average height of each trace on the sacrificial tool is 0.050mm +/-0.003. Similarly, the width of the printed traces on the sacrificial tool is determined by taking the number of scans across each trace and multiplying it by 0.05mm (distance between each scan). This shows that the average width of traces on the sacrificial tool was 0.962mm +/-0.055.

Qualitative comparison of the cross-section plots in Figure 2.14a-b with Figure 2.14c-d indicates that the printed traces are clearly visible and detectable on the surface of the PES sacrificial tooling, whereas once the trace transfer has been completed and the tooling removed via the TEST process, the traces are no longer detectable on the surface of the composite via laser profilometry. It was also observed that, during the handling of the composite test article, trace location could not be detected based on feel alone. Comparison between Figure 2.14b and Figure 2.14d suggest that the approximately 0.050mm tall conductive traces are pressed into the surface of the composite prepreg during the curing stage.

To validate these conclusions, the composite test article was first cut in order to expose the cross-section of the conductive trace. Optical microscopy and ImageJ analysis were then used to measure the cross-sectional area of the transferred conductive trace. The composite edge and cross-section trace are presented in Figure 2.15. In the picture, the trace can be seen on the underside of the composite, and measurements were taken in ImageJ to determine the transferred trace height and thickness for comparison to the trace measured by profilometry on the PES sacrificial tool. The ImageJ results measured the transferred average trace height across the four traces to be 0.055+/- 0.0062mm. The width of the cross section in Figure 2.15 is measured to be 0.945 +/-0.027. F-test analysis of this data indicates that, at the 95% confidence interval, no statistically significant change occurred in the cross-sectional area of the conductive traces before and after transfer.

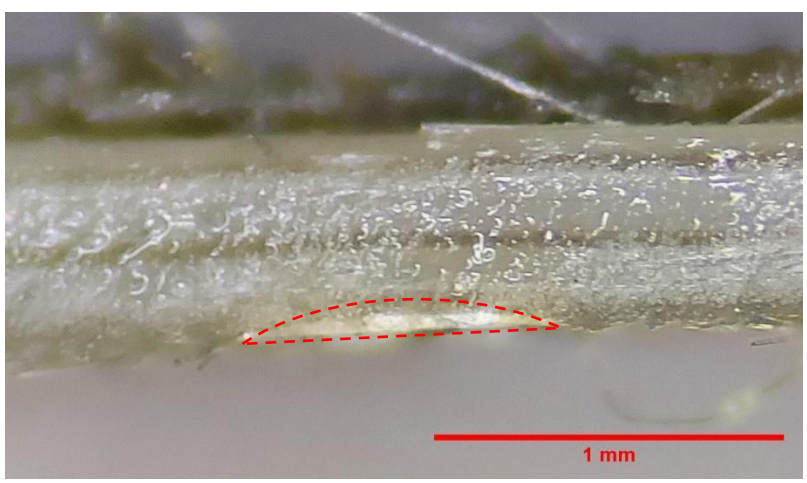

Figure 2.15 Cut edge of composite test article with transferred trace cross-section exposed and outlined in red.

2.6.4 Conclusion

In this experiment, observations regarding the printed conductive trace dimensions are made in order to determine the effect of the TEST process on trace embedding. The PES sacrificial tool and composite specimen with printed conductive traces from Section 2.5.1 served as the test articles for this study. Profilometry scans were taken of the surface of both substrates during their respective stages of the TEST process, and those scans were compiled into the surface plots in Figure 2.15. Individual scans were used to determine the cross-sectional dimensions on the sacrificial tool and on the composite specimen. Trace height and width on the tool measured approximately 0.050mm tall and 0.96mm wide from the individual scans. After completion of the TEST process, profilometry of the traces revealed that they were no longer detectable from the surrounding surface features. The composite specimen was cut to expose the transferred conductive trace on the specimen edge. Optical microscopy and ImageJ analysis revealed that the thickness and height of the transferred trace is unchanged, as the trace is pressed into the surface of the composite during the cure stage of the TEST process.

2.7 RQ5: What is the quality of ink adhesion to the composite surface after TEST process?

2.7.1 Introduction

One of the major concerns with the TEST process is the quality of adhesion between the printed conductive elements and the surface of a structural composite following the transfer. When using the TEST process to fabricate multifunctional composites, the printed device to be transferred is adhered to the composite surface by the composite matrix during the composite cure. These printed features need to be able to be handled during subsequent part installation and need to be able to deform as the structural composite is subjected to mechanical loads. If the printed traces are not sufficiently adhered to the composite surface, delamination, cracking, and discontinuities can form throughout the life of multifunctional composite, which could potentially lead to a loss of conductivity. Therefore, the purpose of this experiment is to qualitatively determine the adhesion between the printed conductive trace and the composite surface after the TEST process. In order to quantify the effect of straining the composite on transferred trace resistance, five sample holders were printed to flex the composite specimen at specific curvature values so that resistance measurements could be taken in a similar fashion to those taken in Section 2.5.1.

2.7.2 Methods

The 50mm 4-probe resistance lines from Section 2.5.1 served as the test specimen for this study. Two methods for determining adhesion were used: (1) ASTM D3359 for Scotch tape adhesion testing and (2) measuring sample resistance under strain. The Scotch tape method was used to qualitatively determine adhesion of the printed conductive traces on both the PES sacrificial tooling and the composite surface after tooling washout. Adhesive backed Scotch tape was applied over the printed conductive traces and peeled off at 180°.

Measuring resistance across the printed traces under increasing flexural strain on the composite is used to determine how well the traces are adhere to the composite surface. Sample holders were designed to have decreasing radius of curvatures (635mm, 317.5mm, 158.75mm, 80.65mm, and 69.85) starting with the unflexed composite sample acting as the control for this experiment. The sample holders were printed out of PLA on an FFF printer at the Virginia Tech University Library. Sample holders are shown in Figure 2.16. The composite specimen was placed in the printed holder, resistance

measurements were taken and recorded, and the process was repeated for the next holder. The radius of curvature becomes sharper as the radius of curvature decreases, and an increase in trace resistance is expected. If a gradual increase in resistance is measured, it is attributed to an elongation of the conductive trace; whereas, if a sharp increase in resistance is observed, it is indicative of cracking or discontinuities forming in the printed trace [45].

Figure 2.16 Composite sample holders with decreasing radius of curvatures, measuring from bottom to top: 635mm, 317.5mm, 158.75mm, 80.65mm, and 69.85mm.

2.7.3 Results

For the Scotch tape adhesion test, results proved that in both cases the printed conductive traces were not removed by the adhesive tape at all. No evidence of the printed conductive traces was visible on the tape after peeling. This qualitatively demonstrated satisfactory adhesion between the printed conductive traces and the composite surface.

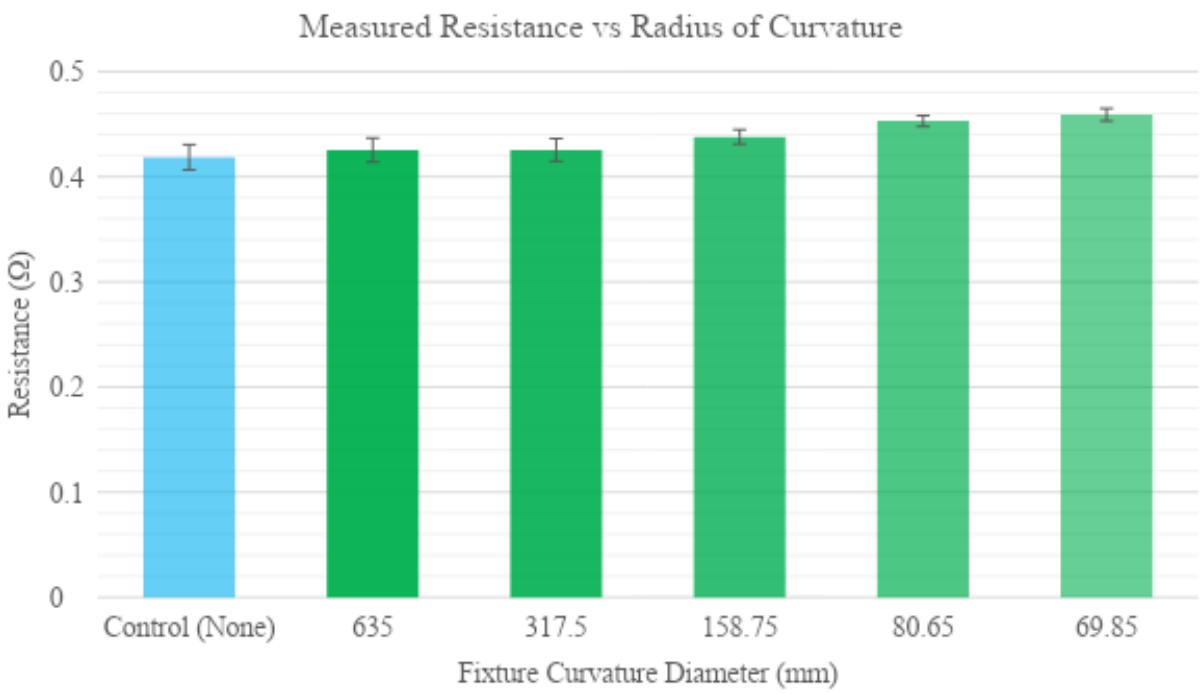

Figure 2.17 Resistance measurements for the unflexed and flexed composite specimen at decreasing radius of curvatures.

The measured resistance of the specimen being strained across different radius of curvatures is shown in Figure 2.17. It is observed that there is a gradual increase in trace resistance corresponding to an increase in flexural strain. This confirms the hypothesis that the printed trace strained with the composite and did not crack or delaminate. Using Equation 2.1 [46], the axial strain (ε_x) can be calculated for the smallest radius of curvature (69.85mm) to be 0.004mm/mm.

$$\varepsilon_x = -\frac{y}{\rho} \qquad \text{Eq 2.1}$$

where y is the distance from the neutral axis and ρ is the radius of curvature.

It should be noted that at no point in time did any portion of the printed trace delaminate from the composite surface, despite frequent flexing and multiple loading and unloading cycles into the sample holders. At no point in the handling of the test article did any of the five traces become discontinuous.

2.7.4 Conclusion

In this experiment, the printed resistance samples from Section 2.5.1 of this work were subjected to adhesion tests in order to understand the bond between the conductive traces and the composite surface. An initial Scotch tape adhesion test resulted showed no part of the printed traces delaminating from the composite surface. To further assess the quality of the adhesion, the composite specimen and printed traces were gradually flexed across more severe curvatures through the use of printed fixtures, and resistance measurements were taken while the specimen was flexed. The data indicated that a gradual increase in resistance occurred with higher strains (as expected) and showed that there were no delaminations or cracks forming within the trace. This study confirms the ability to axially strain the fabricated multifunctional composites up to 0.004mm/mm without delamination or discontinuity. Additional experiments are recommended to test the limit of the strain before delamination.

The experimental results show that the TEST process for fabricating multifunctional composites may be adequate for applications where the expected flexural strain on composites high. Additionally, the measure results and empirical observations show that conductive traces transferred using the TEST process are able to be handled without any concern of delamination.

2.8 TEST Process Conclusions

In this chapter, a novel process for the integration of printed electronics with FRP composites, the TEST process, is demonstrated and characterized. The TEST process was used to demonstrate the ability of combining DIW and transfer printing methods to fabricate multifunctional composites. The four major steps are printing additively manufactured sacrificial composite tooling, printing electronic devices onto the additively manufactured sacrificial tooling, layup and cure of FRP composite prepreg onto the additively manufactured sacrificial tooling, and removal of the additively manufactured sacrificial tooling through via dissolution.

Material requirements for processing compatibility between the additively manufactured sacrificial toolings, conductive inks, FRP composites, and solvents are explored, and a list of material combinations is presented for potential applications of the TEST process. Polyether sulfone (PES), polysulfone (PSU) and ULTEM 9085 are demonstrated as high temperature (>180°C) additively manufactured sacrificial composite tooling materials when dissolved via DCM, DMF, or DMSO.

Resistance measurements were taken on conductive traces before and after the transferring via the TEST process. F-test analysis confirmed that the resistance of conductive traces is not statistically affected by the TEST process. Furthermore, analysis of the trace cross-sectional dimensions before and after transfer revealed that there is no statistically significant change due to the TEST process. Adhesion studies demonstrated that the conductive traces are well adhered to the surface of the composite after the TEST process, although further testing is required to determine the limit of strain before delamination of the transferred traces.

At the conclusion of these experiments, a list of factors which were observed to influence the success of the TEST process was compiled into a fishbone diagram. This diagram, shown in Figure 2.18, highlights key elements within each process step that must be considered to facilitate a successful execution of the TEST process. General trends were observed and are presented here to summarize the rationale behind the TEST process as well as to provide rationale for the application of the TEST process with other materials.

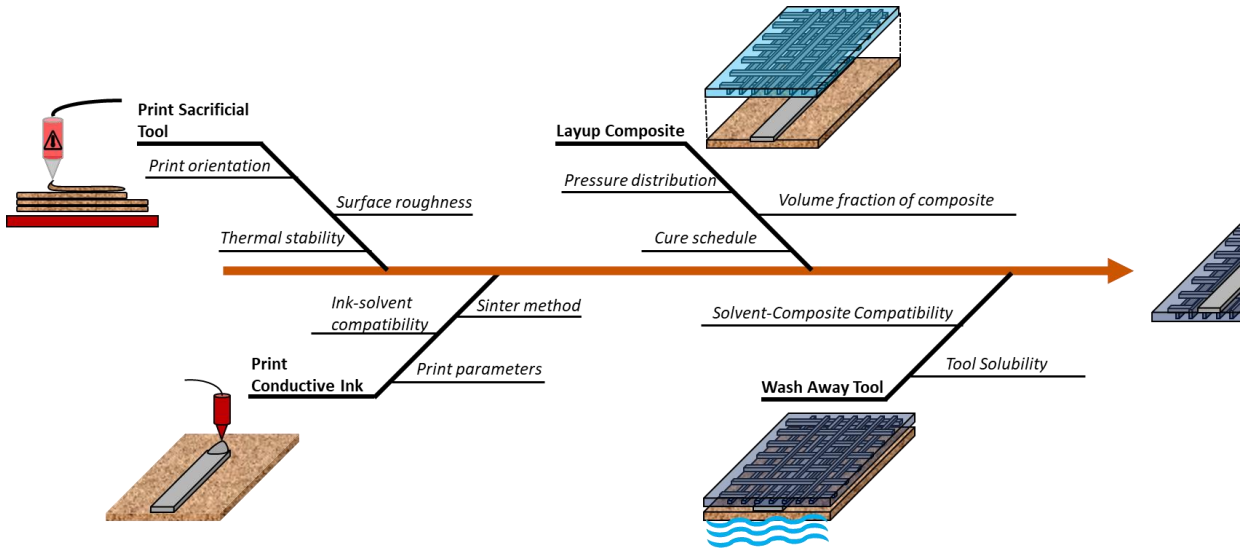

Figure 2.18 Fishbone diagram illustrating the factors at each step in the TEST process which was observed to directly affect the final part transfer quality

Step 1: Print Sacrificial Tool

- *Thermal stability*: The heat deflection temperature of the sacrificial tooling must be higher than the fiber composite cure temperature and the conductive ink sinter temperature (if a thermal sinter is to be used). If the printed sacrificial tooling thermal stability is less than the composite cure temperature or the thermal sinter temperature, the sacrificial tool will deform, and the resulting composite structure will differ from the intended design.
- *Surface roughness*: The surface roughness of the printed sacrificial tool is also important to the TEST process because the printed sacrificial tooling acts as the substrate for the printed conductive ink in the next step. The printed conductive ink will conform to the surface of the printed sacrificial tool, and depending on the viscosity of the conductive ink, it will possess the surface roughness of the tool after it has been sintered and transferred to the surface of the composite. For this reason, the surface roughness of the tooling should be at a minimum the same value as the required surface roughness of the conductive trace. This factor is particularly important for applications involving high frequency devices.
- *Print orientation*: The print orientation of the sacrificial tool affects the surface finish of the final part. It is preferable to abrade across the layer interfaces of the printed sacrificial tool to achieve the required surface finish for printing conductive ink because this orientation requires the removal of the least amount of tooling material. Standard best practice for surface treatment of printed

composite tools is to remove as little material as possible to minimize dimensional differences between the designed tool and the printed tool.

Step 2: Print Conductive Trace

In the second stage of the TEST process, the printing of the conductive ink, the three critical factors which directly relate to the quality of the multifunctional composite are (i) the printing parameters, (ii) the degree and method of sintering for the conductive ink, and (iii) the solubility compatibility of the solvent and the conductive ink.

- *Print Parameters*: From Chapter 1, patterning conductive ink must be performed using the correct parameters specific to each printing process. For DIW, print parameters (from Chapter 1) must be adjusted so that the printed trace width is identical to the selected nozzle inner diameter to ensure that the printed device dimensions match the modeled dimensions.
- *Sinter method:* As discussed above, the method used to sinter the conductive ink can affect the conductivity of printed conductive inks. If a thermal sinter is used, the maximum sinter temperature must be less than the heat deflection temperature of the printed sacrificial tooling to prevent deformation to the sacrificial tooling.
- *Conductive trace resistance to solvent*: The sintered conductive trace will be exposed to the solvent used in the sacrificial tool washout procedure. If the solvent adversely affects the adhesion of the printed conductive traces to the composite surface, then there will consequently be imperfections in the trace transfer. This is unlikely because organic solvents to not typically affect inorganic materials. In rare cases, however, this may contribute to TEST process failures.

Step 3: Layup Composite

- *Volume fraction of composite:* During the composite layup stage of the TEST process, it has been observed that the volume fraction of matrix to reinforcement material plays a role in the transfer of printed conductive traces from the sacrificial tool surface to the final composite structure surface. The uncured matrix material acts as the adhesive that bonds to the printed conductive traces. Composites with low volume fractions have reduced resin content which contributes to regions of printed conductive ink that do not adhere to the composite surface preventing successful transfer. These defects can be mitigated through the use of an unreinforced adhesive mat, provided that the mat is compatible with the selected solvent and the end use application requirements.
- *Pressure distribution:* Pressure of the composite onto the printed conductive ink is important to ensure consistent adhesion between the two materials; any air pockets or unadhered regions will not transfer.
- *Cure schedule:* The cure schedule of the composite prepreg is the final critical factor affecting transfer in this stage of the process. Temperature ramp and dwell and pressure required for the prepreg cure are the criteria by which the sacrificial tooling material are selected and therefore play a critical role in the TEST process.

Step 4: Wash away tool

When the sacrificial tooling is to be removed, the printed conductive trace is well adhered to both the sacrificial tooling and the composite surface, assuming ideal circumstances in previous steps. Potential causes for transfer failure during this stage of the TEST process are listed below:

- *Solvent-composite compatibility:* Solvents used for sacrificial tool washout must not soften the composite matrix material. This may result in reducing the adhesion between the printed conductive trace and the composite surface, preventing successful transfer.
- *Tool solubility:* Solvents used in the test process must fully dissolve the printed sacrificial tooling. The dissolution of the material is critical to ensuring that no film of sacrificial tooling material is left behind, particularly in complex shaped parts where it may be difficult access. Any sacrificial tooling material left behind may negatively affect the added functionality of the multifunctional composite.

Chapter 3: Use of Test Method to Integrate Strain Gauge on Conformal Composite Structure

3.1 Introduction

Structural health monitoring through the use of strain sensing has seen use in several applications including automotive, aerospace, and civil composite structures. Strain gauges are a commonly used device to monitor changes in mechanical strain through the piezoelectric effect. This ability enables engineers to predict part failure and to model damage within composite structures. In recent years, the ability to embed strain sensors within composite structures has been of interest especially in aerospace, civil, mechanical and electromagnetic, namely antenna and radio frequency (RF), applications [3], [9], [31], [33].

Traditional methods of manufacturing strain sensors entail etching involving complex lithographic masks, material waste, and expensive tooling that drive up the cost of manufacturing high resolution components [3], [47]. Such methods are subtractive, whereas additive methods have the potential to at least, partially eliminate the need for lithographic masks, material waste, and high tooling costs for high volume production of embedded sensors. Several additive methods to produce conductive substrates for frequency selective surfaces include screen printing and roll-to-roll manufacturing, namely gravure printing [48]. Interest in printing strain sensors onto composites has also resulted in the utilization of DIW for composite structural health monitoring and in situ damage sensing [15]. Such research has focused on printing sensors directly onto a backing layer which is then placed onto simple, planar fiber-reinforced composite substrates. This process does not entail direct contact between the printed gauge and the composite surface [15]. Printing directly onto prepreg materials is unfavorable because of the resulting poor print quality (Section 1.3). The main limitation to these approaches is the difficulty associated with printing sensors onto non-planar surfaces. The critical advantage to the TEST process is the ability to transfer printed sensors, namely strain gauges, onto conformal and complex composite surfaces using printed sacrificial tooling.

The ability of additive manufacturing methods to pattern conductive inks onto a wide variety of substrates has accompanied the rise in interest of embedded sensors. This capability presents a potential benefit to strain sensing techniques by allowing the printed sensor to be directly integrated with the component's structure, leading to weight reduction, cost savings, and waste reduction. This, combined with the design flexibility and "free complexity" of additive manufacturing, has further established interest in printed strain gauges [49].

The primary goal is to validate the TEST process in a case study using DIW traces printed onto a sacrificial FFF-printed tool and ultimately embedding the traces onto a fiber-reinforced composite via TEST. More specifically, a conductive strain gauge will be printed onto sacrificial tooling, transferred onto a structural composite material, and wired to a Wheatstone bridge configuration for tension testing to validate the efficacy of the printed sensor. In order to validate efficacy of the printed strain gauge, tension testing results need to yield statistically significant changes in strain correlating to the applied uniaxial load.

3.2 Methods

3.2.1 Strain gauge design

The strain gauge design used in this experiment was modeled to have similar geometry to that of commercially available strain gauge patterns. Typically, a strain gauge is designed to detect uniaxial strain by relating the change in electrical resistance to change in strain.

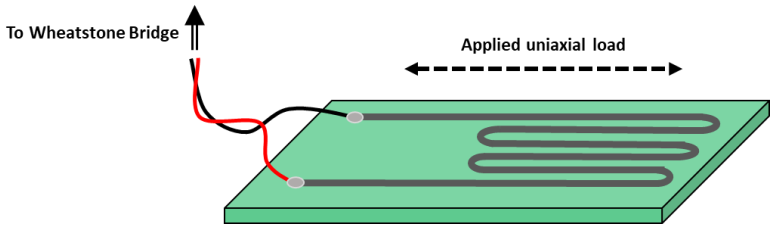

Figure 3.1 Illustration of a uniaxial strain gauge

A strain gauge design, shown in Figure 3.2, was first designed via computer aided design (CAD) software SolidWorks. When developing the strain gauge design, the intent was to mimic traditional strain gauges. Typically, strain gauges are longer in the longitudinal direction because the wire length directly influences the electrical resistance, R, per Equation 3.1, where ρ represents the wire resistivity, L represents the wire length, and A represents the cross-sectional area of the wire. The wire width is 0.1 mm, active grid length is 25 mm, print height is 0.2mm, and the solder tabs are 3 mm x 3 mm to provide sufficient surface area to solder leading wires to strain testing. Referencing ASTM D3039, the standard test method for tensile properties of polymer matrix composite materials, the balanced and symmetric glass-fiber reinforced epoxy $[0/90]_{2s}$ composite had a recommended width of 25.4mm x 25.4mm. Thus, the design constraint for the width of the strain gauge required that the gauge should be less than 25.4mm. In addition, the strain gauge must be located on the center of the gauge and not within the grips of the testing equipment. These two-dimensional constraints led to the design of the 14-loop strain gauge.

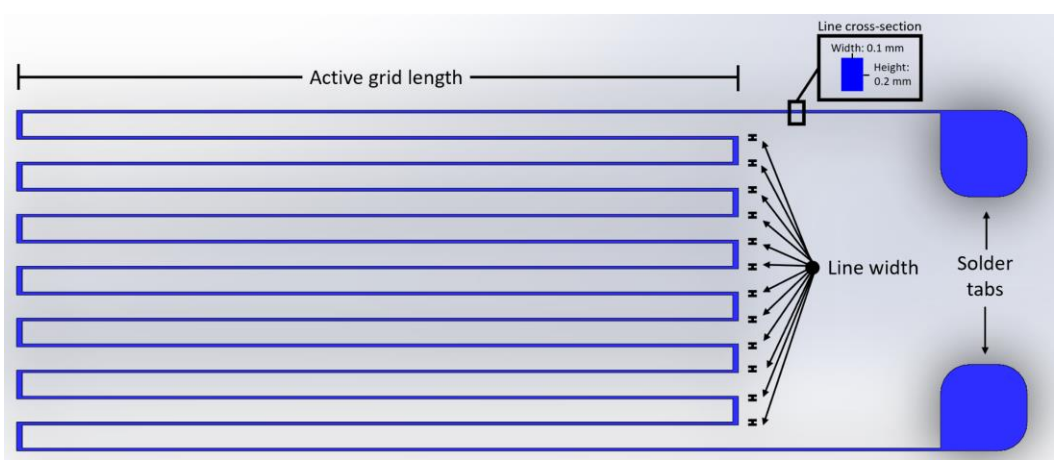

Figure 3.2 CAD image produced via SolidWorks of uniaxial strain gauge to be printed using conductive DIW.

$$R = \rho LA \qquad \text{Eqn. 3.1}$$

Since the wire resistivity dictated by the silver-filled ink material was fixed, the objective was to have a high-resistance strain gauge by maximizing the length and minimizing the cross-sectional area of the wire. The greater the change in *L*, the greater the change in resistance. The length of the wire was predominantly constrained by the composite coupon dimensions, which were determined by the load cell test area. The cross-sectional area of the wire was constrained by the DIW processing route, which relies on nozzle diameter selection and rheological properties of the silver-filled ink. Previous experiments showed that the ink, Dupont CB-028, typically results in a trace width of 0.28mm when processed with previously used 0.25 mm ID nozzle.

3.2.2 Strain Gauge Printing via Direct Ink Write (DIW)

3.2.1 Print sacrificial tool: tool selection and preparation

The first step in the TEST process is the printing of the sacrificial composite tooling. Considering that the strain gauges have been designed to measure uniaxial mechanical strain, the composite tooling has a planar surface that will act as a suitable substrate for the gauges. Therefore, a simple rectangular prism (block) geometry was selected as the sacrificial tooling geometry. The CAD dimensions of this block measured 76.2mm x 76.2mm x 25.4mm.

Polyethersulfone (PES) was selected as the tooling material to be printed on an FDM Fortus 400mc. A high temperature sacrificial tooling material, PES has demonstrated compatibility with the cure schedule of HexPly 8552 S-glass epoxy prepreg in preliminary studies printing 4-point resistance measurement samples. PES was also selected due its high solubility with dimethyl sulfoxide (DMSO), which is the safest, non-toxic solvent used in this study, making it the preferred solvent. In contrast with DMF, PES was previously shown to have no significant effect on composite flexural strength.

The CAD file was sliced, and toolpaths were generated using Stratasys Insight software. In order to facilitate the washing out of the tooling material later, and because tool integrity was not essential for the completion of the experimental objectives, a sparse infill was used for printing this tool. The tool was printed in the XZ plane. Such orientation, mimicking the printing of an airfoil in Section 2.2.3 for an empirical demonstration of the TEST process, was chosen to obtain the desired surface finish via abrasion. The printed tool was then progressively sanded down using 80, 120, 220, 320, 400, and 600 grit abrasive pads for the subsequent DIW printing of the strain gauges. Sanding was necessary to ensure a smooth, level surface compatible with DIW.

3.2.2 Print conductive trace: DIW of strain gauges

The selected modality of additive manufacturing to fabricate the strain gauges was direct ink write (DIW). Directly after printing the strain gauges onto the composite tooling, the assembly was placed in an oven at 180C for one hour to fully dry the ink traces. To determine whether or not the strain gauges were functional, tension testing was performed.

Dupont CB028 silver loaded conductive ink was used for the DIW printing of the strain gauges onto the PES tooling. CB028 was loaded into a 10cc syringe barrel with a 25ga (0.25mm) tip, which was

connected to a Fisnar dispensing unit. The Fisnar dispensing unit acted as a pneumatic controller to apply pressure to the syringe barrel and dispense ink on demand. The 14 loop strain gauge CAD model was then exported as an .stl to Autodesk Netfabb in order to generate .gcode toolpaths. The gcode was loaded into the printer, and four strain gauges were printed at 20psi at 250mm/min with a tip offset distance of 0.2mm. After successfully printing, the tool and printed strain gauges were placed in an oven to dry at 50°C for 30min then sintered at 180°C for 1hr.

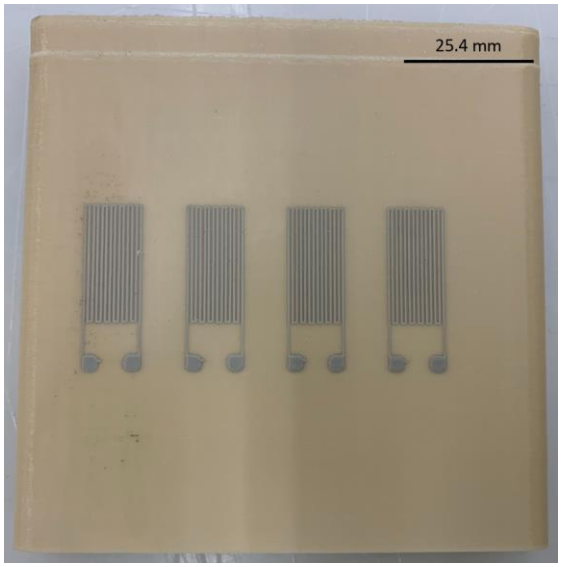

Figure 3.3 Strain gauges printed onto PES sacrificial tooling via conductive DIW

Soldering to the printed silver ink, and silver inks in general, is not feasible. This presents a minor inconvenience when connecting printed electronics to copper terminals or wires. To overcome this challenge, small strips of copper foil were cut and carefully laid in place onto the “solder” tabs of the printed strain gauges. A small amount of ink was extruded onto the copper foil between it and the printed tab. This lightly bonded the copper foil to the gauge, which provided a way of connecting the wires needed to take measurements later in the process. An image of the copper foil tabs being connected to the sintered strain gauges on PES tooling can be seen in Figure 3.3.

Figure 3.4 Copper solder tabs placed onto printed strain gauges

3.2.3 Composite layup onto PES tooling

The composite tool, with printed gauges and tabs, was then laid up with composite prepreg. Hexcel HexPly S-glass/8552 epoxy unidirectional prepreg was used as the structural composite in this experiment with a $[0,90]_{2S}$ fiber orientation layup sequence. This 8-layer laminate sequence was selected for its quasi-isotropic properties in the tensile load case. Each layer of the laminate was laid over the PES tooling with printed gauges and copper tabs, smoothed by hand, and vacuumed to the surface to remove air pockets between the PES and the prepreg. This process was repeated for all eight layers. The laminate and printed sacrificial tooling were wrapped in a vacuum bag and placed into a Wabash Genesis series hydraulic press.

Per the recommended cure schedule, the laminate was initially placed under vacuum and 15 psig pressure, heated up to 107°C with a controlled rate of 2°C per minute, held at 107°C for 60 minutes, then held at 177°C for 120 minutes. After curing, the laminate was securely bonded to the PES tooling, and no visible air pockets were present.

*3.2.*3 Transfer of Printed Strain Gauge via TEST (composite layup and washout)

The cured composite and PES tool was then placed in a bath of DMSO for approximately three hours at room temperature. During that time, the PES printed tool dissolved. Periodically, the composite laminate was removed from the bath in order to inspect the progress of the dissolution. Once the printed strain gauges were visible, and no visible sections of PES remained adhered to the laminate, the tool was considered dissolved and the washout process complete.

Continuity of the printed and transferred conductive traces was verified with a Hewlett Packard 34401A Digital Multimeter and inspection of transfer quality via optical microscopy. Wires were then soldered from the Wheatstone bridge onto the copper tabs that had been integrated into the gauges earlier.

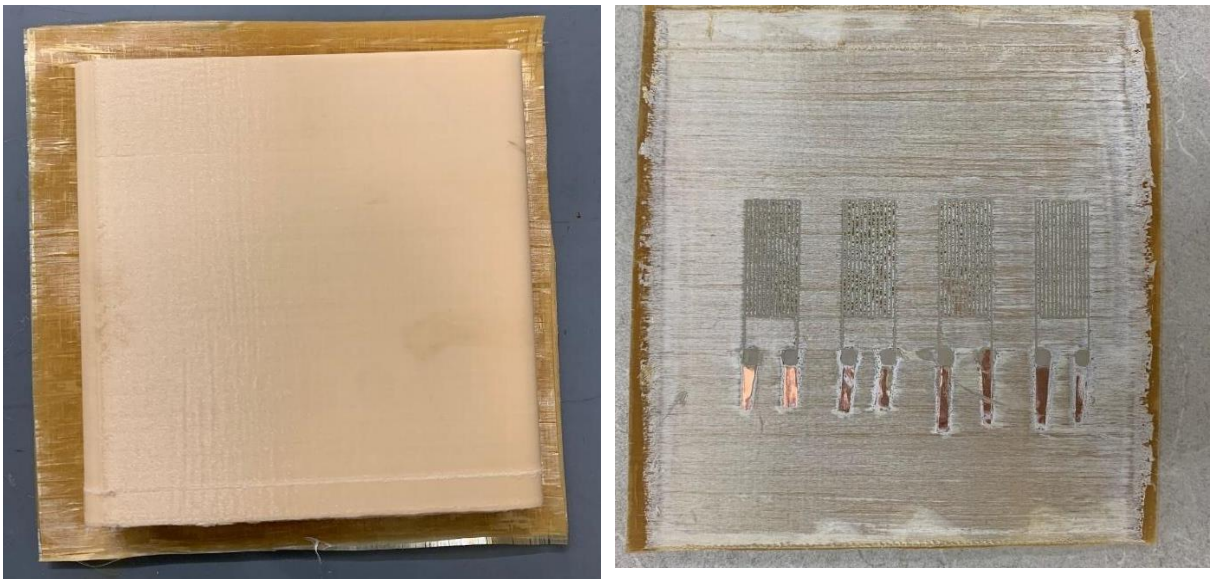

a. b.

Figure 3.5 PES tooling after curing FRP composite laminate (a) and after tool dissolution in DMSO (b), showing the successful transfer of the printed strain gauges from the surface of the PES tooling to the FRP composite surface.

Initial resistance of the strain gauge was critical when setting up the test configuration. A Wheatstone bridge compatible with 120Ω resistors was modified for conducting tension testing the printed strain gauges. Such configuration was available since the most widely used commercially available strain gauges have 120Ω resistance [50]. The average printed strain gauge resistance of 7.5Ω did not match the resistances of the 120Ω legs in the Wheatstone bridge configuration as shown in Figure 3.6. A balanced Wheatstone bridge configuration was accomplished by adding an additional resistor in series with the printed strain gauge in order to reach a resistance closer to 120Ω. The native resistance of the printed strain gauge was not compatible with the Wheatstone bridge testing configuration. Thus, additional resistors were used to increase the resistance of that leg and make the printed strain gauges compatible with the available setup. Output voltage measurements, measured across the green and red legs of the bridge in Figure 3.6, were recorded and used to plot voltage versus strain. Plots illustrating a linear relationship for both stress versus strain and output voltage versus strain are indicators of successful TEST process and functionality of the printed strain gauge.

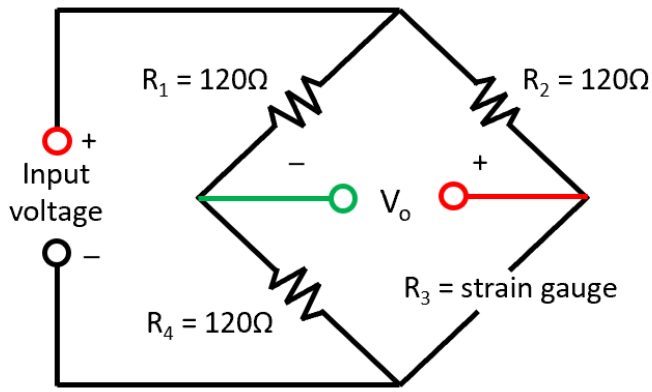

Figure 3.6 Schematic of unbalanced Wheatstone bridge, thus necessitating the use of an additional resistor to increase the resistance of R_4 to match the three 120Ω legs.

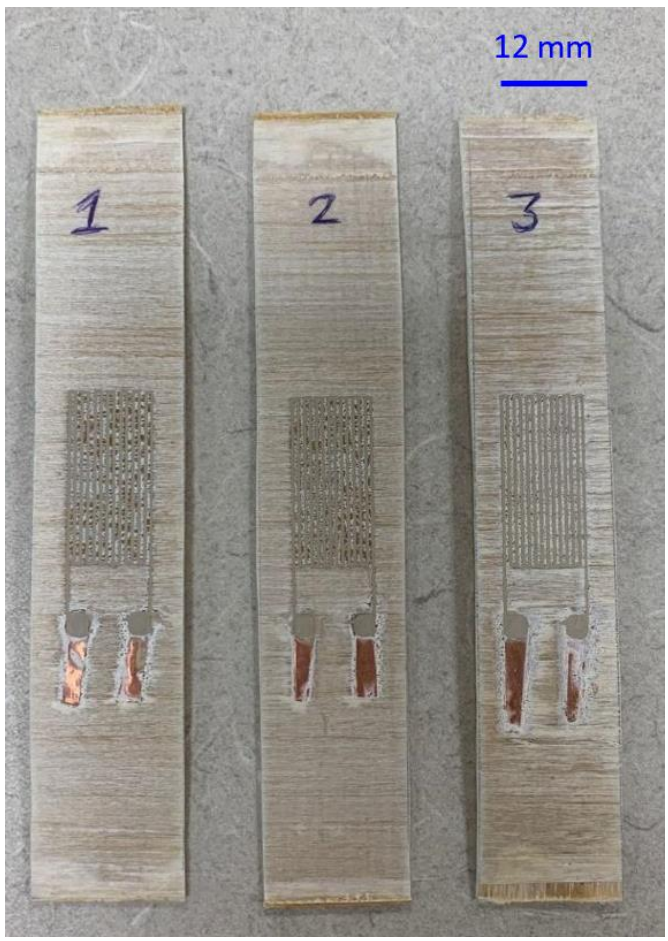

Figure 3.7 Strain gauges embedded onto FRP fiberglass-epoxy composite specimens.

The experimental expectation was that tensile testing would cause the cross-sectional area of the wire to decrease as the coupon elongates. Such experimentation would validate the transfer process by showing a change in strain as a result of increasing the uniaxial tension. MTS Testworks 4 software was

used to regulate the applied load and associated strain. After placing the coupon within the load frame serrated grips, an extensometer was attached to the coupon to directly measure strain. Once all test set-up was complete, testing began by using a handheld load controller to manually increase the tensile load in increments of 100N and obtain discrete load measurements. Input voltages of 2.008V or 5.033V were applied to the Wheatstone bridge. At each load increment, the strain (%) measured via extensometer and output voltage (V) via multimeter was recorded. Strain (%) was converted to strain (mm/mm) and a plot of stress versus strain was generated to observe the relationship between applied load and change in resistance. Load (N) was utilized to calculate stress (MPa) to create stress versus strain plots.

Figure 3.8 Test configuration for tension testing including an extensometer to measure strain.

3.3 Measurement and Results

3.3.1 Initial results of CB028 strain gauge on fiberglass-epoxy composite

Initial resistance measurements of the printed strain gauges via multimeter yielded the following measurements in Table 1. For three coupons containing the transferred DIW gauges, the average strain gauge resistance was measured as 7.5 ± 0.35 Ω. Such consistency reflects repeatability and consistency amongst the prints. The deviations were likely the result of additional ink added to the solder tabs to bond the copper tabs. Data collection was performed by manually applying tensile load to the composite coupon in the Instron load frame.

3.3.4 Results and discussion for CB028 strain gauge on fiberglass-epoxy

Non-destructive tensile testing was performed on the GFRP coupons that contain the printed strain gauges. Figure 3.8 conveys results from the ramp-up tensile test, suggesting a linear relationship between the stress applied via the Instron handheld controller and the strain measured with an extensometer. There was a strong, positive correlation between the two variables, stress and strain, as demonstrated by an R^2 value of 0.9961. The line of best fit for the stress versus strain plot is represented by Equation 3.2. The strong linear fit demonstrates predictability of composite behavior in response to tension applied in discrete increments of 100N.

$$y = 38988x - 39.423 \qquad \text{Eqn. 3.2}$$

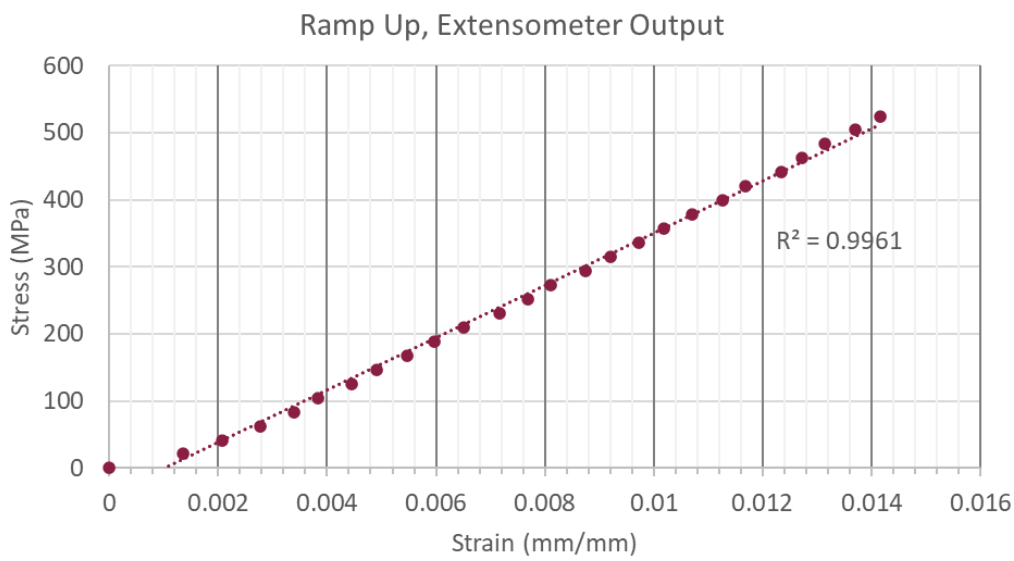

Figure 3.9 Extensometer results from Instron testing shows the linear relationship between stress and strain.

Figure 3.10 is a plot of strain (mm/mm) measured strain gage output voltage based on an input voltage of 5.0326V. An observable plateau is shown at a strain of 0.012 mm/mm. This plateau may be attributed to the maximum output voltage of the strain gauge, which is the upper limit of the output voltage at the given input voltage. There was a strong, positive linear correlation between the two variables, output voltage and strain, as shown by the R^2 value of 0.9489. The line of best fit for the voltage versus strain plot is represented by Equation 3.3. As desired, both the stress versus strain and output voltage versus strain plots illustrated linear trends, therefore suggesting successful operation of the strain gauge. Such conclusions can be drawn because axial strain is a linear function of the output voltage of a wire at constant temperature, input voltage, and strain gauge factor [50].

$$y = 206.12x - 0.4717 \qquad \text{Eqn. 3.3}$$

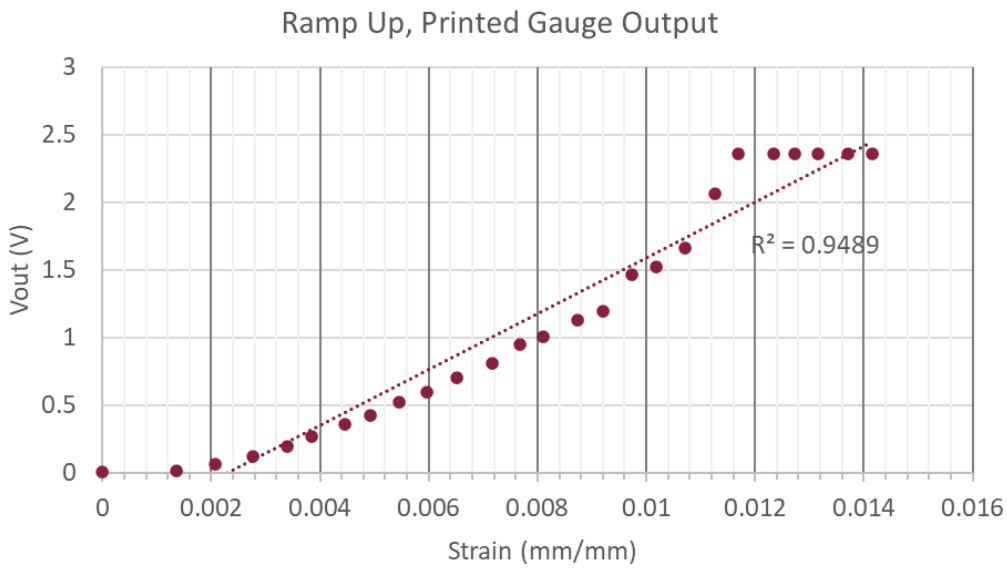

Figure 3.10 Printed strain gauge output voltage versus strain of glass-fiber reinforced polymer (GFRP) composite.

Strain gauge factor, a dimensionless parameter, was calculated via Equations 3.4, 3.5, and 3.6. The printed 14-loop strain gauge tested with an input voltage of 5.0326V had a maximum gauge factor of 0.16. This gauge factor is smaller than that of commercially available strain gauges, which have a gauge factor of 2.0. Higher gauge factors are associated with increased sensitivity. Thus, utilizing a higher resistivity ink for the printed strain gauge will increase sensitivity.

$$K = \frac{\frac{\Delta R}{R}}{\varepsilon} \qquad \text{Eqn. 3.4}$$

$$\frac{\Delta R}{R} = \frac{2 \times \frac{V_{out}}{V_{in}}}{\frac{1}{2} - \frac{V_{out}}{V_{in}}} \qquad \text{Eqn. 3.5}$$

$$\frac{\Delta R}{R} \approx 4 \times \frac{V_{out}}{V_{in}} (V_{out} \ll V_{in}) \qquad \text{Eqn. 3.6}$$

where K is strain gauge factor, ε is strain, R is resistance, V_{out} is output voltage, and V_{in} is input voltage.

The maximum gauge factor of the printed strain gauge was 0.16. While this value is lower than that of traditional strain gauges, such results indicate that the printed strain gauge has less sensitivity than commercially available strain gauges. Increased sensitivity can be accomplished by printing a higher resistivity material. Nonetheless, a correlation was successfully determined between strain applied and output voltage.

3.5 Conclusions

This work demonstrates the potential for the integration of structural health monitoring devices within composite structures. In this experiment, the primary objective of printing, transferring, and

measuring a functioning strain gauge is accomplished. FFF was first used to print a sacrificial PES tool, onto which silver ink was patterned via DIW into a strain gauge pattern and sintered. Fiber reinforced composite material is then laid up onto the surface of the tool, covering the DIW traces, and cured. The composite and tool are then placed in a DMSO solvent bath to dissolve the PES tooling, leaving behind the strain gauges embedded on the surface of the cured composite.

Three functioning strain gauges were patterned onto the surface of a 180°C curing, structural composite laminate. The gauges were demonstrated to measure strain linearly from 0.002-0.012mm/mm. Commercial strain gauges demonstrate proportionality between wire resistance and strain at a given temperature, input voltage, and strain gauge factor [49]. Positive linear trends on the output voltage versus strain graphs show successful functioning of the gauge. For the printed and transferred gauges, the plotted stress versus strain data confirms the linear elastic behavior of the composite material. The plotted output voltage versus strain data yields expected linear behavior.

Future work needs to demonstrate the conformal aspect of this technology, by perhaps integrating a strain sensor in a complex, conformal structure. While successful strain gauge operation was demonstrated on a planar coupon, many composite applications, such as airfoils or pressure vessels, exhibit non-planar geometry and thus would be candidates for sacrificial tooling in the TEST process. An attempt at embedding a sensor in a complex structure was made by implementing the TEST process using a miniaturized pressure vessel as sacrificial tooling. Appendix A.2 outlines the associated material selection, manufacturing method, and challenges. Another consideration to strengthen the tension testing results would be to either select a higher resistance material for printing or increase the active grid length to achieve the 120Ω resistance of the resistors in the original Wheatstone bridge configuration. Achieving such resistance without needing supplemental resistors to be added in parallel with the strain gauge would further validate the initial plots of output voltage versus strain.

Chapter 4: Transfer Process Validation: Production and Characterization of a Composite Frequency Selective Surface at X-band

4.1 Introduction

Frequency selective surfaces (FSS) are devices that act as electromagnetic filters for designer-specified frequencies and bands. These filters have response in both the frequency and spatial domains. An FSS is a resonant structure that derives its filtering characteristics from its geometric and material properties. Most commonly, FSSs take the form of a periodic array of individual conductive elements patterned onto a substrate. The geometry of the individual conductive elements dictates ability to filter different radiation frequencies. In the domain of aerospace composites, FSSs are a critical device for isolating sensor and communication systems from external interference among other applications. Composite FSSs have become critical to the aerospace industry because of the use of embedded conductive traces, as opposed to having a separate structure or apparatus [48]. Embedded traces within composites provide a lightweight means of enabling sensing and communications.

Current approaches for integrating FSSs with composite structures involve adhering a layer of bulk copper onto a composite laminate and either ablating or etching away the excess material until only the desired pattern of conductive material remains [48]. This can often result in a low-yield for the product. This is particularly true for band-stop filters, a type of FSS, which have less than 50% conductive area and therefore require the removal of a majority of the deposited copper. Other methods include printing the FSS on thin films and adhering that film to the composite surface, typically interior to the structure.

Additive Manufacturing (AM) of printed electronics, affords the opportunity to directly deposit only the conductive material necessary for the FSS, thus eliminating the need for an additional subtractive processing step which can lead to waste. For this reason, there has been significant interest in the additive manufacturing of frequency selective surfaces through the use of inkjet, screen printing and microdispensing (DIW) [9], [48], [51], [52]. In this study, conductive DIW is selected primarily for its ability to pattern conformally.

In an effort to further validate the efficacy of the TEST process, the goal of this chapter is to demonstrate its ability to effectively produce high fidelity electromagnetic structures that can meet the specifications and requirements of platforms. This validation experiment is both industrially relevant and an appropriate challenge that must address the following constraints: fabricating a functioning FSS requires strict control over individual element dimensions, the spacing between elements, conductivity of elements, thickness of dielectric (structural composite), overall panel dimensions, alignment of elements, and testing conditions. This experiment expands the application space for the TEST process beyond structural health monitoring and into the RF space. Successful fabrication of an FSS via the transfer process thus requires consistent print quality, tooling accuracy, refined composite processing conditions, successful transfer of printed elements onto composite surface, and adhesion of elements onto a large composite surface area.

To verify the efficacy of the TEST process to form high performance RF devices, an FSS was simulated in HFSS, designed in Ultimaker Cura, and fabricated via DIW printing of conductive ink onto ULTEM sacrificial tooling. The printed FSS and ULTEM tooling were integrated with a structural prepreg via hand lay-up and pressure cured; once the FSS panel was integrated with the surface of the FRP composite, the sacrificial ULTEM tooling was removed, and transmission measurements were performed

in the microwave band, otherwise known as X-band, on the finished FSS. X-Band refers to the electromagnetic spectrum from 8.2 GHz to 12.4 GHz. These measurements were then compared to the expected transmission from simulation.

4.2 Methods

4.2.1 FSS Design

A band-stop FSS was chosen for the demonstration and was modeled in ANSYS high-frequency simulation software (HFSS) to perform in the X-band. The X-band was selected because of its frequent use in aerospace communications, which coincides with the intended application for this process. Furthermore, it is most easily tested in a laboratory environment where structure scale is limited. The design consisted of an array of tri-pole elements with legs positioned at 120° intervals. This particular geometry was selected for its relative simplicity, subsequent ease for printing over a large area, and printability with the given ink, nozzle diameter, and printer positioning precision. Each element possessed only nine changes in direction and could be continuously printed without the need to start or stop extrusion during individual element printing. The array unit cell and element dimensions with the corresponding RF characteristics are shown in Figure 4.1.

Feature	Position	Dimension
Tripole spacing	A	0.60mm
Pole width	B	0.490mm
Pole length	C	6mm
Pole angle	D	120°

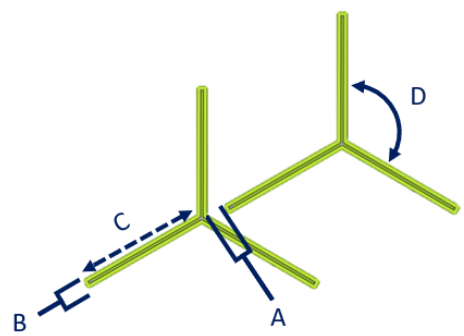

Figure 4.1 Frequency selective surface unit cell with critical dimensions listed in the table on the left.

In the model, there exist two critical angles:

(i) alpha (α, i.e., rotation angle): corresponds to the angle in the X-Y plane where the incident field is propagating

(ii) beta (β, i.e., angle-of-incidence (AoI)): corresponds to the angle from the Z-axis to that of the incident radiation propagation direction.

These angles define the relative angle of incidence to the FSS and the alignment of the incident electric field (E-Field) with the elements of the FSS. Alpha can be changed either by rotating the transmitting and receiving antennas, or by rotating the test specimen about the Z-axis. Using the coordinate system in Figure 4.2, the E-field in red is propagating at zero degrees to the X-axis. Alpha, therefore, is zero in this case. To simplify matters, the alpha angle of zero is labeled as “vertical” and an alpha angle of 90

as “horizontal” as the E-field is aligned and perpendicular to the X-axis. If the antennas were not positioned normal to the surface of the test specimen, the resulting angle would be beta. In the Figure 4.2, beta is zero as the incoming wave is propagating normal to the plane of incidence. This choice provides results for normal incidence to the FSS and is meant to avoid complexities associated with establishing an oblique angle of incidence; the available experimental apparatus has limited capabilities for precision alignment.

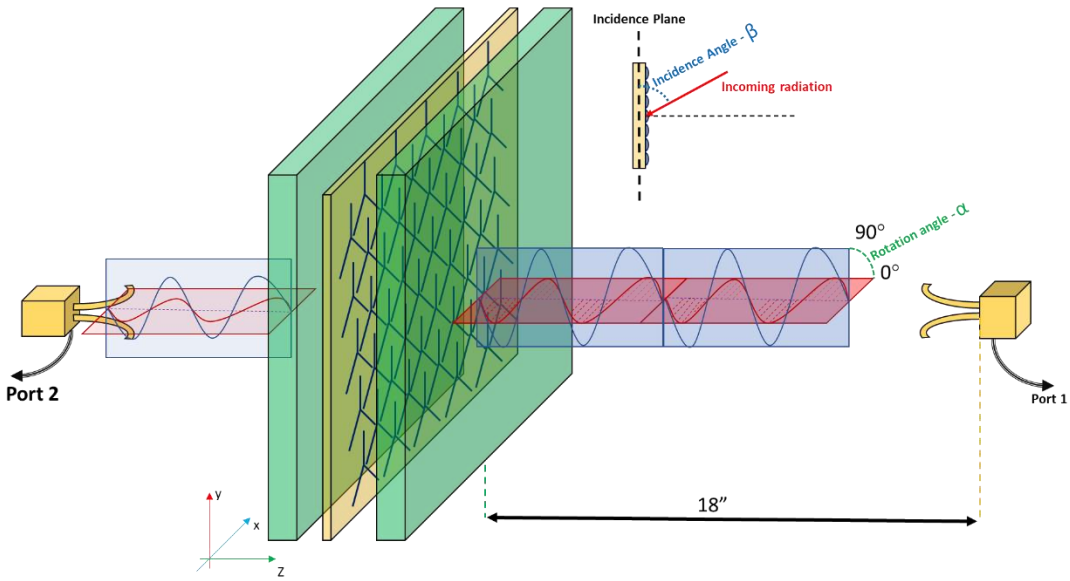

Figure 4.2 Illustration of the test method orientation showing the coordinate system relative to the test specimen and the transmitted waves. Both alpha and beta angles are highlighted.

Recognizing that the physical test fixture and experimental setup are not under ideal conditions, the simulation was run for different beta values. Examining the simulated results will enable interpretation of the experimental results and their comparison to the simulation. From the plot of modeled transmission vs. frequency for the designed FSS geometry (Figure 4.3) , it is observed that the transmission characteristics are identical for both H and V-orientations; there is virtually no difference when beta is equal to 0°(normal incidence). For this case, a prominent null at 9.5GHz is the result. As beta increases to 10°; however, a secondary null is shown beginning to form around 13.9GHz for the V-orientation, while for the H-orientation there is little to no change. This trend becomes more pronounced once beta increases to 45° with the secondary null shifting to approximately 15.6GHz, and the primary null shifting down to 8.9GHz for the V-orientation. Once again, there are no noticeable shifts in response in the H-orientation at 45°.

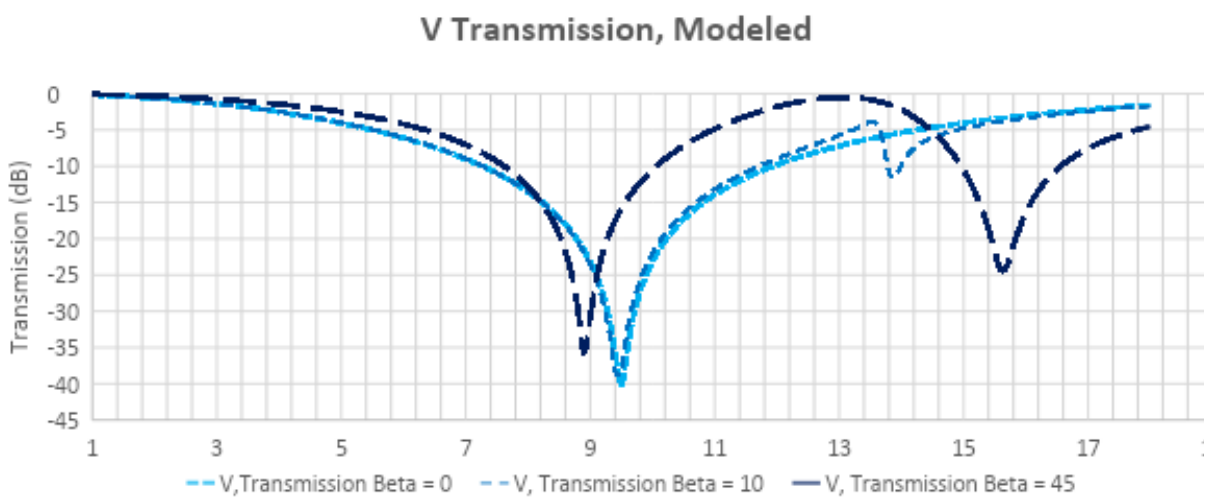

a.

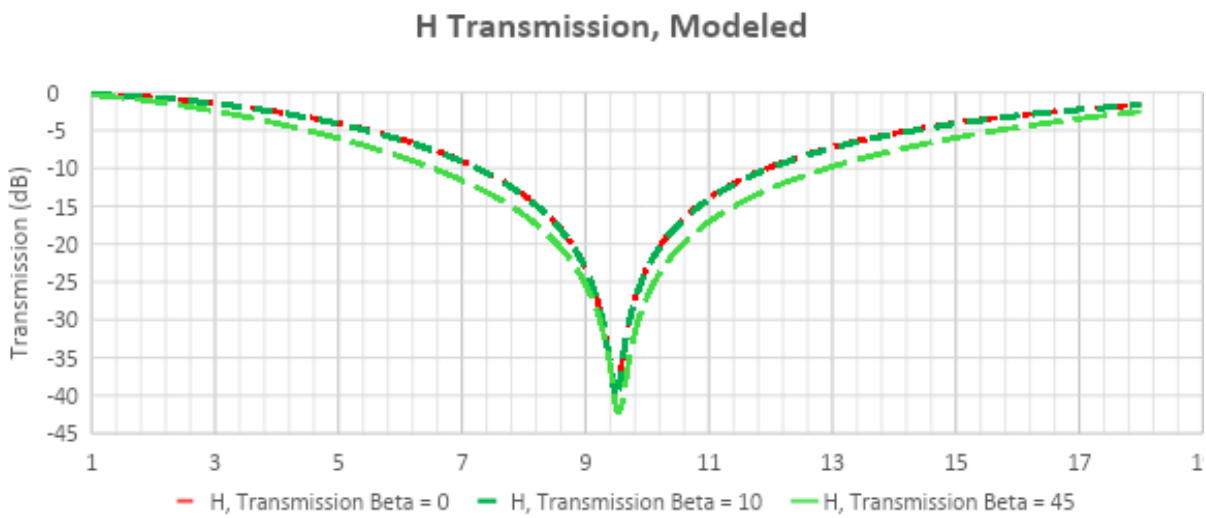

b.

Figure 4.3 Modeled S12 transmission characteristics for the FSS in the V-orientation (a) and H-orientation (b). Each orientation was modeled for beta angles of 0, 10, and 45, in order to visualize how the transmission response changes with changes in the beta angle

4.2.2 Fabrication

Geometric modeling and DIW toolpath planning

The tripole (dimensions in Figure 1) was periodically arrayed over an area measuring 61.0cm x 61.0cm using nTopology. The resulting model was then split into four 30.5cm x 30.5cm sections and meshed as four separate .stl files. The original CAD file was split into four smaller files to fit within the printable area of the custom DIW printer. The CAD file and sacrificial tooling substrates were subdivided into four sections only to fit the processing volume constraints of the equipment used in the TEST process; subdivision of large test articles is not required for the successful execution of the TEST process.

The toolpaths were modified from the .stl files to include z-hops in between each printed element. A z-hop is a line of code within a print file which lowers the platform between the printing of tripole elements to minimize the over-extrusion of the ink crossing between elements and establishing connectivity. Once a complete toolpath was accomplished, the process of selecting and preparing the print substrate commenced.

Step 1: Print sacrificial tool: selection and preparation

Since the chosen substrate geometry was square and planar, it was decided to purchase four, off-the-shelf ULTEM 1000 sheets (30.5cm x 30.5cm x 0.95cm; McMaster-Carr) as the sacrificial tooling substrate. This route was chosen instead of printing the geometry via FFF, as it significantly reduced cost and lead time, and the test specimen geometry did not require complex geometry afforded by FFF. While the tooling for this specific experiment was not printed using an FFF process, the tooling material selected is similar to commercially-available FFF resins (ULTEM 1010 and ULTEM 9085). ULTEM 1000 is an amorphous thermoplastic polyetherimide with a Tg of 217 °C. It therefore satisfies the critical criteria of being thermally stable at the sinter temperature of the chosen conductive ink (Dupont CB028 – 180 °C) and the maximum cure temperature of the FRP composite prepreg (Fibreglast 7781 E-glass/Epoxy - 154°C), while also remaining soluble in the selected solvent (dimethyl formamide). To make the surface of the ULTEM 1000 sheets sufficiently flat for DIW printing they were progressively sanded with a progressive sequence of sandpaper with increasing grit (40, 60, 80, 120, 220, 320, 400, and 600 grit), until a sufficiently smooth surface was obtained for each ULTEM sheet.

Step 2:Print conductive trace - DIW of FSS onto ULTEM 1000

Dupont CB-028 served as the conductive ink for this project. A 0.25mm needle was selected as the deposition head so that as the printhead printed each element in a single contour line, the final width of each printed leg would be 0.49mm (Figure 4.1). After loading CB-028 into a 10cc syringe barrel, the ULTEM substrate was mounted onto the print bed and began depositing the FSS, as seen in Figure 4.4. Dupont CB-028 was pneumatically pressurized at 20psi and extruded through a 0.25mm nozzle that was offset from the substrate surface by 0.2mm. The deposition nozzle traveled at 300mm/min during the printing of each tripole element and at 75mm/min when traveling between individual elements.

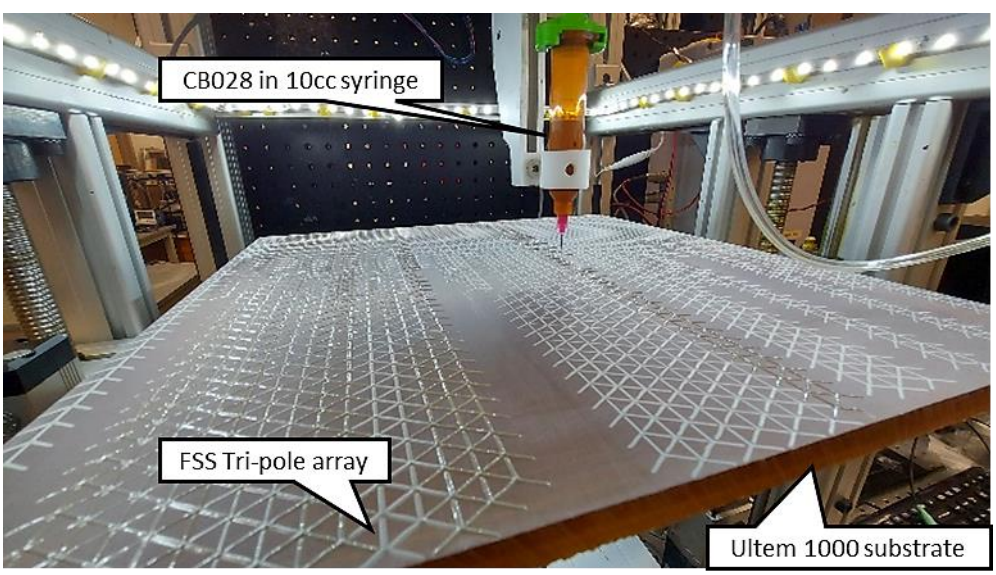

Figure 4.4 Printing of the FSS onto an Ultem 1000 substrate via conductive DIW.

After completing each of the prints on the four 30.5cm x 30.5cm panels, each of the 11,760 elements in the printed array was inspected using optical microscopy to verify that each element remained disconnected from its surrounding elements, thus retaining its resonance behavior. Each panel was allowed to dry before being sintered at 180 °C (Figure 4.5a).

Step 3: Layup composite

Once each panel was successfully printed and sintered, the hand layup process was employed to form the composite laminate to the ULTEM tooling (Figure 4.5b). Fibreglast 7781 E-glass/Epoxy plain weave prepreg was selected for this application for its adequate dielectric properties, while possessing similar processing conditions as other aerospace grade composite materials. These attributes made it a suitable prepreg with which to demonstrate the transfer process. It should be noted that this is also the same composite material that was used for the analysis of the negative effects of solvent exposure on composite mechanical properties in Chapter 2. Two layers of prepreg were laid up onto the tool surface, covering the FSS in a thin composite skin.

The panels were then vacuum bagged and placed into a Wabash Genesis Series hydraulic heated press (Figure 4.5c). The specimen was heated from room temperature to 154°C at a ramp rate of 1°C/min and held for 1hr then cooled to 143°C at a ramp rate of 1°C and held for 2hr then cooled to 132°C at a ramp rate of 1°C/min and held for 4hr before being brought to room temperature and removed from the heated press. A thin composite was used to eliminate complications that may arise due to resulting resonances as the laminate is made thicker. This also allowed for less loss and lower reflection from the bulk material, thereby better isolating the FSS product.

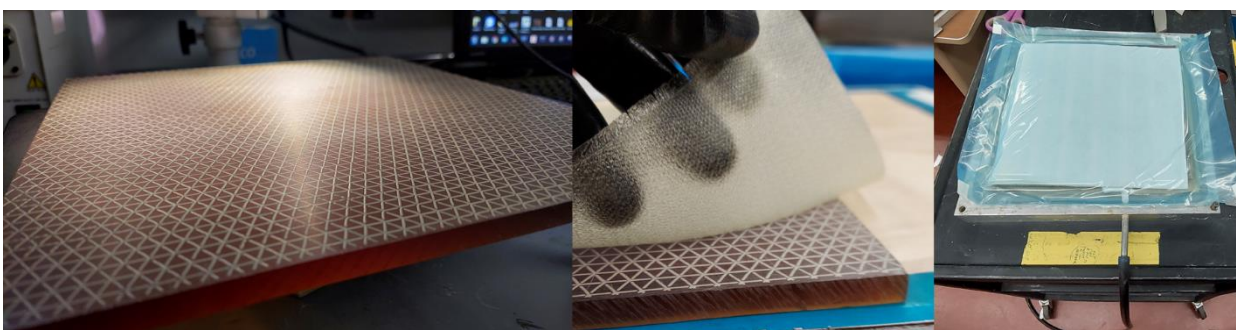

a. b. c.

Figure 4.5 From left to right: Sintered FSS pattern undergoing optical microscopy inspection (a). Hand layup of composite prepreg onto the surface of the Ultem 1000 tool(b). Vacuum bagging of the composite prepreg and the FSS on the Ultem 1000 sacrificial tooling(c).

Step 4: Wash away tool

Before the ULTEM tooling was dissolved, the tool removal process was expedited by utilizing a DeWalt 20V compact cordless router to remove approximately 0.25” of material from the thickness of the tooling. Manual removal of material was deemed acceptable and necessary for time constraints. Once ULTEM material was manually removed, approximately 0.125” of ULTEM remained bonded to the composite surface.

Dimethyl formamide (DMF) was selected as the solvent to dissolve the remaining ULTEM tooling. DMF was selected for its availability in large quantities and ability to dissolve ULTEM tooling without damaging the composite, which was critical for the scale of this experiment. All four 30.5cm x 30.5cm

panels were placed in a polypropylene container with approximately 16 liters of DMF for 48 hours. In order to expedite the process, the panels were periodically removed from the DMF bath and sections of ULTEM were manually removed from the composite surface. Again, this was done in order to reduce the time necessary to fully dissolve ULTEM 1000.

Once the ULTEM had been fully dissolved, each panel was removed from the DMF bath and inspected (Figure 4.6a). As expected, regions where air pockets had formed between the tool and composite during the composite cure did not see successful transfer of printed elements to the composite surface (Figure 4.6b). Fortunately, this primarily occurred around the periphery of each panel, and by trimming the edges of the composite skins, these bare regions could be removed.

Each panel was then trimmed to its final dimensions. Edges which were adjacent to the other sections of the FSS were aligned such that each partial element lined up its complementary partial element on the adjacent panels. The four panels were then compressed between two expanded polystyrene (EPS) sheets (Figure 4.6c) to hold the whole assembly together. Polystyrene has a very low dielectric constant and was expected to have only minor influence on the measurements while providing adequate support to keep the samples flat and aligned. This assembly served as the final, compiled test specimen with which transmission and reflection measurements were extracted.

a. b. c.

Figure 4.6 Successful transfer of the printed tripole FSS onto Fibreglast 7781 E-glass/Epoxy composite (a). Discoloration and defects occurred due to manual removal of the ULTEM sacrificial tooling from the composite surface (b). Four FSS panels aligned and sandwiched between two panels of polystyrene foam, forming the final test specimen (c).

4.3 Measurement

Measurement Setup

A Keysight Programmable Network Analyzer (N5227B-10 MHz to 67 GHz (4 port, 2 sources))(PNA) was used to characterize the transferred arrays. The PNA was connected to two MVG/Satimo QH2000 open boundary wideband antennas to measure transmission and reflection properties of the test specimen from 2-18GHz. The QH2000 antennas are rated for 2 GHz to 32 GHz.

The test fixture consisted of a 1.2m x 2.4m expanded polystyrene (EPS) board with a 0.6m x 0.6m aperture cutout to hold the FSS test specimen. The EPS board was lined with an RF-reflecting aluminum sheet to act as a backstop for incoming RF waves to shape the incoming beam such that it only transmits through the FSS test specimen. Pyramidal, 40dB RF absorber was mounted onto the aluminum sheet to minimize unwanted reflections around the FSS test specimen as well as absorb the radiation reflected by the aluminum sheet. Without an anechoic chamber, there will be undesired reflections from the environment around the test fixture. These reflections are expected to appear in the results in the form of noise. This system is a version of a structure commonly referred to as a "transmission tunnel". The PNA was calibrated using a coaxial test kit up to the antenna input ports. The free space (no test article) was calibrated by normalizing the measurement results by the free space results. Finally, the PNA was configured to time-gate the transmission signal; allowing only the time period representing the time-of-flight between the two horns to be measured.

For maximum achievable repeatability using the available infrastructure, two wideband antennas were mounted onto adjustable tripods which enabled the positioning and alignment of the antennas on either side of the FSS test specimen. Ideally a fixed mounting structure attached to the transmission tunnel would be available using a linear motion rail-mounted system. In the absence of a precision linear motion rail system to position the antennas accurately and reliably at a distance equal to a quarter wavelength from the FSS test specimen, the antennas were positioned with yard sticks. Because the test panel was relatively close in proximity to the antennas and the fact that a precision adjustment of the distance from the test panel was not available, the reflections from the panel were expected to have significant contributions from standing waves between the horn and the panel. The effects of standing waves could be reduced through post-processing using additional measurements with the antennas precisely repositioned relative to the FSS test specimen. Consequently, only transmission measurements were expected to give useful results and reflection measurements have been discarded. The test setup can be seen in Figure 4.7 below, which depicts an illustration of the experiment.

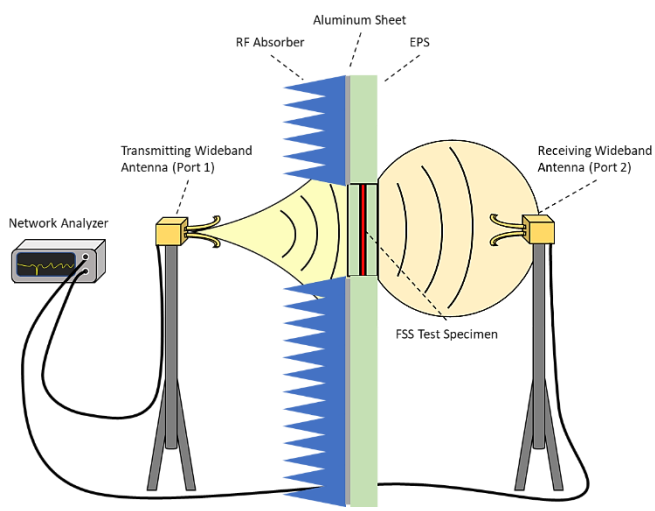

Figure 4.7 Measurement setup for conducting transmission measurements on FSS

Before measurements were performed, calibration of the network analyzer was necessary to remove noise from the system. This is a process to eliminate noise and error contributions due to the VNA and the attached cables. The calibration brings the measurement plane all the way up to the ends of the

cables where the antennas are attached. The first step in this process was to baseline the system up to the ends of the RF cables that would eventually connect to the wideband horns. Using a Keysight Ecal kit, reflections in the cables were accounted for, such that when cables are connected to each other to form a closed loop from port 1 to port 2 on the network analyzer, there is zero gain or loss response. The next step consisted of accounting for the error caused by the testing environment and test fixture. To accomplish this, a baseline was formed in free space by positioning the antennas approximately 0.46m from the fixture window, facing each other, and transmitting a signal from port 1 to port 2. After the measurement was established, the values were stored in memory so that the free space (no test panel) could be normalized to 0 dB across the measurement spectrum, effectively removing the free space effects including scattering from the window's edges.

In the absence of an anechoic chamber, unwanted multipath reflect and scattered signals were eliminated from the measurements by establishing a 4 nanosecond time gate to limit the period of time where the receiving antenna could detect signals. This essentially creates a window of time, starting when transmission begins, and lasts only as long as it takes for the signal to travel in a straight line to the receiving antenna. A signal emitting in an off angle would need to travel a greater distance and be reflected back towards the receiving antenna; this greater distance would thus require more time to reach its destination. An assumption is made regarding the constant velocity of the signal, roughly 1ft/ns. Given a total distance between transmitting and receiving antennas of 0.91m, the time gate is set to form a 3ns window. Completing this, measuring S-parameters for the FSS may commence.

4.4 Results

After printing and before the four individual 30.5cm x 30.5cm panels were cured, the four panels were inspected via optical microscopy for defects. Manual inspection of the as-printed FSS array showed many printed tripole elements were over-extruded during printing which resulted in multiple elements contacting each other. This issue was remedied by manual etching of the areas of the printed tripole elements that were in contact with adjacent elements.

As each of the four individual 30.5cm x 30.5cm panels were laid up and cured, the composite panels were approximately the same size as the processable area in the heated press. This resulted in uneven pressure being applied across the composite during the cure process. This uneven pressure allowed for the formation of small air pockets between the cured laminate and the tool surface. This was noticed around the perimeter of each panel after the cure stage. Overall, it looked as though the overwhelming majority of the composite surface had bonded to the ULTEM tool. These defects are attributed to equipment limitations and are not considered characteristic of the TEST process.

It was also observed that during the ULTEM dissolution stage, regions of the composite that were manually separated from the ULTEM tooling showed a visible color difference from regions that had no manual intervention at all. This resulted in sections of the FSS, composite and printed elements, appearing either darker or lighter, depending on whether DMF alone was used to remove ULTEM (Figure 4.6b-c). By all other appearances, there seems to be no other differences between the transferred elements.

Due to equipment constraints, the antenna horns were not positioned at a precise distance equal from the test specimen. With the small distance to the sample and the fact that the equipment is positioned for measurements at normal incidence, standing waves were expected in the reflection

measurements. Reducing or eliminating the standing waves in reflection measurements would require additional techniques with highly controlled relative positioning. Consequently, the reflection results are not presented. Only transmission from one antenna to the other is reported. The transmission is reported using the S-Parameters, S_{12} or S_{21}, and measured in decibels (dB) [3], [9], [48], [51], [52]. Since reciprocity in the test panel thin substrate is expected, either S_{12} or S_{21} can be used. However, since the absorber was only applied to one side, transmission on the absorber side to receive on the non-absorber side of the fixture was selected.

The test specimen was loaded into the test fixture in the V-orientation and recorded S_{12} behavior from 2-18GHz. The test specimen was removed and rotated into the H-orientation: the process was repeated. The measurement data and simulation results are superimposed in Figure 4.8.

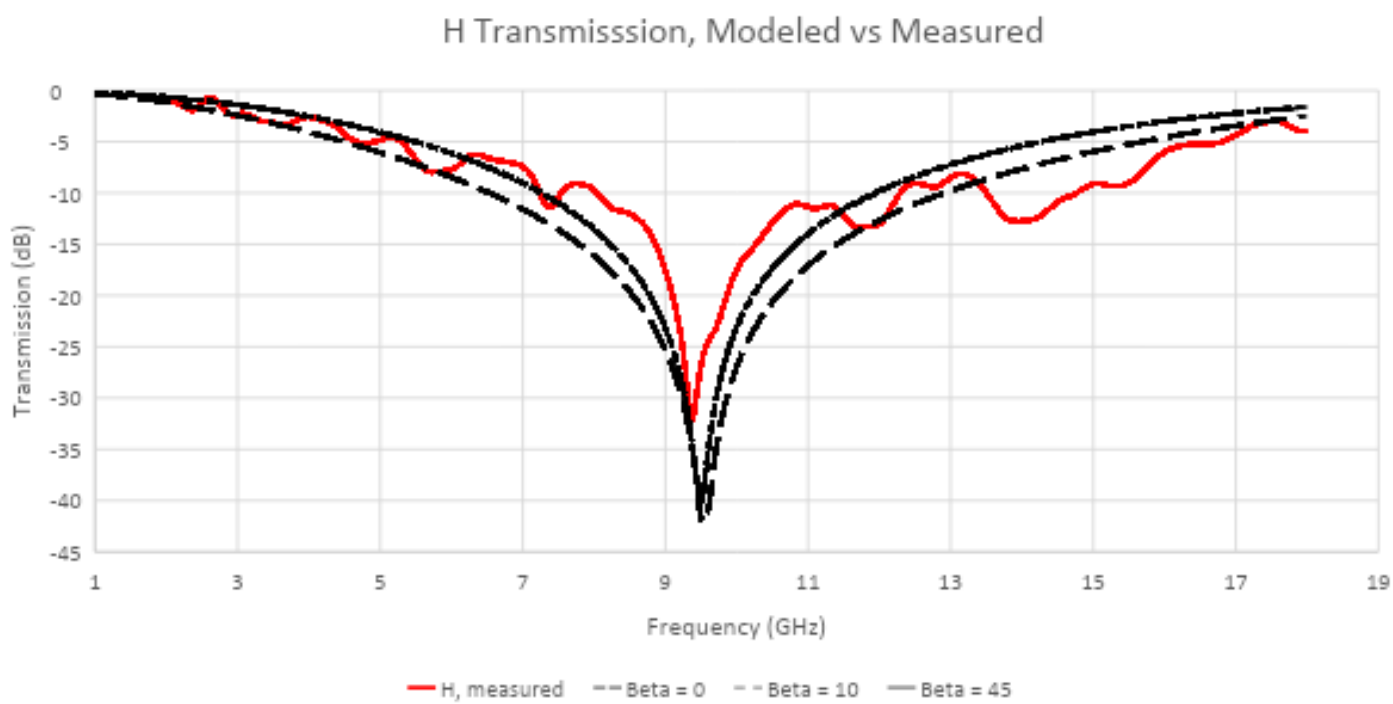

a.

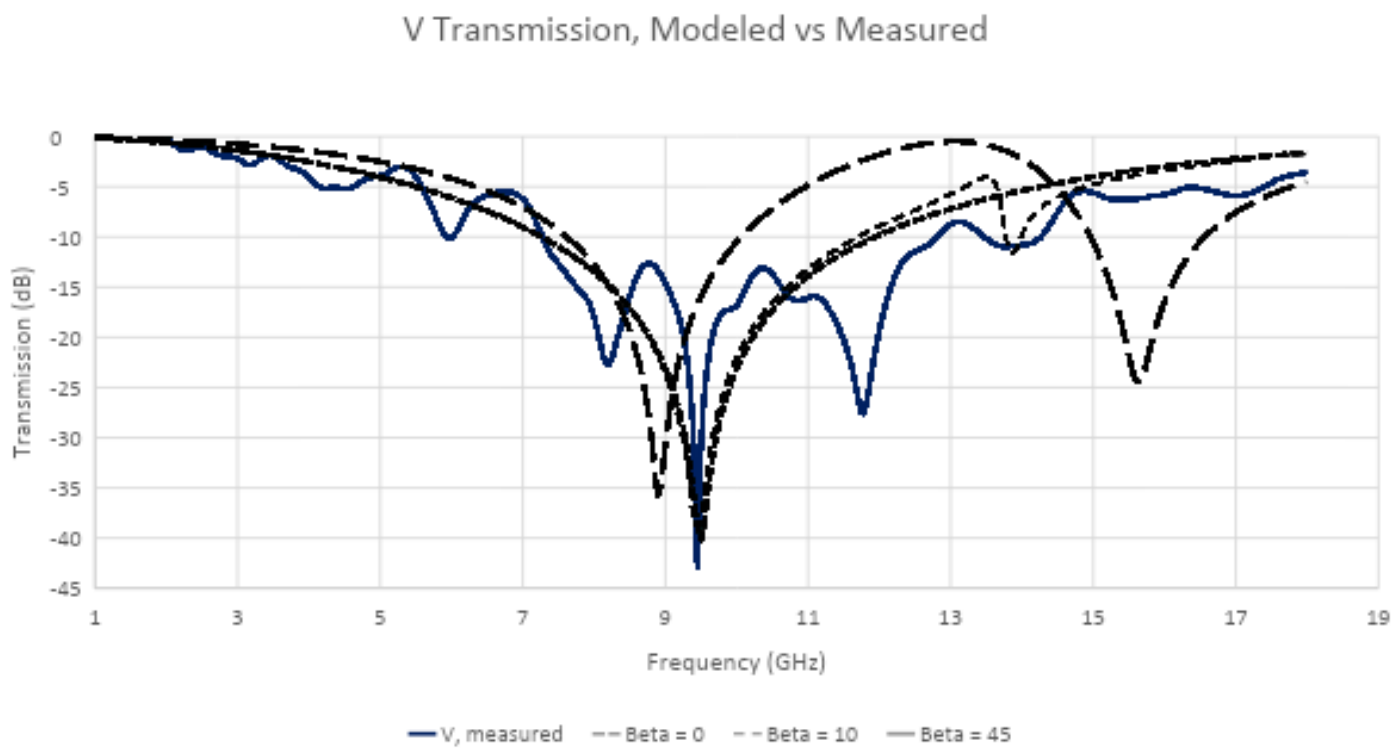

b.

Figure 4.8 Measured transmission response for FSS from 2-18GHz for H-orientation (a) and V-orientation (b). Modeled results at beta angles of 0, 10, and 45 are superimposed over the measured results for comparison.

In the H-orientation (Figure 4.8a), interference effects are observed in the data at and above the target frequency of 9.5GHz. The measured data for the H-orientation shows a prominent null of -35dB at 9.40GHz. This shows good alignment with the simulated results of -40dB at 9.50GHz.

For S_{12} parameters in the V-orientation (Figure 4.8b), two nulls are formed; one at approximately-27dB at 9.4GHz and another at -30dB at 11.75GHz. While this does not align perfectly with the modeled data for when the incoming wave is propagating normal to the plane of incidence (β=0) case, a secondary null at off-incidence angles (β>0), is expected. This error could be attributed to a large number of factors including, but not limited to, imprecision in antenna positioning, imprecision in test specimen mounting, edge effects of test fixture at the interface between test fixture and test specimen, edge gaps and other defects in the test specimen, gaps and misalignments of the subpanels in the test fixture, imprecision in the dimensions of the printed elements, printed elements not being perfect electrical conductors, slight deviation in composite (dielectric) thickness, or solvent effect on dielectric properties of the composite. This secondary null is likely the result of a combination of these factors, and more work is necessary to determine how each factor affects the final S-parameters. Despite this, there is evidence of band stop behavior at the expected frequency range in the V-orientation.

4.5 Conclusions

In this chapter, a novel method for the integration of a FSS onto an aerospace grade composite skin is demonstrated. Successful printing, sintering, transferring, and characterizing a large area (61.0cm X 61.0cm) FSS was accomplished using the TEST process. DIW was used to print an array of 0.5mm wide conductive elements onto the surface of four 30.5cm X 30.5cm ULTEM 1000 sheets. These sheets served in place of additively manufactured tooling, though they were selected from the same class of printable materials (polyetherimide). E-glass/epoxy prepreg was laid up by hand onto the printed arrays and ULTEM tooling and cured. ULTEM tooling was dissolved in a bath of DMF, leaving behind the sintered arrays on the composite surface. The four composite skins were then mounted between two EPS sheets to form the final 61.0cm X 61.0cm FSS test specimen. In order to validate the ability of the transfer process to produce functional FSSs, S-parameters were characterized for the test specimen from 2-18GHz. Due to limitations in the characterization resources, only the S_{12} parameters were investigated for these specimens.

Noisy data due to a large number of potential panel and measurement errors were observed at lower frequencies, but results showed excellent null alignment, depth, and characteristics with predictions in the H-orientation and good null alignment in the V-orientation, indicating that the FSS has a frequency response that is consistent with the design and predictions. The resonance behavior of these arrays was verified in the X-band. From these results, it is clear that the TEST process is capable of integrating large, high-performance RF structures with the surface of structural FRP composites.

This process could be made more efficient through the removal of the manual processes used for this experiment, which could improve these results. Examples include replacing the manual abrasion of the sacrificial tool surface with CNC milling and replacing the manual adjustment of the DIW print nozzle height with an adaptive nozzle offset sensor to maintain a consistent distance between the DIW print nozzle and the substrate. This experiment could be greatly improved by repeating the test in an anechoic chamber. Additionally, the TEST process has yet to be demonstrated with large scale, conformal RF structures. It is hypothesized that, because the process has been demonstrated on a planar specimen, the TEST process can be applied to conformal structures. Further testing is required in order to validate this hypothesis and to identify what process challenges this change introduces.

Chapter 5: Summary, Conclusions, and Future Work

5.1 Summary of motivation

Multifunctional composites have gained significant interest in the last decade for their ability to merge high-strength lightweight structural composite materials with additional functionalities such as sensing, RF communications, EMI shielding, actuation, and much more. By integrating functional devices and materials with structural FRP composites, a reduction in parasitic mass is achieved by rendering wiring harnesses, fasteners, and connectors unnecessary.

Methods of integrating additional functionality have been developed by incorporating electrically conductive or dielectric materials with the structure of the FRP laminate. These methods of integration are achieved through modification of the reinforcing fiber, the polymer matrix, or through the integration of printed electronics with the structural laminate. Functionalities have been added either within the composite laminate or on the surface of the composite laminate.

Modification of the fiber reinforcement or the polymer matrix of the laminate has consistently led to a degradation in mechanical strength, while also providing inconsistent or inadequate functional performance. Embedding of conductive veils or copper wires within structural laminates often results in poor mechanical performance because the embedded device often acts as a defect within the laminate. Embedded devices act as delamination initiators within laminate composites and have been shown to reduce flexural strength by up to 30% in some cases [3], [11]. Additionally, metal coated veils and conductive reinforcement fibers suffer from significantly reduced conductivity and anisotropic conductivity, which has reduced their application within multifunctional composite fabrication [13].

By far the most promising work in recent years has utilized printed electronics to provide functional devices which are then integrated into the structure of composite laminates. Multifunctional composites which utilize printed electronics in their fabrication methods have shown excellent RF performance when compared to finite element simulations [1], [2], [9]. This approach has the added benefit of protecting the functional device from the environment by encapsulating it fully within the structure of the composite laminate. Methods which embed printed devices between laminae of FRP composites still suffer from reduced mechanical performance, particularly in bending [48]. Additionally, printing of conductive inks onto dry and wet (prepreg) fiber reinforcement has been shown to cause device dimensional inaccuracies due to ink wicking/spreading along the reinforcing fibers [3].

The alternative approach is to pattern printed electronic devices onto the surface of cured FRP laminates. This approach involves the printing and sintering of conductive inks onto the surface of cured composites. Thermal stability of the composite matrix poses limitations for the sintering of conductive inks which can occur at temperatures as high as 200°C [22], [26] . Additionally, this approach is compatible with conformal composite structures, but it limited to geometries with curvatures less 45°. This approach leaves the printed device exposed to the environment, as the printed ink is on the external composite surface. The risk of adhesion failure to the external surface of conformal composites poses a risk to the durability of multifunctional composites produced using this method [7], [41], [42].

Perhaps the most promising approach to multifunctional composite fabrication to date involves the integration of electronic devices with the surface of composite laminates through the use of a

transfer process. In the work presented by Nicholson et al., a copper metasurface antenna is patterned via a subtractive laser-profiling method on to a PTFE release liner. Fourteen plies of composite prepreg are laid up onto the patterned metasurface antenna and cured. After curing, the release liner is removed, and the copper antenna has been integrated with the composite surface. This method is used to demonstrate the fabrication of planar and conformal multifunctional composites with excellent RF properties [8], [43]. Additional benefits of this approach are that it is compatible with current aerospace composite industry processing techniques, can be applied to conformal composite structures, and likely does not affect the composite's mechanical performance. This process has yet to be completed using printed electronic devices, which can save considerable time and material compared to the subtractive methods used in this work.

5.2 Summary of work and key results

In this work, a novel process for the fabrication of conformal multifunctional composite structures is presented. The transfer of electronic devices via sacrificial tooling (TEST) process utilizes the advantages of transfer methods and printed electronics to form multifunctional composites without negatively impacting the mechanical strength of the composite structure. The TEST process utilizes additive manufacturing to fabricate a sacrificial composite tool which acts as the print electronics' substrate. A composite laminate is then formed around the sacrificial tool, encapsulating the printed electronic device, and cured. The sacrificial tooling is then dissolved out from the composite part, leaving behind the printed device embossed onto the interior surface of the composite laminate. The four main steps of the TEST process are: additively manufacture a sacrificial composite tool, pattern and sinter conductive ink onto the sacrificial tool, layup and cure composite prepreg onto sacrificial tool, and washout the sacrificial tool.

Additive manufacturing of sacrificial composite tooling has been limited to thermoplastics with Tg <120°C, limiting its application for high-temperature curing aerospace composites. This study has shown that polysulfone (PSU - Tg≈180°C), ULTEM 9085 (Tg≈180°C), and polyethersulfone (PES - Tg≈225°C) can be used as additively manufactured sacrificial composite tooling when dissolved with dimethyl sulfoxide (DMSO), dichloromethane (DCM), or dimethyl formamide (DMF). A list of compatible additively manufactured sacrificial tooling materials, conductive ink sintering methods, composites (based on maximum cure temperatures), and solvents is presented Table 2.1.

The TEST process was demonstrated by printing two PSU sacrificial tools, DIW printing and sintering silver conductive ink onto the sacrificial tools, laying up and curing structural composite onto the sintered traces and sacrificial tool, and dissolving away the sacrificial tooling with DCM. The first demonstration of the TEST process successfully patterned silver conductive traces on the inside surface of a composite box, where it would be otherwise inaccessible for other patterning approaches. The second demonstration of the TEST process successfully patterned a silver patch antenna geometry conformally on the inside surface of a curved composite airfoil structure where geometry limitations prevented the use of other patterning methods (Figure 2.2).

A single test specimen was designed and constructed to study the effects of the TEST process on the resistance, adhesion, and dimensions of conductive traces transferred to structural composites. Additionally, the effects of solvent exposure on composite flexural strength were studied for solvents used in the high-temperature sacrificial tooling washout stage of the TEST process. A PES sacrificial tool was printed using fused filament fabrication, and five 50mm silver ink 4-probe resistance samples were

printed onto its surface. After sintering the printed conductive traces, a $[0,90]_{2S}$ S-glass/epoxy prepreg laminate was laid up over the sintered traces onto the PES sacrificial tool and cured. The PES tool was then dissolved in a solvent bath of DMSO, and the conductive traces were successfully transferred onto the composite surface.

Resistance measurements were taken before and after trace transfer to the composite surface. Resistance of the silver traces on the tool surface measured an average of 0.364Ω +/- 0.004, while trace resistance on the composite surface after transfer measured an average of 0.369Ω +/- 0.006. Statistical comparison of these values via F-test showed that at the 95% confidence interval there is no statistical difference between the resistance values before and after transfer.

Profilometry scans were taken of the printed silver traces on the PES sacrificial tool and the composite surface, before and after transfer respectively. Four distinct cross-sections of the printed traces are visible in the profilometry scans before transfer, whereas scans taken after trace transfer showed no distinguishable difference between the printed trace and the surrounding composite surface.

Adhesion of the transferred silver ink to the composite surface was assessed using two methods: Scotch tape adhesion testing and measuring resistance while flexing the composite structure. The Scotch tape adhesion test qualitatively showed that no silver ink was peeled from the composite surface. The composite specimen was then flexed and held in place while resistance measurements were taken. Trace resistance increased steadily, as expected, and no sharp increases in resistance (indicative of delamination/cracking) were observed.

The effect of solvent on composite flexural strength was determined by performing 3-point bend testing on an E-glass/epoxy composite laminate. Composite laminate test coupons were submerged in DMF and DMSO for 27 hours, dried, and then tested. Dry composite coupons served as the baseline for comparison during the 3-point bend test. Results showed that at the 95% confidence interval there was no statistically significant change in composite flexural strength between the dry samples and samples that were exposed to DMSO. Between the dry samples and samples that were exposed to DMF; however, did show a statistically significant reduction in flexural strength at the 95% confidence interval.

The TEST process demonstrated its ability to integrate structural health monitoring devices onto the surface of composite laminates. Three DIW printed strain gauges were patterned through the TEST process onto $[0,90]_{2S}$ S-glass/epoxy composite laminates for tensile testing with an Instron universal testing machine. The printed strain gauges were shown to measure strain linearly from 0.002-0.012mm/mm when compared to extensometer data. The gauge factor for the printed strain gauge was calculated to be 0.16, which is lower than that of traditional strain gauges. Such results indicate that the printed strain gauge has less sensitivity than commercially available strain gauges.

The final demonstration of the TEST process integrated a DIW printed frequency selective surface onto a structural two-layer E-glass/epoxy composite laminate. FSS was accomplished using the TEST process. DIW was used to print an array of 0.5mm wide conductive elements onto the surface of four 30.5cm X 30.5cm ULTEM 1000 sheets. The composite was laid up by hand onto the printed arrays and cured. ULTEM tooling was dissolved in a bath of DMF, leaving behind the printed arrays on the composite surface. The four composite skins were then mounted between two EPS sheets to form the final 61.0cm X 61.0cm FSS test specimen. S-parameters were characterized for the test specimen from

2-18GHz. The measured S_{12} parameters showed excellent null alignment with simulated models of the FSS.

5.3 List of key contributions

This work has demonstrated and characterized, for the first time, a method to produce conformal multifunctional composite structures by transferring printed electronic devices from the surface of additively manufactured sacrificial composite tooling to the surface of structural, aerospace-grade FRP laminate composites.

This process has demonstrated its ability to pattern thermally sintering (>180°C) conductive ink on the interior surface of complex, closed geometry composite structures where it would be otherwise impossible to access for printing. Additionally, this work verifies the compatibility of the TEST process to work with two high-temperature(>175°C) curing thermoset composites. This process expands the range of materials that can be used for additive manufacturing of sacrificial tooling to include PES, PSU, and ULTEM 9085.

The TEST process was shown to not significantly affect the resistance of conductive traces integrated with FRP laminates. The process was also shown to not significantly affect the flexural strength of the final FRP laminate structure, with the proper solvent selection. Further characterization of the TEST process shows that conductive traces are well adhered to the composite surface, and that the composite laminates can be strained to 0.004mm/mm without causing cracks or delaminations.

This work implements the TEST process to integrate functioning strain gauges directly into the surface of structural composite laminates and compares the performance of those strain gauges with extensometer readings. A gauge factor of 0.16 is recorded for the strain gauges.

The TEST process is further utilized to integrate a frequency selective surface, operating in the X-band, with a structural composite laminate to demonstrate its potential RF applicability. An FSS array of tripole elements is simulated, designed, printed via DIW onto ULTEM tooling. That printed array is then transferred via the TEST process onto a structural composite laminate and its transmission characteristics are measured from 2-18GHz. The measured results align well with the simulated data, with prominent nulls forming at the expected frequency (9.5GHz).

5.4 Future work

Additively manufactured sacrificial tooling plays a critical role in the TEST process presented in this thesis. Subsequently, further studies should be conducted into suitable additive manufacturing materials and methods that can tolerate the TEST processing conditions outlined in Chapter 2 of this work. ExOne binder jetted sacrificial sand tooling was briefly studied in this work (see Appendix A.1) and should be investigated further for its potential use in the TEST process.

In this work, DIW is exclusively used to print the functional devices to be integrated with structural composites via the TEST process. Alternative printing methods suggested in this work include screen printing (for planar applications), aerosol jet, and inkjet (for planar applications). These methods should be explored in combination with particle-free conductive inks to broaden the list of printed electronic methods and materials compatible with the TEST process.

Many of the test articles and functional devices in this thesis possessed planar geometries. While the TEST process was proven conformally, there must be further studies conducted that produce

conformal and functional models. Conformal antennas and conformal strain gauges, in particular, could potentially be an attractive next step for the demonstration of the TEST process.

While the primary focus of this thesis is to bridge current manufacturing capability gaps for multifunctional composites, the TEST method developed in this work does not necessarily require the final part structure to be an FRP laminate. Adapting the TEST process to form other multifunctional materials requires further exploration into processing conditions and their compatibility with the TEST process. Examples could include multifunctional ceramics or multifunctional polymer structures fabricated via the TEST process.

References

[1] D. D. L. Chung, “A review of multifunctional polymer-matrix structural composites,” *Composites Part B*, vol. 160, no. December 2018, pp. 644–660, 2019, doi: 10.1016/j.compositesb.2018.12.117.

[2] K. J. Narayana and R. Gupta Burela, “A review of recent research on multifunctional composite materials and structures with their applications,” *Materials Today: Proceedings*, vol. 5, no. 2, pp. 5580–5590, 2018, doi: 10.1016/J.MATPR.2017.12.149.

[3] Peter Pa, “Additive Manufacturig of Electromagnetic Multifunctional Composites,” 2015.

[4] M. S. Mirotznik, D. Ph, J. Smith, P. Pa, P. Ransom, and B. Good, “Multifunctional Structural Composites ‘ Engineering the EM Properties of Structures ’ Electromagnetically functionalized structural composites : Long term vision,” 2011.

[5] D. A. Roper, “ADDITIVE MANUFACTURING OF GRADED DIELECTRICS,” 2014.

[6] T. C. Baum, R. W. Ziolkowski, K. Ghorbani, and K. J. Nicholson, “Embroidered Active Microwave Composite Preimpregnated Electronics-Pregtronics,” *IEEE Transactions on Microwave Theory and Techniques*, vol. 64, no. 10, 2016, doi: 10.1109/TMTT.2016.2600369.

[7] S. Biswas, “Fabrication of Conformal Load Bearing Antenna using 3D Printing,” *2018 IEEE Antennas and Propagation Society International Symposium and USNC/URSI National Radio Science Meeting, APSURSI 2018 - Proceedings*, pp. 235–236, 2018, doi: 10.1109/APUSNCURSINRSM.2018.8608257.

[8] K. J. Nicholson, S. Member, T. C. Baum, and K. Ghorbani, “Conformal Voronoi Metasurface Antenna Embedded in a Composite Structural Laminate,” *IEEE TRANSACTIONS ON ANTENNAS AND PROPAGATION*, vol. 69, no. 7, p. 3717, 2021, doi: 10.1109/TAP.2020.3044663.

[9] P. Pa, M. S. Mirotznik, R. McCauley, S. Yarlagadda, and K. Duncan, “Integrating metamaterials within a structural composite using additive manufacturing methods,” *IEEE Antennas and Propagation Society, AP-S International Symposium (Digest)*, pp. 1–2, 2012, doi: 10.1109/APS.2012.6349224.

[10] P. Pa, M. S. Mirotznik, and S. Yarlaggada, “High frequency characterization of conductive inks embedded within a structural composite,” in *IEEE Antennas and Propagation Society, AP-S International Symposium (Digest)*, Oct. 2015, vol. 2015-October, pp. 1310–1311. doi: 10.1109/APS.2015.7305044.

[11] R. Healey, K. J. Nicholson, J. Wang, J. Patniotis, T. Lynch, and W. K. Chiu, “Conformal load-bearing antenna structures—mechanical loading considerations,” *Sensors*, vol. 22, no. 1, Jan. 2022, doi: 10.3390/s22010048.

[12] C. González, J. J. Vilatela, J. M. Molina-Aldareguía, C. S. Lopes, and J. LLorca, “Structural composites for multifunctional applications: Current challenges and future trends,” *Progress in Materials Science*, vol. 89, pp. 194–251, Aug. 2017, doi: 10.1016/J.PMATSCI.2017.04.005.

[13] L. Yao *et al.*, “Fabrication and characterization of microstrip array antennas integrated in the three dimensional orthogonal woven composite,” *Composites Part B: Engineering*, vol. 42, no. 4, pp. 885–890, Jun. 2011, doi: 10.1016/J.COMPOSITESB.2011.01.006.

[14] K. Blake Perez and C. B. Williams, “Combining Additive Manufacturing and Direct Write for Integrated Electronics-A Review”.

[15] G. Y. Lee, M. S. Kim, H. S. Yoon, J. Yang, J. B. Ihn, and S. H. Ahn, “Direct Printing of Strain Sensors via Nanoparticle Printer for the Applications to Composite Structural Health Monitoring,” *Procedia CIRP*, vol. 66, pp. 238–242, 2017, doi: 10.1016/j.procir.2017.03.279.

[16] K. H. Church, H. Tsang, R. Rodriguez, P. Defembaugh, and R. Rumpf, “Printed Circuit Structures, the Evolution of Printed Circuit Boards,” *IPC APEX EXPO*, 2013.

[17] J. Chang, T. Ge, and E. Sanchez-Sinencio, “Challenges of printed electronics on flexible substrates,” in *Midwest Symposium on Circuits and Systems*, 2012, pp. 582–585. doi: 10.1109/MWSCAS.2012.6292087.

[18] Y. Khan, A. Thielens, S. Muin, J. Ting, C. Baumbauer, and A. C. Arias, “A New Frontier of Printed Electronics: Flexible Hybrid Electronics,” *Advanced Materials*, vol. 32, no. 15, 2020, doi: 10.1002/adma.201905279.

[19] R. Su, S. H. Park, Z. Li, M. C. Mcalpine, and U. States, “3D printed electronic materials and devices 13,” 2019.

[20] P. C. Joshi *et al.*, “Direct Digital Additive Manufacturing Technologies: Path Towards Hybrid Integration,” *IEEE*, 2012.

[21] N. Thakur and H. Murthy, “Nickel-Based Inks for Inkjet Printing: A Review on Latest Trends,” *American Journal of Materials Science*, vol. 2021, no. 1, pp. 20–35, doi: 10.5923/j.materials.20211101.03.

[22] W. Yang, E. J. W. List-Kratochvil, and C. Wang, “Metal particle-free inks for printed flexible electronics,” *Journal of Materials Chemistry C*, vol. 7, no. 48, pp. 15098–15117, Dec. 2019, doi: 10.1039/C9TC05463D.

[23] Y. Cai, X. Yao, X. Piao, Z. Zhang, E. Nie, and Z. Sun, “Inkjet printing of particle-free silver conductive ink with low sintering temperature on flexible substrates,” *Chemical Physics Letters*, vol. 737, Dec. 2019, doi: 10.1016/J.CPLETT.2019.136857.

[24] T. E. Oja, C. B. Williams, B. A. Davis, and M. D. Bartlett, “Characterization of Additively Manufactured All-Aromatic Polyimide as a Dielectric Substrate for Conductive Direct-Write Silver Inks,” 2020.

[25] Y. Mukai and M. Suh, “Enhancing the Electrical Properties of Inkjet-Printed Silver Ink by Electrolyte Sintering, Photonic Sintering, and Electroless Plating,” *Science of Sintering*, vol. 53, pp. 119–126, 2021, doi: 10.2298/SOS2101119M.

[26] K. A. Ohiri, N. M. Nowicki, T. J. Montalbano, M. Presley, and N. S. Lazarus, “Electroplating of Aerosol Jet-Printed Silver Inks,” vol. 2100362, pp. 1–6, 2021, doi: 10.1002/adem.202100362.

[27] D. P. Parekh, D. Cormier, and M. D. Dickey, *Additive Manufacturing (Chapter 8)*, 2nd ed. CRC Press Taylor&Francis Group, 2020.

[28] H. Bukhari and K. Sarabandi, “Ultra-wideband printed slot antenna with graded index superstrate,” *IEEE Transactions on Antennas and Propagation*, vol. 61, no. 10, pp. 5278–5282, 2013, doi: 10.1109/TAP.2013.2274208.

[29] P. E. Parsons, Z. J. Larimore, A. Lu, and M. S. Mirotznik, “Miniaturization of an additively manufactured microstrip patch antenna using magnetodielectrics,” *2016 IEEE Antennas and Propagation Society International Symposium, APSURSI 2016 - Proceedings*, pp. 819–820, 2016, doi: 10.1109/APS.2016.7696118.

[30] Y. Zhu, J. Li, and G.-L. Huang, “A Lightweight 3-D Printed Dual-Band High-Gain Slotted Spherical Antenna,” *IEEE Antennas and Wireless Propagation Letters*, vol. 1225, no. c, pp. 1–1, 2020, doi: 10.1109/lawp.2020.2971836.

[31] R. Colella, F. P. Chietera, F. Montagna, A. Greco, and L. Catarinucci, “Customizing 3D-Printing for Electromagnetics to Design Enhanced RFID Antennas,” vol. 7281, no. c, 2020, doi: 10.1109/JRFID.2020.3001043.

[32] D. E. Anagnostou, A. A. Gheethan, A. K. Amert, and K. W. Whites, “A direct-write printed antenna on paper-based organic substrate for flexible displays and WLAN applications,” *IEEE/OSA Journal of Display Technology*, vol. 6, no. 11, pp. 558–564, 2010, doi: 10.1109/JDT.2010.2045474.

[33] J. Castro, E. Rojas, A. Ross, T. Weller, and J. Wang, “High-k and low-loss thermoplastic composites for Fused Deposition Modeling and their application to 3D-printed Ku-band antennas,” *IEEE MTT-S International Microwave Symposium Digest*, vol. 2016-Augus, pp. 29–32, 2016, doi: 10.1109/MWSYM.2016.7540068.

[34] G. Tong, Z. Jia, and J. Chang, “Flexible Hybrid Electronics: Review and Challenges,” *Proceedings - IEEE International Symposium on Circuits and Systems*, vol. 2018-May, Apr. 2018, doi: 10.1109/ISCAS.2018.8351806.

[35] F. C. Krebs, “Fabrication and processing of polymer solar cells: A review of printing and coating techniques,” *Solar Energy Materials and Solar Cells*, vol. 93, no. 4, pp. 394–412, 2009, doi: 10.1016/J.SOLMAT.2008.10.004.

[36] N. J. Wilkinson, M. A. A. Smith, R. W. Kay, and R. A. Harris, “A review of aerosol jet printing—a non-traditional hybrid process for micro-manufacturing,” *International Journal of Advanced Manufacturing Technology*, vol. 105, no. 11, pp. 4599–4619, Dec. 2019, doi: 10.1007/S00170-019-03438-2.

[37] N.N., “Aerosol Jet ® Printed Electronics Overview,” p. 6, 2009, [Online]. Available: http://www.optomec.com/wp-content/uploads/2014/04/AJ_Printed_Electronics_Overview_whitepaper.pdf

[38] K. A. Ohiri, N. M. Nowicki, T. J. Montalbano, M. Presley, and N. S. Lazarus, “Electroplating of Aerosol Jet-Printed Silver Inks,” *Advanced Engineering Materials*, vol. 23, no. 10, Oct. 2021, doi: 10.1002/adem.202100362.

[39] K. K. B. Hon, L. Li, and I. M. Hutchings, “Direct writing technology-Advances and developments,” *CIRP Annals - Manufacturing Technology*, vol. 57, no. 2, pp. 601–620, 2008, doi: 10.1016/j.cirp.2008.09.006.

[40] M. A. Meitl *et al.*, “Transfer printing by kinetic control of adhesion to an elastomeric stamp,” 2005, doi: 10.1038/nmat1532.

[41] S. Biswas, “DESIGN AND ADDITIVE MANUFACTURING OF BROADBAND BEAMFORMING LENSED ANTENNAS AND LOAD BEARING CONFORMAL ANTENNAS,” 2019.

[42] S. Biswas and M. Mirotznik, “Additively Manufactured Conformal Load-Bearing Antenna Structure (CLAS),” *IEEE Transactions on Components, Packaging and Manufacturing Technology*, 2020, doi: 10.1109/TCPMT.2020.3019220.

[43] E. Gupta, Z. Larimore, M. Mirotznik, and K. Nicholson, “Fabrication of conformal metasurface RF devices using 6-axis hybrid additive manufacturing; Fabrication of conformal metasurface RF devices using 6-axis hybrid additive manufacturing,” 2021, doi: 10.1109/ICEAA52647.2021.9539837.

[44] V. Sastri, “Chapter 8 High-Temperature Engineering Thermoplastics:Polysulfones, Polyimides, Polysulfides, Polyketones,Liquid Crystalline Polymers, and Fluoropolymers,” in *Plastics in medical devices : properties, requirements and applications* , 2010, pp. 175–215.

[45] K. B. Perez, J. H. Bøhn, K. Meehan, and K. Blake Perez, “Hybridization of PolyJet and Direct Write for the Direct Manufacture of Functional Electronics in Additively Manufactured Components,” 2013.

[46] “Beam Bending.” https://www.continuummechanics.org/beambending.html (accessed Apr. 01, 2022).

[47] M. R. Khosravani and T. Reinicke, “3D-printed sensors: Current progress and future challenges,” *Sensors and Actuators, A: Physical*, vol. 305, Apr. 2020, doi: 10.1016/J.SNA.2020.111916.

[48] R. Mccauley, “MATERIAL DESIGN METHODOLOGY FOR STRUCTURAL AND MICROWAVE MULTIFUNCTIONAL COMPOSITE LAMINATE SYSTEMS,” 2013.

[49] Y. H. Chang, K. Wang, C. Wu, Y. Chen, C. Zhang, and B. Wang, “A facile method for integrating direct-write devices into three-dimensional printed parts,” *Smart Materials and Structures*, vol. 24, no. 6, p. 065008, May 2015, doi: 10.1088/0964-1726/24/6/065008.

[50] J. M. Cimbala, “Stress, Strain, and Strain Gages,” 2013.

[51] J. A. Miller, J. C. Batchelor, and E. A. Parker, “FSS printed using conducting ink,” 2010. doi: 10.1109/APS.2010.5562321.

[52] A. A. Dewani, S. G. O’Keefe, D. v. Thiel, and A. Galehdar, “Window RF Shielding Film Using Printed FSS,” *IEEE Transactions on Antennas and Propagation*, vol. 66, no. 2, pp. 790–796, Feb. 2018, doi: 10.1109/TAP.2017.2780893.

Appendices

A.1 TEST process using ExOne Printed Sand sacrificial tooling

In Figure A.1 below, four 4-probe conductivity samples were printed via DIW of Dupont CB-028 onto a sample of ExOne printed sand sacrificial composite tooling. This sample was donated by ExOne to the lab; design and printing of the sacrificial tooling was not an option for this demonstration. The printed sand sacrificial tooling surface had been sealed with a proprietary “blue” coating to prevent resin wicking into the porous structure of the sand. This sacrificial tooling material is attractive for its ability to remain dimensionally stable up to 180°C while remaining water-soluble. This removes the need for harsh solvents to be used in the washout stage of the TEST process.

The conductive traces were sintered onto the sand tool in open air with a convection oven at 180°C. Four layers of Hexcel HexPly S2GL/8552 was laid up around the sample. A hole in the shape of the letters “VT” was cut into the layup to provide solvent access and the layup was then cured at 107°C with a ramp rate of 2°C per minute, held at 107°C for 60 minutes, then held at 177°C for 120 minutes. After curing the composite and tool were placed into a water bath and left for several hours (≈4 hours). The specimen was then removed from the bath and inspected.

In Figure A.1b, the cured composite “box” can be seen with the sacrificial sand tooling removed from its interior. Visual inspection indicates the successful transfer of the sintered silver traces to the composite surface, where it would otherwise be inaccessible for printing. The “box” was cut open so further examination of the transferred traces could be conducted. Using optical microscopy, visual inspection of the surface showed that the uneven surface of the “blue” coating was imparted onto the conductive traces and composite surface (Figure A.1a). This meant that the cross-section of the transferred traces was inconsistent and therefore, no meaningful resistivity study could be conducted on the traces.

The severe surface deviations of the ExOne printed sand tooling, the inability to print and seal future sand tooling, and the lack of access to these materials severely limited the use of ExOne sand tooling in this work. In principle, with a surface smooth enough to act as a print substrate, ExOne sand sacrificial composite tooling is compatible with the TEST process. Future studies are needed to understand its full range of benefits and challenges.

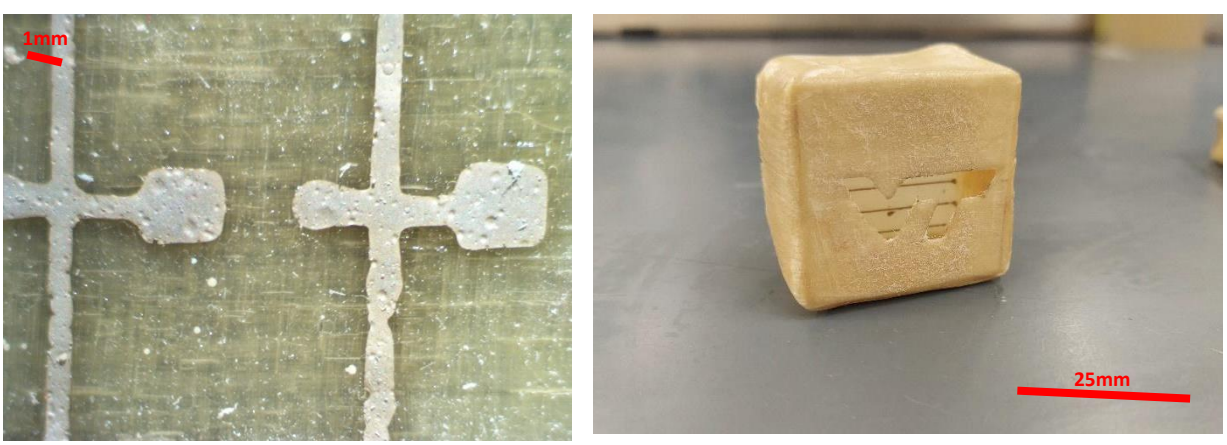

a. b.

Figure A.1.1 TEST Process transfer demonstration using ExOne printed sand sacrificial composite tooling surface (a) and cured composite box (b)

A.2 Composite pressure vessel experiment

In an effort to test the strain gauge on an industry-relevant complex part, a pressure vessel was printed out of Ultem via FDM as sacrificial tooling for a composite lay up. Figure A1 illustrates the CAD model with relevant dimensions generated on SolidWorks. The process flow of this study included the following: (i) DIW printing the strain gauge out of silver-loaded ink onto the sacrificial FDM printed pressure vessel tooling as shown in Figure A2, (ii) using additional silver ink to attach copper wires to the strain gauge solder tabs (iii) drying the ink in a box oven at 180°C for 1 hour, (iv) hand laying up 3 layers of carbon fiber twill prepreg onto the sacrificial tooling, (iv) vacuum bag curing the assembly at 154°C for 1 hour, (v) soaking the cured assembly in DMF solvent to dissolve the Ultem sacrificial tooling, (iv) measuring change in strain by applying pressure causing the vessel to expand. Steps (i) through (iv) were completed with the remaining steps incomplete as a result of combined difficulties with the sacrificial tooling and composite weave pattern.

Figure A.2.1 Pressure vessel dimensions for FDM printed sacrificial tooling

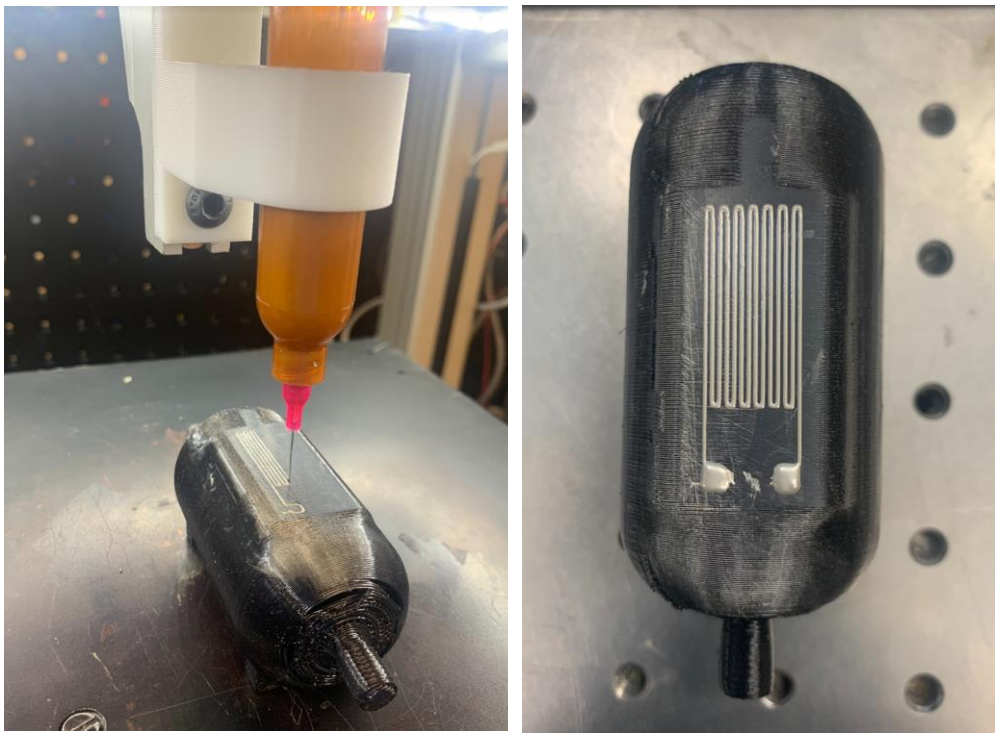

Figure A.2.2 DIW printing silver ink strain gauge onto Ultem pressure vessel sacrificial tooling

The main pain points that prevented the completion of this study were the challenges of dissolving the Ultem tooling which necessitated a large volume of DMF solvent and adhering the printed strain gauge onto the carbon fiber twill weave. With regards to dissolving the Ultem tooling, the narrow neck opening resulting in limited contact between the Ultem and solvent, high viscosity of partially dissolved Ultem, and lack of mechanical agitation to push the Ultem out of the tooling, prevented testing efforts. Additional difficulties encountered included handling the pressure vessel to avoid pulling the wires off the solder tabs while dissolving the Ultem. With regards to ensuring complete adherence of the strain gauge to the carbon fiber composite, concerns arose as a result of the twill weave geometry which had slight gaps between fiber tows. Such weave pattern was not ideal as a printed trace transfer substrate, nor ideal for an airtight pressure vessel design.

Future experiments should include printing a larger scale pressure vessel (2X original size) and adding a single layer of adhesive to the 3 layers of carbon fiber prepreg in hopes of ensuring an airtight seal to eliminate air leaks during testing and to eliminate noise in measurements from the conductivity of carbon fibers.

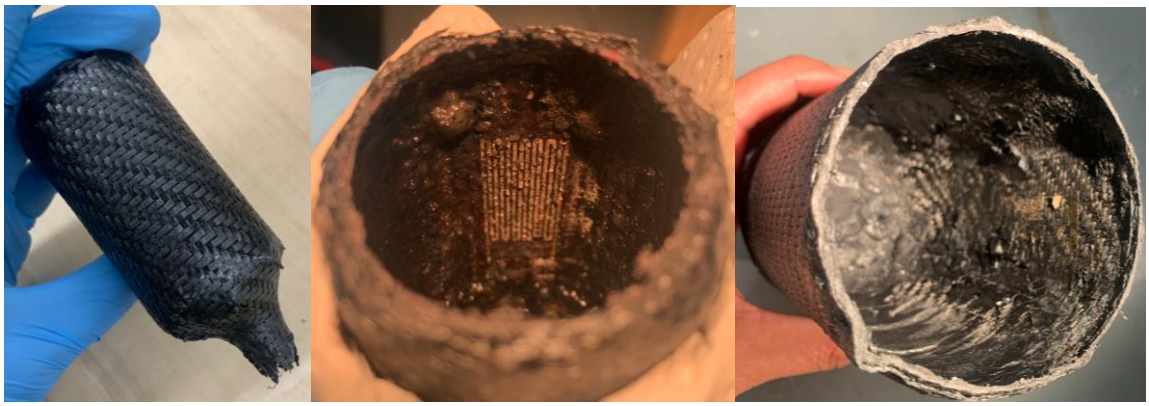

Figure A.2.3 Cured composite pressure vessel on sacrificial tooling (left), interior of original size pressure vessel with undissolved Ultem and damaged strain gauge not fully adhered to composite (middle), and large-scale pressure vessel (2X original size) with undissolved Ultem covering the damaged printed strain gauge (right).